	<p style="text-align: center;">SMOS L2 OS Table Generation Requirements Document</p>	<p>Doc: SO-TN-ARG-GS-0014 Issue: 3 Rev: 18 Date: 16 March 2021 Page: i</p>
---	--	--

Title: **SMOS L2 OS Table Generation Requirements Document**

Doc code: **SO-TN-ARG-GS-0014**

Issue: **3**

Revision: **18**

Date: **16 March 2021**

	Name	Function	Company	Signature	Date
Prepared	SMOS Team		Expert Support Laboratories		
Reviewed	M. Arias	Project manager	ARGANS		
Released	R. Sabia	Technical Officer	ESA		

Proprietary/Copyright Information

This material contains proprietary and/or copyright information of ARGANS Ltd. (ARGANS) and may not be copied, used, or disclosed without permission of ARGANS.

© Copyright ARGANS Ltd. (2021)

COMMERCIAL IN CONFIDENCE



Change Record

<u>Issue</u>	<u>Revision</u>	<u>Date</u>	<u>Description</u>	<u>Approval</u>
Draf	1	17-06-2005	Initial version	
Draft	2	20-12-2005	Major update before Critical design Review	
Draft	3	20-01-2006	Minor revision after Critical Design Review	
1	0 (and 0b)	27-06-2006	Consolidation from draft	
1	1 (and 1b, 2, 2a)	24-09-2006	For Core-v2 review	
2	0 (and 0a, 0b)	29-06-2007		
2	1	07-12-2007	Cove V3	
2	2 (1a and 1b)	15-02-2008	Post Core V3 FAT	
3	0	14-11-2008	For V4 pre-QR	
3	1	16-12-2008	Updated after V4 pre-QR RIDs	
3	2	17-02-2009	For V4 TRR	
3	3	29-06-2009	Post V4 FAT	
3	4	07-01-2010	Build 0311	
3	5	09-06-2010	Build 0316	
3	6	07-12-2010	Build 0317	
3	7	27-05-2011	Build v0500 pre-FAT	
3	7	22-06-2011	Post v0500 FAT	
3	8	07-11-2011	Build v0550 pre-FAT	
3	8	17-11-2011	Post v0550 FAT	
3	9	30-11-2012	Build v0600	
3	9	25-01-2013	Post v0600 FAT	
3	10	13-09-2013	Pre v0610 FAT	
3	10	29-11-2013	v611 delivery	
3	11	11-03-2015	V62x reprocessing update	
3	12	31-07-2015	beta delivery 06_25	
3	13	29-04-2016	Build 06_60	
3	14	08-07-2016	Post v06_61 FAT	
3	15	21-01-2019	Build v0670	
3	16	09-10-2020	Pre v0700 FAT	
3	17	12-02-2021	Build v0700	
3	18	16-03-2021	Post v07_00 FAT	

Proprietary/Copyright Information

This material contains proprietary and/or copyright information of ARGANS Ltd. (ARGANS) and may not be copied, used, or disclosed without permission of ARGANS.

© Copyright ARGANS Ltd. (2021)

COMMERCIAL IN CONFIDENCE



SMOS L2 OS
Table Generation Requirements Document

Doc: SO-TN-ARG-GS-0014
Issue: 3 Rev: 18
Date: 16 March 2021
Page: iii

	Page #	Section #	Comments	
issue 1.0	44	2.4.6	Bistatic scattering coefficients.	30-06-2006
issue 1.0b	5	2.1	Added general quality index to LUTs list	21-07-2006
	6	2.2.2	Changed section title to distinguish from 2.4.2	
	32	2.4.2	Several TBD cleared	
	32	2.4.2	Tg_young and old seas removed	
	32	2.4.2	σ_{Tb_model} split in 3	
	32	2.4.2	Tg_TEC_gradient added	
	52	2.4.6	Modified atmosph. coefficients	
	54	2.4.9	Several TBD cleared	
	54	2.4.9	Tg_quality_SSSX added to table	
	56	2.4.11	Added General Quality Index section	
	several		"Decision tree" changed to "Measurement discrimination"	


issue 1.1	2-3	1.3	Update numbering of Reference Documents	15-09-2006
	4	1.4	Minor corrections	
	5	2.1	Replaced LOCEAN by IPSL	
	18	2.2.3.2	Extended incidence coverage of the LUT	
	23	2.2.5	Comment on new approach	
	23	2.2.5.1.2	TBD removed	
	25	2.2.5.1.3	Typo corrected and TBC removed	
	25	2.2.5.2	Section title detailed	
	24	2.2.5.2.1	Conditions of validity (flat sea) added	
	25	2.2.5.2.1	Removed "provided by ESA"	
	26	2.2.5.2.3	Updated table and text	
	27	2.3.1.3	'gain' and 'bias' replaced by 'scale factor' and 'offset'	
	27-39	2.3.1	Removed TBD and changed values in all tables	
	29	2.3.1.4	New section.	
	33-35	2.3.1.4	Two new tables for parameters U^* & SWH	
	35	2.3.1.5	Former section 2.3.1.4. Added missing parameters and std dev	
	40	2.4.2	Removed TBD and Tg_resol_max_coast_ocean	
	41	2.4.3	Modified some coefficients	
	several	index+several	Sections renumbered from 2.4.6	
	62	2.4.10	Removed Tg_quality_SSSX	
	63	2.4.12	Changed [] to dl	

Proprietary/Copyright Information

This material contains proprietary and/or copyright information of ARGANS Ltd. (ARGANS) and may not be copied, used, or disclosed without permission of ARGANS.

© Copyright ARGANS Ltd. (2021)

COMMERCIAL IN CONFIDENCE

	SMOS L2 OS Table Generation Requirements Document	Doc: SO-TN-ARG-GS-0014 Issue: 3 Rev: 18 Date: 16 March 2021 Page: iv
---	--	---

	66-75	Appendix B	New section on celestial sky glitter corrections	
--	-------	------------	--	--

issue 1.1b	1	1.3, 1.4	Tables of documents and acronyms substituted by reference to SO-L2-SSS-ACR-013	12-12-2006
	23-33	2.2.6	Appendix B moved to new section	
	34-37	2.3.1.3, 2.3.1.4	Sections merged	
	40	2.3.1.5	Added number of sigma_TEC values	
	42	2.4.2	Modified Tb_modelX	
	67	Appendix A	Changed file names in matrix	

issue 1.2	15	2.2.3.3	LUT definition updated, possibility of Hermite interpolation added.	1-2-2007
	44-46	2.4.4	Typographic errors corrected in tables	
	59-60	2.4.7	Updated atmosphere coefficients	

issue 1.2a	3-9	2.2.2	Remove tables for neighbours. Merge distance to coast table and sea-ice mask + some naming corrections.	1-6-2007
	9-10	2.2.2	Add table for SSS climatology	
	11	2.2.3	Threshold to apply roughness 1	
	14	2.2.4	Threshold to apply roughness 2	
	35	2.4.2	Tg_dlandX removed from table (already defined in 2.2.2.1)	
	36	2.4.2	Tm_angle_sun removed (not used). Tm_WS1,2 removed (duplicated from 2.4.4)	
	38	2.4.4	Threshold to apply roughness 3	
	46	2.4.5	Values for Tg_WS_foam_MX	
	60	2.4.12	Updated Dg_SSS_quality coefficients	


issue 2.0	11	2.2.3.2	Explanation on threshold for roughness 1 correction	15-6-2007
	56	2.4.8	User parameters for cardioid	
	56-60	2.4.9-2.4.13	Renumbered sections	
	61	Appendix A	Table 9 updated	
	1	1.3 and 1.4	Updated reference to Software Release Document	
		2.4.7	Atmospheric model parameters controlled.	
issue 2.0a	iv	Change log	Issues 2.0, 2.0a, 2.0b renumbered to 1.2, 1.2a, 2.0 for coherence with deliveries to ESA	20-7-2007
	58	2.4.11	Thresholds for A_card inversion	
	i	Cover, headers	Date and issue number corrected in cover page and page headers (were not updated in 20.7.07 delivery)	10-9-2007

Proprietary/Copyright Information

This material contains proprietary and/or copyright information of ARGANS Ltd. (ARGANS) and may not be copied, used, or disclosed without permission of ARGANS.

© Copyright ARGANS Ltd. (2021)

COMMERCIAL IN CONFIDENCE

	SMOS L2 OS Table Generation Requirements Document	Doc: SO-TN-ARG-GS-0014 Issue: 3 Rev: 18 Date: 16 March 2021 Page: v
---	--	--

	v	Change log	Correction to change log (renumbering of issues was not noted)	
--	---	------------	---	--

issue 2.0b	35	2.4.2	Typos corrected in Tg_ice_concentration, Tg_low_SST_ice, Tg_max_rainfall	8-10-2007
	36	2.4.2	4 Tm for sun changed from TBD to TBC (values taken from config file)	
	36	2.4.2	a_factor changed to nsig	
	57	2.4.9	Sentence on SBC completed	
	63	Actions	Three new action items noted	

issue 2.1 (named 2.0c when it was distributed first to ESLs)	16	2.2.5.1.3	Galactic map precision corrected from 0.5 K to 0.05 K and text modified	24-10-2007
--	----	-----------	--	------------

issue 2.1a (issued twice by mistake 13-12-07 and 1-2-08)	18	2.2.5.2, 2.2.5.3	Computation of error maps convoluted by WeF	29-1-2008
	36	2.4.2	Thresholds for polarised gal. noise	29-1-2008
	36	2.4.2	Tg_DT_ice corrected to Tm_DT_ice	10-12-2007
	36	2.4.2	Tm_out_of_range set to 100 K	12-12-2007
	36	2.4.2	Tm_DT_ice units set to K, not °C	12-12-2007
	36	2.4.2	Tg_WS_gal = 2 m/s introduced as maximum to discard measurements contaminated by erroneous gal. noise	12-12-2007
	56	2.4.8	Tg_lat_ice_Acard set to 50° Tg_SST_ice_Acard set to 271 K	12-12-2007
	63	Actions	New TBC/TBD column in table	24-1-2008
	63	Actions	Need to confirm % or [0-1] in 2.4.2	31-1-2008
	63	Actions	Removed two “ambiguous” actions on comments to be added	12-12-2007


issue 2.2 (initially named 2.1b)	29	2.3.1.1	Note: α is noted Fac_omega in DPM	8-2-2008
	35	2.1.4	Dual pol acquisition time, solid angle of Sun and sky background Tb added to physical constants table	
	36	2.4.2	Added missing % to some values	
	36	2.4.2	TBC on sunglint thresholds removed	
	37	2.4.2	Sigmas for cardioid model	
	39-42	2.4.4	Modified table format	
	58	2.4.11	Tg_lambda_diaMax set to 100	

Proprietary/Copyright Information

This material contains proprietary and/or copyright information of ARGANS Ltd. (ARGANS) and may not be copied, used, or disclosed without permission of ARGANS.

© Copyright ARGANS Ltd. (2021)

COMMERCIAL IN CONFIDENCE

	SMOS L2 OS Table Generation Requirements Document	Doc: SO-TN-ARG-GS-0014 Issue: 3 Rev: 18 Date: 16 March 2021 Page: vi
---	--	---

	58-59	2.4.11	SSS_prior and Acard_prior values	
	59	2.4.11	δ SSS and δ Acard set to 0.01 like the rest of variables	
	60	2.4.11	Coefficients for Tb/SSS sensitivity computation	
	60	2.4.11	Thresholds for overall quality index	
	63	Appendix A	TGRD to IODD traceability matrix updated	
	64	Pending actions	Note to recall that several values are just guesses that require future confirmation	

	Page #	Section #	Comments	Date
issue 3.0	36	2.4.2	Values for Tg_swell, Tg_old_sea, Tg_young_sea	11-5-2008
	36	2.4.2	Values for Radius_front, Tg_SST_front, Tg_SSS_front	11-5-2008
	59	2.4.11	Values for Tg_Acard_max, Tg_Acard_min, Tg_sigma_max_Acard	6-3-2008
	64	Pending actions	Removed action above. Added comment on future changes	6-3-2008
	i, ii, all	cover, headings	Formatted to ARGANS version	9-6-2008
	v-vi	Change log	Names and dates of past issues explained where there was confusion	2-7-2008
	56	2.4.9	Removed Scene Dependent Bias Correction section that had been previously removed from ATBD	1-7-2008
	15	2.2.5	Changed section title and removed introduction	7-7-2008
	15-17	2.2.5.1	Removed Original Sky Map subsection	7-7-2008
	60	Appendix A	AUX_CNFO2 changed to AUX_CNFOSD/F	30-10-2008
		2.3.1.3, 2.3.1.4	Extended AGDPT description	12-11-2008

	Page #	Section #	Comments	Date
issue 3.1		2.3.1	Updated AGDPT description & tables	16-12-2008

	Page #	Section #	Comments	Date
issue 3.2		2.2.3.2	Corrected LUT sequence (swapped SSS & SST)	08-01-2009


	Page #	Section #	Comments	Date
issue 3.3	33	2.4.4	Renamed Tm_WR1/2 to WS_range_min/max	03-04-2009
issue 3.3	28	2.3.1.3	Corrected UN10/VN10 ending value and interval to match ATBD	11-05-2009
issue 3.3	8	2.2.2.1	Corrected total # bytes & AUX_DISTAN file size	18-05-2009

Proprietary/Copyright Information

This material contains proprietary and/or copyright information of ARGANS Ltd. (ARGANS) and may not be copied, used, or disclosed without permission of ARGANS.

© Copyright ARGANS Ltd. (2021)

COMMERCIAL IN CONFIDENCE

	SMOS L2 OS Table Generation Requirements Document	Doc: SO-TN-ARG-GS-0014 Issue: 3 Rev: 18 Date: 16 March 2021 Page: vii
---	--	--

issue 3.3	30-31	2.4.2	Corrected values for Tg_sunlint_max%, Tg_moonglint_max%, Tg_gal_noise_max% - all 10%	27-05-2009
issue 3.3	26	2.2.7	Removed unimplemented neural network	29-06-2009

	Page #	Section #	Comments	Date
issue 3.4	32-40	2.4.4	Roughness model 3 extended to cubic dependency on incidence angle	01-12-2009

	Page #	Section #	Comments	Date
issue 3.5		Appendix B	Added: Ocean Target Transformation (OTT)	09-06-2010

	Page #	Section #	Comments	Date
issue 3.6		2.2.5	New roughness model 3 – complete rewrite of previous section 2.4.4, moved to 2.2.5, & subsequent sections renumbered	07-12-2010
		2.2.4	Updated roughness model 2	

	Page #	Section #	Comments	Date
issue 3.7		2.4.2	Corrected Tg_max_rainfall to 0.002 m/h (was 2 mm/h); added Tg_num_RFI_max, RFI_std, RFI_nsig, & Tg_num_outliers_max%	27-04-2011
	ii		Corrected change record version (was 318) , JCD comment 8ii(2)	15-06-2011
	vii		Added Tg_num_outliers_max% to change log above, JCD comment 8ii(4)	15-06-2011
			See Appendix of FAT minutes for JCD comments referenced above.	22-06-2011

	Page #	Section #	Comments	Date
issue 3.8	56	Appendix B	Updated description of OTT generation and added new example OTTs	07-11-2011
	9	2.2.2.2	Updated to WOA2009, updated hyperlink	07-11-2011
		Appendix B	Corrected captions for figures 13 & 14 & various typos (see JCD comments 8)	17-11-2011
		Appendix C	Moved pending actions into a new Appendix	17-11-2011


	Page #	Section #	Comments	Date
issue 3.9	53	2.4.13	Updated SSS quality index coefficients	26-06-2012

Proprietary/Copyright Information

This material contains proprietary and/or copyright information of ARGANS Ltd. (ARGANS) and may not be copied, used, or disclosed without permission of ARGANS.

© Copyright ARGANS Ltd. (2021)

COMMERCIAL IN CONFIDENCE

	SMOS L2 OS Table Generation Requirements Document	Doc: SO-TN-ARG-GS-0014 Issue: 3 Rev: 18 Date: 16 March 2021 Page: viii
---	--	---

	33	2.4.2	Removed Tg_gal_noise_pol_max, Tm_gal_noise_pol, Tm_out_of_range; added Tg_current_RFI_max_X/Y, Tg_num_meas_outliers_min, Tg_num_meas_RFI_outliers_min, Tg_num_RFI_outlier_max, Tm_out_of_range_affov/eaffov, Tm_out_of_range_stokes3_affov/eaffov, Tm_out_of_range_stokes4_affov/eaffov, Ts_snapshot_out_of_range, Ts_meas_min, Ts_std, Ts_std_stokes3/4, RFI_c1/2.	14-01-2013
	20,28	2.2.7.1 & 2.2.7.3	Updated description of derivation of GAL2OS LUTs: now using geometric optics model & double set of LUTs (for ascending/descending orbits).	30-11-2012
	49	2.4.10	Removed sentence stating there are no RFI tests described in ATBD	17-12-2012

	Page #	Section #	Comments	Date
issue 3.10		2.1, 2.2.7, Appendix A	Removed reference to neural network, added OTT, corrected IODD section cross-references	03-09-2013
		2.3.2	Added new section "Ocean Target Transformation Tables"	03-09-2013
		Appendix B & C	Removed – no longer needed	03-09-2013
		Appendix A	Corrected AGDP, OTT, Cardiod IODD section cross-references	11-10-2013
		Table 2	Added not cross-referencing "global quality index" to IODD field 271-302	11-10-2013
		2.2.6.1.4	Added references to "New GAL_OS (weighted by WEF) generated using two different methods" & Nicolas Floury's TN.	12-11-2013

	Page #	Section #	Comments	Date
issue 3.11		2.4.12	Renamed section "TEC and Faraday rotation; added table for TEC retrieval from Stokes 3.	02-03-2015
		2.3.2	Added tables for selection & computation of ascending & descending orbit OTTs.	02-03-2015
		2.4.6	Added new section 2.4.6 "Switches & Filters"	11-03-2015


	Page #	Section #	Comments	Date
issue 3.12		2.2.5	Updated with new empirical model from L1 v620	11-06-2015
		2.2.8	New section "Land (Mixed Scene) Contamination"	23-07-2015
	Page #	Section #	Comments	Date
issue 3.13		2.4.5	Renamed "Galactic Noise bistatic scattering"	26-05-2016
		2.4.6	New section "Sun glint" inserted, subsequent sub-sections renumbered.	26-05-2016
		Appendix A	Updated IODD cross-references.	

Proprietary/Copyright Information

This material contains proprietary and/or copyright information of ARGANS Ltd. (ARGANS) and may not be copied, used, or disclosed without permission of ARGANS.

© Copyright ARGANS Ltd. (2021)

COMMERCIAL IN CONFIDENCE

	SMOS L2 OS Table Generation Requirements Document	Doc: SO-TN-ARG-GS-0014 Issue: 3 Rev: 18 Date: 16 March 2021 Page: ix
---	--	---

	Page #	Section #	Comments	Date
issue 3.14	41	2.2.8.5	Clarified definition of 3 rd & 4 th modified Stokes vectors in land-sea correction LUT (AUX_MSOTT_).	08-07-2016

	Page #	Section #	Comments	Date
issue 3.15			Various typo correction and version numbering updating for L2OS v670 delivery	11-08-2017

	Page #	Section #	Comments	Date
issue 3.16	n/a	Whole document	Update of headers and footer, reformatting to newer Word editor. Reformatting of equations and improvement of general readability.	09-10-2020
	3	2.2.1	Update of list of LUTs, including extended description as was incomplete.	09-10-2020
	42	2.2.8	Addition of SMOS-based climatology LUT computation to obtain SSS anomalies, to be part of L2OS v700	09-10-2020
	63	2.4.3	Add coefficients for Somaraju and trumpf dielectric constant	09-10-2020
	87	2.4.6.2	Introduction of AUX_SUN_BT computation from SERCO solar flux data.	09-10-2020
	99	Appendix A	Update of table to include new AUX files and updates references to sections in ATBD.	09-10-2020

	Page #	Section #	Comments	Date
issue 3.17	N/A	2.4.6.2	Reallocation of solar flux studies to Annex A	12-02-2021
	N/A	Annex A	Addition of the list of solar fluxes studied.	12-02-2021
	81	2.4.6.2	Inclusion of process to adapt solar fluxes to the LUTs used in L2OS data processor.	12-02-2021
	All pages	2.2.8	Full reformulation of the LSC LUT computation for L2OS v700 (3 rd mission reprocessing)	12-02-2021

In the current issue 3.18

Issue 3.18	Page #	Section #	Comments	Date
	56-29	2.2.9	Correction of small typos. Clarification of the period used to generate the LUT for 3 rd mission reprocessing.	16-03-2021
	59	2.2.9.4	Clarification of post-filtering carried out in the LUT to remove non-physical values.	16-03-2021
	133	Appendix B	Addition of AUX_SUN_BT in the traceability matrix	16-03-2021

Proprietary/Copyright Information

This material contains proprietary and/or copyright information of ARGANS Ltd. (ARGANS) and may not be copied, used, or disclosed without permission of ARGANS.

© Copyright ARGANS Ltd. (2021)

COMMERCIAL IN CONFIDENCE

Table of Contents

1. INTRODUCTION	1
1.1. PURPOSE OF DOCUMENT	1
1.2. SCOPE OF DOCUMENT	1
1.3. REFERENCE AND APPLICABLE DOCUMENTS	1
1.4. ABBREVIATIONS	1
1.5. NOTATIONS AND CONVENTIONS	1
2. LOOK-UP TABLE SPECIFICATIONS.....	1
2.1. LIST OF LOOK-UP TABLES	1
2.2. PRE-COMPUTED TABLES FOR THE DURATION OF SMOS MISSION	3
2.2.1. List of LUTs	3
2.2.2. Geographical information	4
2.2.2.1. Distance to the coast and sea-ice mask	4
2.2.2.2. Sea Surface Salinity	10
2.2.3. Roughness 1	11
2.2.3.1. Content	11
2.2.3.2. Generation method	12
2.2.3.3. LUT format.....	12
2.2.4. Roughness 2	14
2.2.4.1. Contents.....	14
2.2.4.2. Generation Method	14
2.2.4.3. LUT format.....	17
2.2.5. Roughness 3	19
2.2.5.1. Content	19
2.2.5.2. Generation method	19
2.2.6. Galactic Noise 1	20
2.2.6.1. Sky map weighted by a centrosymmetric WEF (flat sea)	20
2.2.7. Galactic Noise 2	23
2.2.7.1. Mathematical formulation.....	23
2.2.7.2. Numerical Integration of Scattered Galactic Radiation	26
2.2.7.3. Look up Tables Implementation	32
2.2.8. Land (Mixed Scene) Contamination	35
2.2.8.1. Brief introduction to land-sea contamination biases	35
2.2.8.2. Brief Overview of the empirical land-sea contamination bias correction calculation.....	36
2.2.8.3. Weighted moments of the land sea contamination.....	38
2.2.8.4. Weighted Filtering and adjusting the merged lookup table.....	42
2.2.8.5. Using the convolution kernel to fill gaps in the filtered lookup table	44
2.2.8.6. Contents of the MATLAB LSC LUT files	50
2.2.8.7. Example C++ code to compute dimension and global indices.....	50
2.2.8.8. The total model solution	52
2.2.8.9. Notes.....	55
2.2.8.10. References	55
2.2.9. SMOS-based climatology LUT for SSS anomaly computation	56
2.2.9.1. Purpose	56
2.2.9.2. Mathematical Formulation.....	56
2.2.9.3. Calculation of LUT	57
2.2.9.4. Generation of LUT	59
2.2.9.5. Contents of LUT.....	59
2.3. TIME VARYING TABLES	60
2.3.1. Auxiliary Geophysical Data Processor Tables.....	60
2.3.1.1. Physical constants.....	60
2.3.1.2. First guess, uncertainty on priors and bias correction	60
2.3.1.3. Scale factor and offset correction for the geophysical parameters used in the iterative retrieval	61
2.3.2. Ocean Target Transformation Tables.....	62

Proprietary/Copyright Information

This material contains proprietary and/or copyright information of ARGANS Ltd. (ARGANS) and may not be copied, used, or disclosed without permission of ARGANS.

© Copyright ARGANS Ltd. (2021)

COMMERCIAL IN CONFIDENCE

2.4. USER PARAMETERS TABLES	67
2.4.1. <i>Physical constants</i>	67
2.4.2. <i>Measurement discrimination</i>	68
2.4.3. <i>Dielectric Constant</i>	70
2.4.3.1. Klein & Swift	70
2.4.3.2. Somaraju and Trumpf	71
2.4.4. <i>Foam</i>	72
2.4.4.1. Generation method	73
2.4.4.2. Foam coverage model	73
2.4.5. <i>Galactic Noise bistatic scattering</i>	76
2.4.5.1 Formulation of scattering coefficients	76
2.4.5.2 Lookup table implementation	83
2.4.6. <i>Sun glint</i>	88
2.4.6.1. Bistatic scattering cross-sections	88
2.4.6.2. Solar flux LUT	90
2.4.7. <i>Switches & Filters</i>	91
2.4.8. <i>Atmosphere</i>	95
2.4.9. <i>Cardioid model</i>	95
2.4.10. <i>2.4.10 RFI</i>	96
2.4.11. <i>2.4.11 Convergence</i>	96
2.4.12. <i>2.4.12 TEC and Faraday rotation</i>	100
2.4.13. <i>Global SSS quality index</i>	101
APPENDIX A: SOLAR FLUX DATASETS FOR SUN GLINT CORRECTION	103
A.1. ONE SECOND SOLAR FLUX DATA	103
A.2. DAILY NOON SOLAR FLUX DATA	107
A.3. USE OF SOLAR FLUX DERIVED FROM SMOS DATA	109
APPENDIX B: TGRD TO IODD TRACEABILITY MATRIX	120

List of Tables

Table 1: Data record of distance to coast and sea ice table	9
Table 2: Variables in the MATLAB LSC Lookup Table Files	51
Table 3: Quantities in the total Scene Brightness Model	54
Table 4: Solar Flux Lookup Table for the L2OS Processor	91
Table 5: Solar Flux sources alternatives	111
Table 6: Quantities in the total Scene Brightness Model	119
Table 7: TGRD to IODD traceability matrix	120

Proprietary/Copyright Information

This material contains proprietary and/or copyright information of ARGANS Ltd. (ARGANS) and may not be copied, used, or disclosed without permission of ARGANS.

© Copyright ARGANS Ltd. (2021)

COMMERCIAL IN CONFIDENCE

List of Figures

Figure 1: maximum ice extent annual climatology for both the Arctic (left) and Antarctica (right)..... 5

Figure 2: Plots showing the polar stereographic projections used for the Southern (left) and Northern (right) hemispheres..... 6

Figure 3: (a) and (b): Example dwell-line averaged bias between SMOS and SMAP (8-day running mean) retrieved SSS for July 2016 for descending and ascending passes, respectively. (c) and (d): Corresponding bias in first Stokes parameter divided by two T_p (K)..... 35

Figure 4: Example projection fo the four-dimensional land-sea contamination lookup table (LSC LUT) grid lines onto earth for a particular scene. Blue lines are latitude-longitude grid cell boundaries and the red lines are director cosine grid cell boundaries. Black dots show the locations where the LSC biases are computed before interpolation to the LUT cells..... 36

Figure 5: Flowchart showing the basic steps in producing the land-sea contamination lookup table. 37

Figure 6: Flowchart showing stages of the process of merging the first four moments of the land sea contamination biases evaluated over the mission. At each stage the calculation is parallelized for efficiency. 41

Figure 7: (a): Example slice through the unfiltered LSC LUT at grid cell $(i\xi, i\eta) = (41, 41)$ with the boundaries of filtered regions indicated by the green curves. The curves outline both a rectangular area in the northwest Atlantic Ocean (heavily affected by RFI) and areas where the temporal standard deviation of the monthly 25 km ISAS SSS from 2013-2016 exceeds 0.4. (b): The same as in (a) except filtered to remove all biases inside the green curves as well as biases for which the sum of the weights is below 0.1, the fraction of land in the front half-space is below 0.005, or the standard deviation of the bias exceeds the 95th percentile for the given polarization and $(i\xi, i\eta)$ location..... 42

Figure 8: Same slice as in Figure 7 through the LSC correction (a) before and (b) after correcting for open ocean (far from land) biases..... 43

Figure 9: Convolution kernel (a) weighting and (b) influence functions for land occupying an LSC LUT cell with center at director cosine position index $(i\xi, i\eta) = (40, 40)$. Integration of the product of the weighting function $C^p(\xi_k, \eta_k; \xi, \eta)$ (with k fixed) and the land-sea mask over the entire FoV yields the total LSC at position (ξ_k, η_k) . By contrast, the influence function $C^p(\xi, \eta; \xi_i, \eta_i)$ (with i fixed) is the bias over the EAF-FoV associated with the presence of land at position (ξ_i, η_i) . Hence these two functions are different slices through the same four-dimensional function $C^p(\xi_k, \eta_k; \xi_i, \eta_i)$. Units are kelvin.. 48

Figure 10: (a): Ascending pass LSC at grid cell $(i\xi, i\eta) = (41, 41)$ computed using only the convolution kernel method. (b): Difference between convolution kernel solution and the bias-corrected LSC LUT solution. Units are kelvin. 49

Figure 11: Example of SMOS absolute bias determination 56

Figure 12: Flowchart showing the steps involved in producing the final daily (unpolarized) sun brightness temperature time series to be used in the Level 2 Ocean Salinity Processor..... 90

Proprietary/Copyright Information

This material contains proprietary and/or copyright information of ARGANS Ltd. (ARGANS) and may not be copied, used, or disclosed without permission of ARGANS.

© Copyright ARGANS Ltd. (2021)

COMMERCIAL IN CONFIDENCE

Figure 13: Time series of the six-day running mean of daily median of the 1-s sun brightness temperatures reported by stations in Sagamore Hill, Palehua, and San Vito. This running mean is used to compute the sun glint model solutions. Gray shading shows the range of sun brightness temperatures obtained by computing the daily maximum and minimum of the smoothed solar fluxes +/- two standard deviations. 106

Figure 14: Linear fit between 10.7 cm and 21 cm sun brightness temperatures. 108

Figure 15: Left: Time series of daily L-band sun brightness temperature obtained from linear fit to 10.7 cm brightness temperature as described above. Right: zoom on 2015/2016 brightness temperatures, showing the slow overall decrease in solar flux during this period. 109

Figure 16: Scatterplots of actual versus nominal sun glint (first Stokes divided by two, as discussed in the text) for four distinct 2-min time intervals during which sun glint strongly affects the measured brightness. (a)-(c) are three-time intervals on 27 Jan 2012, and (c) corresponds to a solar flare during which there is a large increase in the solar flux lasting just a few minutes. (d) is a two-min interval on 27 Dec 2017 which corresponds to a quiet sun period (and low sun brightness temperature). The black lines correspond the linear fits at the wind speed provided by the CCMP product, while the red and blue lines are linear fits for CCMP wind speed +/- 2 m/s, respectively. 114

Figure 17: Daily time series of sun Tb from various sources, include the rescaled Pentiction 10.7 cm measurements, the RedLab/Serco reference and SMOS time series, and 20-min averages of the linear fit using both CCMP and ECMWF wind speed to compute the nominal sun glint solutions. Upper panels are for 21 dec 2014 (active sun), while the lower panels are for 21 Dec 2018 (quiet sun). Vertical bars in the left panels show the range of linear fit sun Tb within each 20-min averaging wind, while the bars in the right panels show the range associated with varying the CCMP wind speed by +/- 2 m/s in the nominal sun glint solution. 115

Figure 18: Time series of verious sources of sun Tb over the months of December and January for (a) 2014-2015 and (b) 2018-2019. Shown are both the nominal (i.e, as provided) and rescaled RedLab/Serco fluxes, where the rescaling is obtained as the median of the ratio between the linear fit and RedLab sun Tb time series over the entire mission. A median filter with a running 1-day window has been applied to the 2-min linear fit sun Tb time series to make it comparable to the daily time series. 115


Figure 19: Dwell-line average bias between SMOS and the total forward ocean scene brightness (first Stokes parameter divided by two) model including sun glint computed using four sources of solar flux (SMOS-model). 116

Proprietary/Copyright Information

This material contains proprietary and/or copyright information of ARGANS Ltd. (ARGANS) and may not be copied, used, or disclosed without permission of ARGANS.

© Copyright ARGANS Ltd. (2021)

COMMERCIAL IN CONFIDENCE

	<p style="text-align: center;">SMOS L2 OS Table Generation Requirements Document</p>	<p>Doc: SO-TN-ARG-GS-0014 Issue: 3 Rev: 18 Date: 16 March 2021 Page: 1</p>
---	--	--

1. Introduction

1.1. Purpose of document

This document is the Table Generation Requirements Document for the SMOS Level 2 Sea Surface Salinity Processor.

1.2. Scope of document

The Table Generation Requirements Document provides information on the generation of numerical values for variable parameters and fixed constants that are required for the SMOS SSS L2 processor. The document provides the fixed values and look-up tables and explains the method to compute those variables that are defined through mathematical expressions or must be obtained from external sources.

1.3. Reference and applicable documents

See Software Release Document SO-RN-ARG-GS-0019.

1.4. Abbreviations

See Software Release Document SO-RN-ARG-GS-0019.

1.5. Notations and conventions

Notations and conventions in TGRD are the same as in the ATBD document.

2. Look-up table specifications

2.1. LIST OF LOOK-UP TABLES


Table Name	Section	Description	Sampling requirements	Source	Notes
<i>Pre-computed Tables for the duration of the SMOS mission</i>					
Land sea mask-Measurement discrimination	2.2.2.1	USGS 1km land-sea mask		L1 processing-ACRI	
Sea ice mask-Measurement discrimination	2.2.2.2			IFREMER	
Roughness_1	2.2.3	Pre-computed Tb roughness data for model 1		LOCEAN	
Roughness_2	2.2.4	Pre-computed Tb roughness data for model 2		IFREMER	

ARGANS Ltd.

Commercial in Confidence

Page 1

Use, duplication, or disclosure of this document or any information contained herein is subject to the restriction on the title page of this document.

	SMOS L2 OS Table Generation Requirements Document	Doc: SO-TN-ARG-GS-0014 Issue: 3 Rev: 18 Date: 16 March 2021 Page: 2
---	--	--

Roughness_3	2.2.5	Pre-computed Tb roughness data for model 3		BEC	
Galactic noise 1	2.2.6	Pre-computed Tb using some input variables		LOCEAN	
Galactic noise 2	2.2.7	Pre-computed sky glitter harmonics		ODL	
Land (Mixed Scene) Contamination	2.2.8	Pre-computed global snapshot Tb correction		ODL	
SMOS climatology	2.2.9	Pre-computed climatology using SMOS salinities		LOCEAN/ACRI	
<i>Time Varying Tables</i>					
ADGP tables	2.3.1			IFREMER	
OTT	2.3.2	Corrects spatial biases & drift in L1		OTT post-processor	
<i>User Parameter Table</i>					
Physical Constants	2.4.1	Definition of some physical constants		ICM	
Measurement discrimination	2.4.2	Coefficients definition that appear in this module		ICM	
Dielectric constant	2.4.3	Coefficients definition that appear in this module		ICM LOCEAN ACRI-ST	
Roughness_3	2.4.4	Coefficients definition that appear in this module		ICM	
Foam	2.4.5			IFREMER	
Bistatic scattering coefficients	2.4.6			IFREMER	
Atmosphere	2.4.7	Coefficients definition that appear in this module		IPSL	
Bias correction	2.4.8	Coefficients definition		ICM	
RFI	2.4.9	No applicable		ICM	
Convergence	2.4.10	Coefficients definition		ICM	
Faraday rotation	2.4.11	Rotation angle to be applied on surface polarisation frame due to Faraday effect along target to satellite path.		L1 processing	see [R.D. 13]

ARGANS Ltd.

Commercial in Confidence

Page 2


Use, duplication, or disclosure of this document or any information contained herein is subject to the restriction on the title page of this document.

Global quality index.	2.4.12	Definition of a global quality index of the retrieved SSS.		LOCEAN	
-----------------------	--------	--	--	--------	--

2.2. PRE-COMPUTED TABLES FOR THE DURATION OF SMOS MISSION

2.2.1. List of LUTs

Table Name	Section	Description	Sampling requirements	Source	Notes
Land-sea mask	2.2.2.1	Land-sea mask to be applied in the Measurement discrimination		L1 Processing	
Sea ice mask	2.2.2.1	Sea ice mask to be applied in the Measurement discrimination		ECMWF climatology	
Roughness_1	2.2.3	Two-scale model		LOCEAN	
Roughness_2	2.2.4	SSA model		IFREMER	
Roughness_3	2.2.5	Empirical model		BEC	
Galactic noise 1	2.2.6	Sky map		LOCEAN	
Galactic noise 2	2.2.7	Scattering contribution of the galactic glint		ODL	
Land contamination	2.2.8	Systematic biases between L1C TBs and forward model according to the position in the FOV (xi, eta) and land fraction in the fundamental hexagon.	L1b datasets	ODL	
SMOS-based climatology	2.2.9	SSS climatologic values retrieved from SMOS SSS retrievals and accounting for remaining systematic biases, to support production of SSS anomaly.	L2 OS UDP datasets	ACRI-ST	

	<p style="text-align: center;">SMOS L2 OS Table Generation Requirements Document</p>	<p>Doc: SO-TN-ARG-GS-0014 Issue: 3 Rev: 18 Date: 16 March 2021 Page: 4</p>
---	--	--

2.2.2. Geographical information

2.2.2.1. Distance to the coast and sea-ice mask

Extended Land/sea mask for L2 SSS processor.

Needs

1. Is the ISEA grid point in land, in sea, in water in land, in island in water in land?
2. Distance to coastline (coastline is the border between land and sea, or land and water, or island and water).
3. Is distance to coastline less than Tg_dland1?
4. Is distance to coastline less than Tg_dland2?
5. Is the grid point within a sea-ice region for a given month according to the climatology?

Material

- isea4h9_cell_in_column_20040702.gz file. Below are the 10 first lines of the file:


```
1, 0000000000, 11.250, 58.283
2, 0100000000, -168.750, 58.283
3, 0100000001, -168.750, 58.400
4, 0100000010, -168.750, 58.518
5, 0100000011, -168.750, 58.636
6, 0100000100, -168.750, 58.755
7, 0100000101, -168.750, 58.873
8, 0100000110, -168.750, 58.991
9, 0100000111, -168.750, 59.109
10, 0100001000, -168.750, 59.228
```
- GSHHS - A Global Self-consistent, Hierarchical, High-resolution Shoreline Database, see <http://www.soest.hawaii.edu/wessel/gshhs/gshhs.html>.

For sea ice mask, we make use of the products delivered by the National Snow and Ice Data Centre (NSIDC), available at

ftp://sidads.colorado.edu/pub/DATASETS/PASSIVE_MICROWAVE/POLAR_STEREO/ANCILLARY/OCEANMASKS

NSIDC has created monthly ocean masks for users who want to know the maximum sea ice extent during a particular month, or who wish to mask out false sea ice concentrations caused by weather effects and/or land contamination. The ocean masks are a binary indicator (ice/no ice). They were derived for each month from the [Bootstrap Sea Ice Concentrations from Nimbus-7 SMMR and DMSP SSM/I](#) data set. The first processing step involved averaging the sea ice concentrations for each series of months throughout the time series, November 1978 through December 2003, to create 12 monthly ice concentration climatology for the entire

ARGANS Ltd.

Commercial in Confidence

Page 4

Use, duplication, or disclosure of this document or any information contained herein is subject to the restriction on the title page of this document.

series. To derive the monthly ocean masks, individual pixels containing any fraction of ice in these monthly-averaged sea ice concentrations were flagged as "ice-covered", and all other non-land pixels were flagged as "open water".

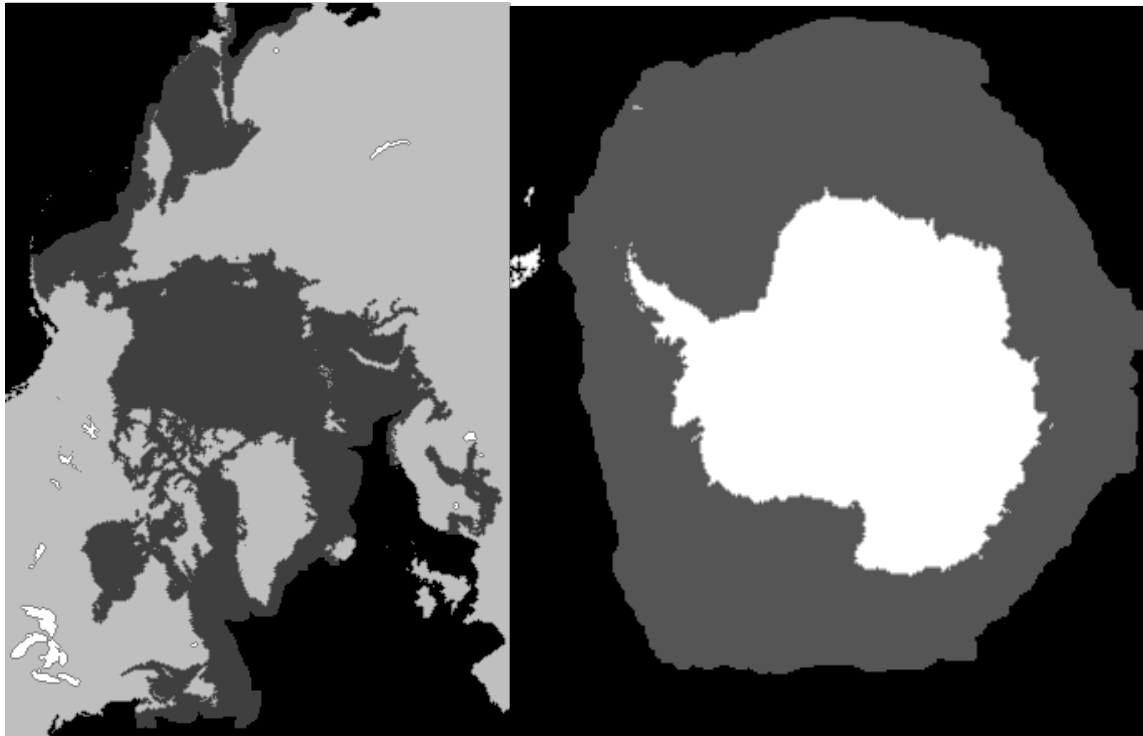


Figure 1: maximum ice extent annual climatology for both the Arctic (left) and Antarctica (right).

Ocean mask data are in flat, binary files with an image size of 304 x 448 pixels (bytes) for Arctic data, and 316 x 332 pixels (bytes) for Antarctic data. Ocean mask files exist for each month of the year as well as annually. An example of the file name convention for the monthly masks is 'oceanmask.apr.1979-2003.n' (or .s) for the April Northern Hemisphere ocean mask. Pixel values, coded for water, ice, coast, land, or lakes, are indicated below:

- 0 = water
- 1 = ice
- 2 = coast
- 3 = land
- 4 = lakes

For the maximum annual sea ice extent products, if ice was present in any of the twelve-monthly ocean masks, the corresponding pixels were classified as ice in the final ice extent image. A buffer of 2 pixels (approximately 50 km) was then set around this edge to produce the final ice extent boundary. Data files for the maximum ice extent grids for the entire time series are in flat one-byte binary format (304 x 448 pixels for the Arctic, and 316 x 332 pixels for the Antarctic region). The file naming convention is 'max_extent_mask.1979-2003.n' (or .s).

The projection for all the above data files is polar stereographic, true at 70 degrees latitude. A description of the projection is provided at:

http://nsidc.org/data/docs/daac/nsidc0079_bootstrap_seaice.gd.html

Figure 2 shows some aspects of the grid projection.

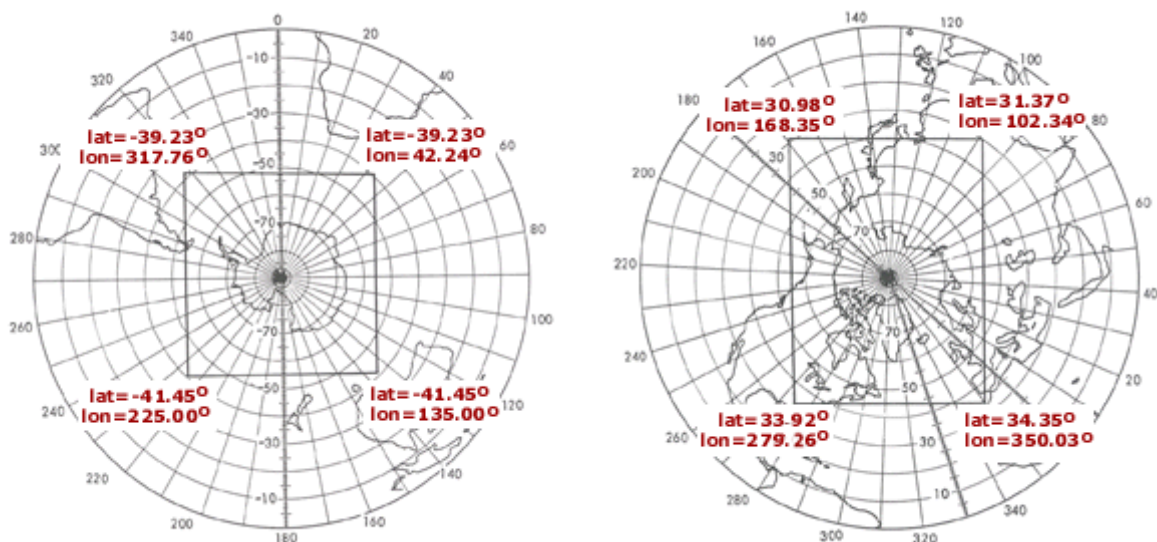



Figure 2: Plots showing the polar stereographic projections used for the Southern (left) and Northern (right) hemispheres.

The polar stereographic projection used specifies a projection plane (i.e., the grid) tangent to the earth at 70 degrees. The planar grid is designed so that the grid cells at 70 degrees latitude are 25 km by 25 km.

The polar stereographic formulae for converting between latitude/longitude and X-Y grid coordinates have been taken from Map Projections Used by the U.S. Geological Survey (Snyder 1982). Several different ellipsoids were compared to the Hughes ellipsoid and in each case, differences were less than 1 km over the SSM/I grids. However, differences of up to 9 km were

ARGANS Ltd.

Commercial in Confidence

	<p style="text-align: center;">SMOS L2 OS Table Generation Requirements Document</p>	<p>Doc: SO-TN-ARG-GS-0014 Issue: 3 Rev: 18 Date: 16 March 2021 Page: 7</p>
---	--	--

found if a sphere rather than an ellipsoid was used. Thus, it is an explicit requirement that an ellipsoid be used in processing the data.

FORTRAN code for performing the necessary transformations is provided at:

[ftp://sidads.colorado.edu/pub/DATASETS/PASSIVE MICROWAVE/POLAR STEREO/TOOLS/GE O COORD/FORTRAN/](ftp://sidads.colorado.edu/pub/DATASETS/PASSIVE_MICROWAVE/POLAR_STEREO/TOOLS/GE_O_COORD/FORTRAN/).

Since the mask is only used as a flag, the processor shall use the monthly maximum sea ice extent maps, which will provide a conservative mask for processing. The processor will ingest masks that have been pre-processed onto the ISEA4H-9 grid. This pre-processing shall involve looping over all grid cells in the ISEA grid, computing the corresponding grid point on one of the two sea ice extent maps, and then setting the ISEA cell mask value to 1 if any of the four neighbouring polar stereographic grid points contains ice and to 0 otherwise.

The data files

For the 2 621,442 grid points, the following data shall be generated:

- Distance to coastline,
- Flags according to the distance to the coast.
- Flags for possible presence of sea ice.

The table describes the binary data record. Flag F6 is true for the 12 grid points for which the cell is a pentagon instead of a hexagon.

File size is $15 \times 2\,621,442 = 37.5\text{Mbytes}$ (1Mbyte = 1024×1024 bytes)

Data field	Description	Unit	type	C format	length (byte)
GridPoint_ID	Grid point identifier	DI	Unsigned long (ul)	%lu	4
Flag	flag with (1=True, 0=False): F1. Fg_land_sea_coast1 (Most Significant Bit) F2. Fg_land_sea_coast2 F3. spare F4. spare F5. spare F6. spare F7. spare F8. spare	dl	unsigned char	%d	1
Dist	Distance to coastline	km	float	%f	4
Tg_resol_max_ocean	Maximum resolution of footprint. Default value is 100.	km	float	%f	4
sea_ice_flag	flag with (1=True, 0=False): SC1. Within maximum extend of sea ice in January month (LSB, i.e. 2 ⁰) SC2. Within maximum extend of sea ice in February month (first bit after LSB, i.e. 2 ¹) SC3. Within maximum extend of sea ice in March month SC4. Within maximum extend of sea ice in April month SC5. Within maximum extend of sea ice in May month SC6. Within maximum extend of sea ice in June month SC7. Within maximum extend of sea ice in July month SC8. Within maximum extend of sea ice in August month	dl	short	%d	1

	SC9. Within maximum extend of sea ice in September month				
	SC10. Within maximum extend of sea ice in October month				
	SC11. Within maximum extend of sea ice in November month				
	SC12. Within maximum extend of sea ice in December month				
				Total	15

Table 1: Data record of distance to coast and sea ice table.

For the land/sea/coast mask, four categories have been defined in ATBD. Two booleans are defined for the four states:

(Fg_land_sea_coast1;Fg_land_sea_coast2)

(false;false)=Land

(false>true)=Water, with distance to coast \leq Tg_dland1

(true>true)=Water, with distance to coast \leq Tg_dland2 and $>$ Tg_dland1

(true>false)=Water, with distance to coast $>$ Tg_dland2 $>$ Tg_dland1.

Dland1 and Tg_dland2 are two distances to coast in km.

With such definition, Fg_land_sea_coast1 flag defines if the grid point is strongly contaminated by land and Fg_land_sea_coast2 flags defined coastal grid points.

Finding Methods

The following approach is adopted to find ISEA grid point neighbours in the GSHHS vector shoreline. For each grid point of the DGG, all points of the vector shoreline are sorted by increasing order of angle (see figure below). The nearest point of the vector shoreline gives the distance to the coast.

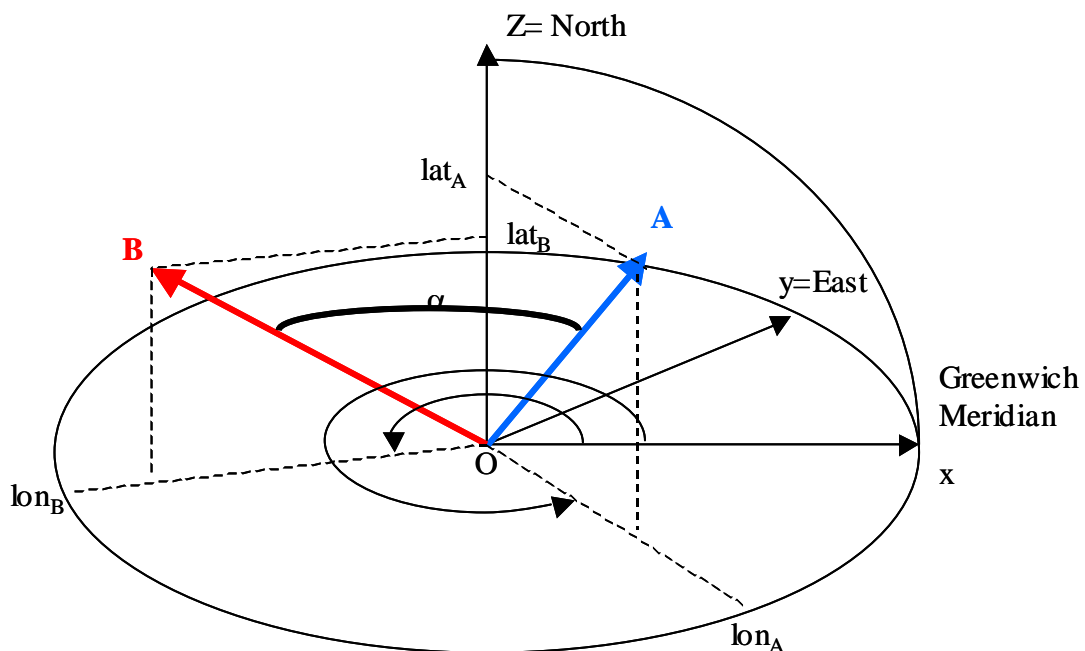
For Fg_land_sea_coast1 and Fg_land_sea_coast2 flags definition, thresholds Tg_dland1 and Tg_dland2 will be defined later and may change during SMOS mission. Baseline is Tg_dland1=60km and Tg_dland2=100km. One shall be able to update the dataset with new values for Tg_dland1 and Tg_dland2 (only flags F1 and F2 are affected) quickly (less than 1 hours) and easily (one command line). If Tg_dland1 and Tg_dland2 shall be modified often during validation and SMOS mission phases, they will be added to the processor configuration

file. Tg_land_sea_coast1 and Tg_land_sea_coast2 will be computed on the fly by the processor using the Dist information.

For the coastline, the GSHHS data base provides vector shorelines at several resolutions (25, 5, 1 and 0.2km). Preliminary generations of auxiliary data files are based on the 25km resolution dataset. The final generation will be based on the 1km resolution dataset.

Obviously, the general method above has been optimised to keep computation time within reasonable limits.

$$\cos(\alpha) = \cos(\text{lat}_A) \cos(\text{lat}_B) \cos(\text{lon}_A - \text{lon}_B) + \sin(\text{lat}_A) \sin(\text{lat}_B)$$



2.2.2.2. Sea Surface Salinity

The Sea surface Salinity LUT is based on the World Ocean Atlas 2009 climatology provided by the *Ocean Climate Laboratory* of the National Oceanographic Data Centre (NODC). These data are delivered monthly over the planet at one-degree resolution in latitude and longitude. Documentation can be found at

<ftp://ftp.nodc.noaa.gov/pub/WOA09/DOC/woa09documentation.pdf>


The LUT is built on the 2621442 grid points of the ISEA grid at which nearest neighbour values of the WOA grid are computed by maximizing $\cos(\alpha)$ (see details in section 2.2.2.1 above).

ARGANS Ltd.

Commercial in Confidence

Page 10

Use, duplication, or disclosure of this document or any information contained herein is subject to the restriction on the title page of this document.

	SMOS L2 OS Table Generation Requirements Document	Doc: SO-TN-ARG-GS-0014 Issue: 3 Rev: 18 Date: 16 March 2021 Page: 11
---	--	---

At each grid point of the ISA grid, twelve values, one per month, are written along with the grid point ID.

File size is 13 x 4 x 2 621,442 = 130Mbytes (1Mbyte = 1024 x 1024 bytes)

Data field	Description	Unit	type	C format	length (byte)
GridPoint_ID	Grid point identifier	DI	Unsigned long (ul)	%lu	4
SSS_jan	Monthly mean of Sea Surface Salinity for January month according to climatology.	psu	fl	%f	4
SSS_feb	Same as above for February.	psu	fl	%f	4
SSS_mar	Same as above for March.	psu	fl	%f	4
SSS_apr	Same as above for April.	psu	fl	%f	4
SSS_may	Same as above for May.	psu	fl	%f	4
SSS_jun	Same as above for June.	psu	fl	%f	4
SSS_jul	Same as above for July.	psu	fl	%f	4
SSS_aug	Same as above for August.	psu	fl	%f	4
SSS_sep	Same as above for September.	psu	fl	%f	4
SSS_oct	Same as above for October.	psu	fl	%f	4
SSS_nov	Same as above for November.	psu	fl	%f	4
SSS_dec	Same as above for December.	psu	fl	%f	4
Total					52


Table 2: Data record of SSS climatology map.

2.2.3. Roughness 1

2.2.3.1. Content

The roughness contribution to T_b , $T_{b,rough}$, is decomposed as the sum of an omnidirectional signal plus first and second harmonics (ATBD, § 4.2.1.2):

$$T_{brough} = \begin{bmatrix} Th_0 + Th_1 \cos(\varphi_a) + Th_2 \cos(2\varphi_a) \\ Tv_0 + Tv_1 \cos(\varphi_a) + Tv_2 \cos(2\varphi_a) \\ U_1 \sin(\varphi_a) + U_2 \sin(2\varphi_a) \\ V_1 \sin(\varphi_a) + V_2 \sin(2\varphi_a) \end{bmatrix}$$

	<p style="text-align: center;">SMOS L2 OS Table Generation Requirements Document</p>	<p>Doc: SO-TN-ARG-GS-0014 Issue: 3 Rev: 18 Date: 16 March 2021 Page: 12</p>
---	--	---

Since the model computation is very heavy, a tabulation of $T_{b_{rough}}$ is provided. Tabulations of $Th_0, Th_1, Th_2, Tv_0, Tv_1, Tv_2, U_1, U_2, V_1$ and V_2 are given in this table, as functions of incidence angle, SSS, SST, and wind speed assuming a neutral atmosphere, WSn .

2.2.3.2. Generation method

ASCII file provided by IPSL/LOCEAN.

The tabulation of $T_{b_{rough}}$ will be provided at the following geophysical values:

SST(°C) = [0 5 10 15 20 25 30]
SSS(psu) =[30 33 36 39]
 WSn (m/s)=[2 2.5 3 4 5 6 7 8 9 10 11 12 13 14 15 17 19 21 23 25 27 29 30]
 ϑ (°)=[0 4 8 12 16 20 24 28 32 36 40 44 48 52 56 60 64 68]

and all the $T_{b_{rough}} = 0$ K for $WSn=0$ m/s.

A switch allows to choose between linear and Hermite interpolation methods. In case the linear interpolation is selected, then the interpolation must be done linearly in the following order: 1- interpolation in SSS; 2- interpolation in SST; 3- interpolation in WSn ; 4- interpolation in incidence angle; this ensures a precision of 0.05K on each parameter.

No extrapolation out of the tabulation ranges is performed: in case any parameter goes out of range, the corresponding boundary value is taken. In case $0m/s < WSn < 2m/s$, the interpolation (linear or Hermitian) is performed between $T_{b_{rough}}(WSn=0m/s) = 0K$ and $T_{b_{rough}}(WSn=2m/s)$.

Roughness correction is always applied ($Tg_WS_roughness_M1 = 0m/s$).

Reprocessing is not foreseen on a regular basis. It is probable though, for improvement after SMOS launch based on the analysis of SMOS products.

2.2.3.3. LUT format

The ASCII file consists of 18 lines of header, followed by the LUT. The column separator is one blank space.

The FORTRAN code, that was written by E. Dinnat and used to generate the LUT, will be delivered to ACRI.

In the following table, which describes the content of the LUT, **the quantities useful for the processor appear in bold.**



Data field	Description	Unit	type	FORTTRAN format	length (byte)
freq	Frequency of SMOS radiometer	GHz	float	f9.5	
SST	Sea surface temperature	°C	float	f5.2	
SSS	Sea surface salinity	psu	float	f6.3	
WSn	Neutral wind speed at 10 m	ms ⁻¹	float	f6.2	
ustar	Friction velocity	ms ⁻¹	float	f6.2	
theta	Incidence angle	deg.	float	f4.1	
TvN	Tv for a flat sea	K	float	f7.3	
ThN	Th for a flat sea	K	float	f7.3	
Tv0	Omnidirectionnal component of Tv _{rough}	K	float	f7.3	
Th0	Omnidirectionnal component of Th _{rough}	K	float	f7.3	
Tv1	first harmonic component of Tv _{rough}	K	float	f6.3	
Th1	first harmonic component of Th _{rough}	K	float	f6.3	
U1	first harmonic component of U _{rough} (3 rd Stokes parameter)	K	float	f6.3	
V1	first harmonic component of V _{rough} (4 th Stokes parameter)	K	float	f6.3	
Tv2	second harmonic component of Tv _{rough}	K	float	f6.3	
Th2	second harmonic component of Th _{rough}	K	float	f6.3	
U2	second harmonic component of U _{rough} (3 rd Stokes parameter)	K	float	f6.3	
V2	second harmonic component of V _{rough} (4 th Stokes parameter)	K	float	f6.3	
lam_d	Cutoff wavelength	m	float	e9.3	
Stab	Stability parameter	-	float	f5.2	
Re(eps)	Real part of the dielectric constant	-	float	f6.2	
l(eps)	Imaginary part of the dielectric constant	-	float	f6.2	
Var_u	Variance of the slopes – upwind direction	-	float	e9.3	
Var_c	Variance of the slopes – crosswind direction	-	float	e9.3	
Foam	Foam contribution	K	float	f5.1	

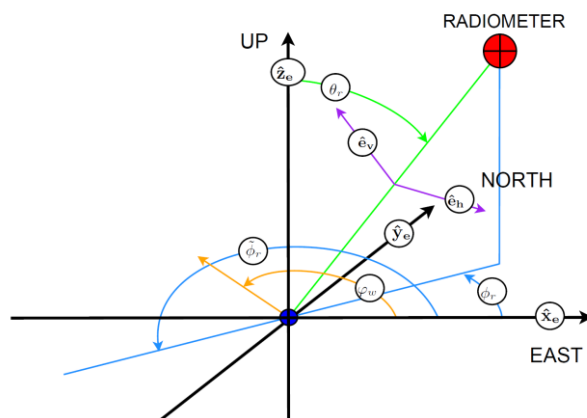
2.2.4. Roughness 2

2.2.4.1. Contents

The surface roughness correction module based on the empirical roughness emission model 2 produces a wind-excess emissivity Stokes vector of the following form:

$$\begin{pmatrix} \Delta T_h \\ \Delta T_v \\ \Delta U \\ \Delta V \end{pmatrix} = \begin{pmatrix} T_h^{(0)} + T_h^{(2)} \cos 2(\phi_r - \phi_w) \\ T_v^{(0)} + T_v^{(2)} \cos 2(\phi_r - \phi_w) \\ U^{(2)} \sin 2(\phi_r - \phi_w) \\ V^{(2)} \sin 2(\phi_r - \phi_w) \end{pmatrix}$$

where the angle is the difference between the emission azimuth and downwind direction as shown below:




As discussed in the ATBD, the final wind-excess emissivity harmonics functions of five parameters: SST, SSS, incidence angle, 10-m neutral equivalent wind speed, and inverse wave age. This is the most general dependence considered, and in the current empirical approach only the dependence upon the neutral equivalent wind speed is retained, since we have not yet been able to determine other dependencies from the SMOS data unambiguously.

2.2.4.2. Generation Method

As discussed in some detail in the ATBD, the current version of the roughness model 2 is empirical and based upon many SMOS ascending passes over the central Pacific Ocean. We choose ascending passes to minimize errors associated with Faraday rotation and scattered galactic noise (which tend to be strongest for descending passes in September).

The ascending orbits considered are a subset of those from March 1 through the end of May 2010 for which overpass times range from 1300 UTC through 1600 UTC. Such passes are

ARGANS Ltd.

	<p style="text-align: center;">SMOS L2 OS Table Generation Requirements Document</p>	<p>Doc: SO-TN-ARG-GS-0014 Issue: 3 Rev: 18 Date: 16 March 2021 Page: 15</p>
---	--	---

located over the Pacific Ocean and provide brightness temperatures that are free from land contamination, which remains a significant problem for SMOS.

We identified all snapshots for which boresight latitude lies between 55 degS and 30 degN. We then extracted all SMOS brightness temperatures within the extended alias-free field of view for which the x-component of the director cosine coordinates is smaller than 0.1 in magnitude and for which the y-component is equal to or larger than the value at nadir. This provides a manageable subset of data for which the polarization basis rotation required to transport the instrument basis brightness temperatures into surface basis components is generally small. More importantly, this subset of data can be transported to the surface basis in dual-pol mode away from nadir.

We used GPS-derived total electron content to compute the Faraday rotation and transported all brightness temperatures into the surface polarization basis. As the period considered included dual-pol and full-pol mode data, we chose to perform the rotation on (Tx,Ty) only, assuming that the third Stokes parameter in the surface basis is identically zero.

Before performing the rotation to the surface basis, we subtracted from the full brightness temperatures (Tx,Ty) our best estimate of all contributions to brightness except for surface roughness emission. These contributions included rough surface scattered celestial sky noise evaluated using the model described in this document and evaluated at a wind speed of 3 m/s.

Assuming that the residual brightness temperatures are associated with surface roughness emission, we then binned the data by incidence angle and by surface wind speed. We used bin sizes of 5° for incidence angle and 1 m/s for wind speed and computed the median residual brightness temperatures for each bin and these median residuals are taken to be associated with roughness emission. For neutral equivalent wind speed, we used both ECMWF and NCEP winds to obtain a measure of possible uncertainty in the results. One might suppose that using buoy winds would yield better results, however in this case the aim is to obtain a roughness correction for SMOS as a function of the surface winds used in the processor and as such it is preferable to use the same wind information as is used in the retrieval of salinity.

The binned SMOS residual brightness temperatures only provide sufficient information for roughness model development up to a wind speed of about 22 m/s. Beyond this very little data exist outside of tropical cyclones. Therefore, to extend the model beyond this wind speed we extrapolate, for each incidence angle bin, the linear fit to the median residuals between 17 and 22 m/s. This extrapolation is used to provide solutions to 40 m/s.

As a final correction step to the residuals, we force the residual brightness temperatures at each incidence angle to be zero at zero wind speed. The adjustment required to achieve this

is applied uniformly to residuals at all wind speeds within each incidence angle bin, and the adjustment is performed separately for T_h and T_v .

The third Stokes parameter is currently set to zero for all wind speeds and incidence angles.

MATLAB Variable Name	Physical Quantity	Independent Variables
sss	SSS (S) [PSU]	sss
sst	SST (T_s) [K]	sst
theta_i	radiometer incidence angle (θ_i) [°]	theta_i
u_{10N}	10-m neutral equivalent wind speed [m/s]	ws10
omega	inverse wave age (Ω) [nd]	omega
dT_h_0	$T_h^{(0)}$ [K]	sss,sst,theta_i,ws10,omega
dT_v_0	$T_v^{(0)}$ [K]	sss,sst,theta_i,ws10,omega
dT_h_2	$T_h^{(2)}$ [K]	sss,sst,theta_i,ws10,omega
dT_v_2	$T_v^{(2)}$ [K]	sss,sst,theta_i,ws10,omega
dT_U_2	$U^{(2)}$ [K]	sss,sst,theta_i,ws10,omega
dT_V_2	$V^{(2)}$ [K]	sss,sst,theta_i,ws10,omega

The actual values of the dimensions in this lookup table are given in the following table:

Dimension	Number of Values	Units	Coordinate Values
SST	20	K	273, 276, 279, 282, 285, 288, 291, 294, 297, 299, 299.5, 300, 300.5, 301, 301.5, 302, 302.5, 303, 304, 306
SSS	22	PSU	0.0, 24.0, 28.0, 30.0, 32.0, 33.0, 33.5, 33.75, 34.0, 34.25, 34.5, 34.75, 35.0, 35.25, 35.5, 35.75, 36.0, 36.25, 36.5, 37.0, 38.0, 40.0
Radiometer incidence angle	28	Deg	0, 3, 6, 9, 12, 15, 18, 21, 24, 27, 30, 33, 36, 39, 42, 45, 48, 51, 54, 57, 60, 63, 66, 69, 72, 75, 78, 81
10 m Neutral equivalent wind speed	23	m s ⁻¹	0,1,2,3,4,5,6,7,8,9,10,11,12,13,14,15,16,17,18,19,20,21,40
Inverse wave age	11	Nd	0.5, 0.8, 1.0, 1.1, 1.2, 1.3, 1.5, 1.7, 1.9, 2.2, 2.5

The discretization above is based on consideration of the global probability distribution of the dimension parameters as well consideration of the trade-off between lookup table size and resolution of nonlinear variations of emissivity corrections.

In producing this discretization, we estimated the error associated with linear interpolation by computing the difference between the value of each emissivity Stokes component at a given location in the lookup table with the corresponding value obtained by linearly interpolating the emissivity values at all immediately surrounding values in the 5 dimensions. The error was then estimated as the magnitude of the difference between the interpolated values and the actual values from the lookup table. Analysis of the errors revealed that for the above discretization 85% of the lookup table values for H and V polarization zeroth harmonics have wind-excess emissivity errors less than 2×10^{-4} (or roughly 0.06 K in terms of brightness temperature for an SST of 300 K). 85% of the second azimuthal harmonics for H and V have errors less than $.5 \times 10^{-4}$. Analysis of the spatial structure of the errors revealed that errors for H and V zeroth harmonics more than 2×10^{-4} tend to occur at low and high friction velocities, generally outside the range of validity of the roughness correction model. Note that these error estimates are maximal since they are derived from a LUT with double the grid spacing along each dimension relative to the actual LUT.

If the processor requires wind excess emissivity outside the range of the lookup table, the processor shall linearly extrapolate along each dimension for which the dimension parameters are out of the LUT range.

Roughness correction with model 2 will not be applied if wind speed is below a threshold $Tg_WS_roughness_M2$ (for the moment set to 0m/s).

2.2.4.3. LUT format

The lookup table is provided as a MATLAB file which contains arrays describing each dimension and the wind-excess emissivity Stokes vector harmonics. The file contents are summarized in the following table.

MATLAB Array Name	Definition	units	Number of values	Type
sst	Sea surface temperature dimension values	K	20	double
sss	Sea surface salinity dimension values	PSU	22	double
theta_i	Radiometer incidence angle dimension values	deg	28	double

ws10	10-m neutral equivalent wind speed	m s ⁻¹	23	double
omega	Inverse wave age dimension values	nd	11	double
dT_h_0	H-pol wind-excess emissivity Tb-zeroth harmonic	K	3116960	double
dT_v_0	V-pol wind-excess emissivity Tb-zeroth harmonic	K	3116960	double
dT_h_2	H-pol wind-excess emissivity Tb-second harmonic coefficient	K	3116960	double
dT_v_2	V-pol wind-excess emissivity Tb-second harmonic coefficient	K	3116960	double
dT_U_2	Third Stokes parameter wind-excess emissivity Tb-second harmonic coefficient	K	3116960	double
dT_V_2	Fourth Stokes parameter wind-excess emissivity Tb-second harmonic coefficient	K	3116960	double

In the above table, emissivity correction arrays are dimensioned by the dimensions listed in the first five rows of the table, with the fastest varying dimension (using the FORTRAN indexing convention) being the SST and the slowest varying dimension being the inverse wave age. So, arrays are dimensioned as, for example, de_h_0(sst,sss,theta_i,ust,omega).

Given that each data value for coordinate values and emissivity consumes 4 bytes (MATLAB double precision), the total size of the lookup table is approximately 75 MB.

2.2.5. Roughness 3

2.2.5.1. Content

The roughness contribution to T_b , $T_{b_{rough}}$, is defined as shown in ATBD, § 4.4:

$$T_{b_{rough}} = \begin{bmatrix} T_h \\ T_v \end{bmatrix}$$

$T_{b_{rough}}$ is provided with a Look Up Table (LUT). Tabulations of T_h , T_v are given as functions of incidence angle and Wind speed assuming a neutral atmosphere (WS_n).

$T_{b_{rough}}$ is obtained from SMOS measurements by considered the geometric and Faraday rotation, the atmospheric and external contributions, and subtracting the T_b due to flat sea, galactic noise, and sun glint contributions.

2.2.5.2. Generation method

A pre-computed lookup table for $T_{b_{rough}}$ is provided as a function of incidence angle and neutral wind speed. The LUT is a DBL file provided by SMOS-BEC (ICM), created with a matlab program that find the neural network fitting of the SMOS $T_{b_{rough}}$ with the ECMWF geophysical parameters cited above.

The model regression analysis will be performed with auxiliary data coming from ECMWF models since such data are globally available at high temporal frequency and can therefore maximize the collocation dataset of SMOS and auxiliary information. A comprehensive analysis of the different error contributions (notably measurement and auxiliary data errors, and fitting errors) will be carried out, as well as a correlation analysis among the different parameters (notably the roughness ones), to derive the most suitable model.

To obtain the $T_{b_{rough}}$ for a given combination of geophysical parameters and incidence angle, the processor shall interpolate $T_{b_{rough}}$, using multi-linear interpolation, from a 2dimensional lookup table dimensioned as specified in the following table:

Dimension	Number of Values	Units	Coordinate Values
Radiometric Incidence angle	76	Deg	[0,1,2,3... $\Delta \theta =1$...73,74,75]
Neutral Wind speed WS_n	111	m/s	[0 ... $\Delta WS=0.25$... 20][21 ... $\Delta WS=1$...50]

The discretization above is based on consideration of the global probability distribution of the dimension parameters as well consideration of the trade-off between lookup table size and resolution of nonlinear variations of $T_{b_{rough}}$ corrections.

The linear interpolation must be done linearly in the following order: 1- interpolation in incidence angle; 2- interpolation in WS_n .

No extrapolation out of the tabulation ranges is performed: in case any parameter goes out of range, the corresponding boundary value is taken.

Roughness correction with model32 will not be applied if wind speed is below a threshold $Tg_WS_roughness_M3$ (for the moment set to 0).

Data field	Description	Unit	type	length (byte)
theta	Incidence angle	deg.	float	76*4
WSn	Neutral wind speed at 10 m	m/s	float	111*4
Th rough	TH due to roughness	K	float	76*111*36
Tv rough	TV due to roughness	K	float	76*111*36

2.2.6. Galactic Noise 1

2.2.6.1. Sky map weighted by a centrosymmetric WEF (flat sea)


2.2.6.1.1.1. Content

For a roughened sea, the effect of the WEF on galactic noise contamination is assumed to be negligible compared to scattering effects. However, for a flat sea, the WEF must be considered.

When processing the SMOS data, the radiometric contribution due to sky should in principle be computed using a variable weighting function, since this weighting function depends on the location of the target in the antenna director cosine reference frame. This is a significant complication to the processing.

An alternate option consists in assuming that the weighting function is a constant one and flagging and underweighting or deleting the data for which this assumption does not hold.

ARGANS Ltd.

	<p style="text-align: center;">SMOS L2 OS Table Generation Requirements Document</p>	<p>Doc: SO-TN-ARG-GS-0014 Issue: 3 Rev: 18 Date: 16 March 2021 Page: 21</p>
---	--	---

Keeping in mind the sensitivity of brightness temperatures to surface salinity, it is proposed that an uncertainty DTB of about 0.05 K on the sky contribution can be tolerated.

Static map, to be provided by IPSL

2.2.6.1.1.2. Generation method

Since the actual angular resolution is not infinitely narrow, the relevant sky contribution is obtained through multiplying the sky map by a weighting function.

The basic weighting function component is the interferometric SMOS directional power gain pattern. It has been shown (Waldteufel and Zine, 2005) that this pattern could be approximated by a constant centrosymmetric function $WEF(\rho_{DC})$ in the frame of director cosines (DC: ξ, η) in the antenna plane, everywhere in the field of view.

$$WEF(\rho_{DC}) = (\text{sinc}(kf \cdot \rho_{DC})^{kk} / (1 + kg \cdot \rho_{DC})^{kh})$$

$$WEF = \max(0, WEF)$$

with:

$\rho_{DC} = \sqrt{(\xi' - \xi)^2 + (\eta' - \eta)^2}$ is the distance in the DC coordinates; $= \sin(\theta_d)$ where θ_d is the angle between the line of sight and the current point.

$(\xi, \eta), (\xi', \eta')$ are the director cosines for the target on Earth surface and the current point, respectively.

$$\text{sinc}(x) = \sin(x)/x \quad (x \neq 0); \quad \text{sinc}(0)=1$$

$$kf=73.30; \quad kk=1.4936; \quad kg=524.5; \quad kh=2.1030$$

for the exact Blackmann apodisation function.

We compute maps of errors due to the centrosymmetric assumption as the maximum difference (in absolute value) between the sky map convoluted by a centrosymmetric WeF and the sky map convoluted by elongated WeFs.

We also compute another error map as:

$$\Delta I = | I_{CSWeF} - I_{ss_CSWeF} |$$

where I_{ss_CSWeF} is the sum of I and of $Tb_{\text{strong_sources}}$ (cf. §2.2.5.1.3), convoluted by the centrosymmetric WeF.

ARGANS Ltd.

Commercial in Confidence

Page 21

Use, duplication, or disclosure of this document or any information contained herein is subject to the restriction on the title page of this document.

Reprocessing is not foreseen on a regular basis, although it remains possible if better sky maps are provided in the future (for example, polarimetric data).

2.2.6.1.1.3. LUT format

Data field	Description	Unit	type	format	length (byte)
I_CSWeF	Total intensity integrated with a centrosymmetric WeF	K	float		
Q_CSWeF	Second Stokes parameter map weighted by a centrosymmetric WeF	K	float		
U_CSWeF	Third Stokes parameter map weighted by a centrosymmetric WeF	K	float		
Error_I_CSWeF	Map of errors on I due to centrosymmetric WeF assumption	K	float		
Error_Q_CSWeF	Map of errors on Q due to centrosymmetric WeF assumption	K	float		
Error_U_CSWeF	Map of errors on U due to centrosymmetric WeF assumption	K	float		
delta_I	Potential error due to strong point sources	K	float		

2.2.6.1.1.4. References

Waldteufel, P., and S. Zine; Approximating the weighting function to be used in the SMOS L2 processor. Note SO-TN-CBSA-GS-0010, 32 pp (2005).

Waldteufel, P.; Impact of the variable angular apodization function on galactic contribution. Note SO-TN-CBSA-GS-0013, 14 pp (2006).

Nicolas Floury; Generation of a sky map to be used in Lvl1 and Lvl2 processors. Note SMOS_TN_SKYMAP_ESA-EEP-1376_iss_3_rev_0, 30 pp (2013).

Xiaobin Yin & Jacqueline Boutin; New GAL_OS (weighted by WEF) generated using two different methods. Note Gal_OS_V3_final.pdf, 4pp (2013)

2.2.7. Galactic Noise 2

The following formulation has been proposed as an alternative for the galactic noise correction:

Sky Glitter Harmonics Coefficients Lookup Table Implementation Method

2.2.7.1. Mathematical formulation

To evaluate the sky glitter correction at surface level and linear polarization p , namely T_p^s , and for a given L1C data, it was shown in the ATBD that the processor has to evaluate the following function:

$$\begin{aligned}
T_p^s(\alpha_{spec}, \delta_{spec}, \theta_{spec}, \psi_{uh}, u_{10}, \phi_w) = & e^{-\tau sec \theta_{spec}} [A_p^{(0)}(\alpha_{spec}, \delta_{spec}, \theta_{spec}, \psi_{uh}, u_{10}) \\
& + A_p^{(2)}(\alpha_{spec}, \delta_{spec}, \theta_{spec}, \psi_{uh}, u_{10}) \cos(2\phi_w^r) \\
& + B_p^{(2)}(\alpha_{spec}, \delta_{spec}, \theta_{spec}, \psi_{uh}, u_{10}) \sin(2\phi_w^r)]
\end{aligned} \tag{1}$$


where:

Parameter	Description
α_{spec}	Right ascension of the specular direction with respect to the radiometer look direction [deg]
δ_{spec}	Declination of the specular direction with respect to the radiometer look direction [deg]
θ_{spec}	Specular Incidence angle at target, which is directly the radiometer incidence angle at target [deg]
ψ_{uh}	Upper Hemisphere orientation angle [deg]
u_{10}	10-meter height wind speed at target [m/s]
ϕ_w^r	Relative angle between the direction towards which the 10-meter wind is blowing and the scattering direction towards the radiometer [deg]
τ	Atmospheric attenuation coefficient evaluated at target

by interpolating pre-computed Look up tables (LUTS) for the coefficients $A_p^{(0)}$, $A_p^{(2)}$ and $B_p^{(2)}$, at the actual values for α_{spec} , δ_{spec} , θ_{spec} , ψ_{uh} , u_{10} , ϕ_w^r , τ determined for the considered L1C data.

The coefficients $A_p^{(0)}$, $A_p^{(2)}$ and $B_p^{(2)}$ are defined by:

ARGANS Ltd.

	SMOS L2 OS Table Generation Requirements Document	Doc: SO-TN-ARG-GS-0014 Issue: 3 Rev: 18 Date: 16 March 2021 Page: 24
---	--	---

$$\begin{aligned}
A_p^{(0)} &= \frac{1}{4\pi \cos \theta_s} \int_0^{\pi/2} \int_0^{2\pi} T_{sky}(\theta_o, \varphi_o, \vartheta_g, \phi_g, t) a_p^{(0)} \sin \theta_o d\varphi_o d\theta_o, \\
A_p^{(2)} &= \frac{1}{4\pi \cos \theta_s} \int_0^{\pi/2} \int_0^{2\pi} T_{sky}(\theta_o, \varphi_o, \vartheta_g, \phi_g, t) a_p^{(2)} \sin \theta_o d\varphi_o d\theta_o, \\
B_p^{(2)} &= \frac{1}{4\pi \cos \theta_s} \int_0^{\pi/2} \int_0^{2\pi} T_{sky}(\theta_o, \varphi_o, \vartheta_g, \phi_g, t) b_p^{(2)} \sin \theta_o d\varphi_o d\theta_o.
\end{aligned} \quad (2)$$

where (θ_s, φ_s) is the scattering direction from the target (defined by its geodetic latitude ϑ_g and geodetic longitude ϕ_g) towards the radiometer, $\vec{n}_o = (\theta_o, \phi_o)$ are the upper hemisphere downwelling sky radiation direction at target, t is the time of observation and T_{sky} is the unpolarized sky brightness temperature in the upper hemisphere. The coefficients $a_p^{(0)}$, $a_p^{(2)}$ and $b_p^{(2)}$ in (2) are the so-called combined scattering cross section coefficients defined by

$$\begin{aligned}
a_p^{(0)}(\theta_o, \varphi_s - \varphi_o, \theta_s, u_{10}) &= a_{pp}^{(0)}(\theta_o, \varphi_s - \varphi_o, \theta_s, u_{10}) + a_{pq}^{(0)}(\theta_o, \varphi_s - \varphi_o, \theta_s, u_{10}), \\
a_p^{(2)}(\theta_o, \varphi_s, \varphi_o, \theta_s, u_{10}) &= a_{pp}^{(2)}(\theta_o, \varphi_s, \varphi_o, \theta_s, u_{10}) + a_{pq}^{(2)}(\theta_o, \varphi_s, \varphi_o, \theta_s, u_{10}), \\
b_p^{(2)}(\theta_o, \varphi_s, \varphi_o, \theta_s, u_{10}) &= b_{pp}^{(2)}(\theta_o, \varphi_s, \varphi_o, \theta_s, u_{10}) + b_{pq}^{(2)}(\theta_o, \varphi_s, \varphi_o, \theta_s, u_{10}),
\end{aligned} \quad (3)$$

in which:

$$\begin{aligned}
a_{\alpha\alpha_o}^{(0)}(\theta_o, \varphi_s - \varphi_o, \theta_s, u_{10}) &= \sigma_{\alpha\alpha_o}^0(\theta_o, \varphi_s - \varphi_o, \theta_s, u_{10}), \\
a_{\alpha\alpha_o}^{(2)}(\theta_o, \varphi_s, \varphi_o, \theta_s, u_{10}) &= \sigma_{\alpha\alpha_o}^2(\theta_o, \varphi_s - \varphi_o, \theta_s, u_{10}) \cos(2\Phi_{si}^0), \\
b_{\alpha\alpha_o}^{(2)}(\theta_o, \varphi_s, \varphi_o, \theta_s, u_{10}) &= \sigma_{\alpha\alpha_o}^2(\theta_o, \varphi_s - \varphi_o, \theta_s, u_{10}) \sin(2\Phi_{si}^0)
\end{aligned} \quad (4)$$

where $\Phi_{si}^0(\theta_o, \varphi_o - \varphi_s, \theta_s) = \Phi_{si}(\theta_o, \varphi_o - \varphi_s, 0^\circ, \theta_s)$ and where Φ_{si} is the angle of the difference between the horizontal projections of the scattered and incident wavevectors, defined by:

$$\Phi_{si}(\theta_o, \phi_o, \phi_s, \theta_s) = \tan^{-1}\left(\frac{q_{Hy}}{q_{Hx}}\right) = \tan^{-1}\left(\frac{\sin \theta_o \sin \phi_o + \sin \theta_s \sin \phi_s}{\sin \theta_o \cos \phi_o + \sin \theta_s \cos \phi_s}\right) \quad (5)$$

and where the $\sigma_{\alpha\alpha_o}^0$ coefficients are the dimensionless bistatic scattering cross section for scattering of the incoming wave of polarization α_o into the outgoing wave of polarization α . As noted in the ATBD doc, the above representation (2) of the scattered signal harmonics is not convenient for interpolation, however, since much of the variation in scattered signal is expected to be related to changes in the specular location in the celestial sphere, and this specular location can change dramatically with changing radiometer incidence and azimuth angles. However, we can use transformations involving ψ_{uh} , Φ_{si}^0 , and ϕ_w^r , and express the harmonic coefficients in terms of the specular location in the celestial sphere along with the orientation angle ψ_{uh} , so that we obtain the representation given in (1).

$$\begin{aligned}
 T_p^S(\alpha_{spec}, \delta_{spec}, \theta_{spec}, \psi_{uh}, u_{10}, \phi_w) = & e^{-\tau \sec \theta_{spec}} [A_p^{(0)}(\alpha_{spec}, \delta_{spec}, \theta_{spec}, \psi_{uh}, u_{10}) \\
 & + A_p^{(2)}(\alpha_{spec}, \delta_{spec}, \theta_{spec}, \psi_{uh}, u_{10}) \cos(2\phi_w^r) \\
 & + B_p^{(2)}(\alpha_{spec}, \delta_{spec}, \theta_{spec}, \psi_{uh}, u_{10}) \sin(2\phi_w^r)]
 \end{aligned} \tag{6}$$

where

$$\psi_{uh} = \tan^{-1} \left(\frac{\hat{h}^c \cdot \tilde{y}^u}{\hat{h}^c \cdot \hat{h}^u} \right) \tag{7}$$

with

$$\begin{aligned}
 \tilde{h}^u &= T_{ac} \hat{h}^u, \\
 \tilde{v}^u &= T_{ac} \hat{v}^u,
 \end{aligned} \tag{8}$$


and with upper hemisphere basis vectors in the topocentric frame defined as

$$\begin{aligned}
 \hat{h}^u &= -\sin \phi_{pec} \hat{x}^u + \cos \phi_{pec} \hat{y}^u, \\
 \hat{v}^u &= -\cos \phi_{pec} \sin \theta_{spec} \hat{x}^u - \sin \phi_{pec} \sin \theta_{spec} \hat{y}^u + \sin \theta_{spec} \hat{z}^u,
 \end{aligned} \tag{9}$$

where \hat{x}^u , \hat{y}^u , and \hat{z}^u are basis vectors for the topocentric Earth frame that determines the upper hemisphere. Analogous basis vectors can be defined in the celestial frame as

$$\begin{aligned}
 \hat{h}^c &= -\sin \alpha_{spec} \hat{x}^c + \cos \alpha_{spec} \hat{y}^c, \\
 \hat{v}^c &= -\cos \alpha_{spec} \sin \delta_{spec} \hat{x}^c - \sin \alpha_{spec} \sin \delta_{spec} \hat{y}^c + \sin \delta_{spec} \hat{z}^c,
 \end{aligned} \tag{10}$$

To pre-compute LUTs for $A_p^{(0)}$, $A_p^{(2)}$ and $B_p^{(2)}$, we select a target location on Earth, fix the azimuth angle of the vector pointing from the target to the radiometer, ϕ_s , and vary the radiometer incidence angle θ_s , wind speed u_{10} , and orientation angle ψ_{uh} over some representative range of values. For each set of values for these parameters, we scan the full range of specular right ascension and declination and compute the coefficients $A_p^{(0)}$, $A_p^{(2)}$ and $B_p^{(2)}$. In the pre-launch version of the processor the Kirchhoff model for rough surface scattering was used to derive the coefficients. In the present version of the processor, however, a geometrical optics model is employed, and in this model only the zero-order harmonics are nonzero so that there is no impact from wind direction.

	<p style="text-align: center;">SMOS L2 OS Table Generation Requirements Document</p>	<p>Doc: SO-TN-ARG-GS-0014 Issue: 3 Rev: 18 Date: 16 March 2021 Page: 26</p>
---	--	---

2.2.7.2. Numerical Integration of Scattered Galactic Radiation

2.2.7.2.1.1. Use of a reduced spatial resolution sky map

The natural way for formulate the numerical method would be to generate a discrete grid over the upper hemisphere $U_{ij}(\theta_i, \varphi_j)$, to interpolate the bistatic scattering coefficients and the galactic radiation and to then integrate the product of the scattering coefficients and the radiation over this grid by some numerical quadrature technique.

This approach has the disadvantage that one must interpolate both the scattering coefficients and the galactic noise onto U_{jk} . An alternative approach is to perform the numerical integration on the discrete grid on which the galactic noise data are provided. In this method, we simply interpolate the bistatic coefficients onto the discrete galactic map and integrate the product of these coefficients with the galactic radiation over the map.

Letting δ denote declination and α right ascension, the original discrete galactic map provides data on a grid $G_{ij}(\delta_0 + i(\Delta\delta), \alpha_0 + j(\Delta\alpha))$ such that the discrete brightness temperature field for a given polarization has the form

$$T_{ij} = T(\delta_0 + i(\Delta\delta), \alpha_0 + j(\Delta\alpha)), \quad (11)$$

where T is the continuous brightness temperature field, and i and j are positive integers such that,

$$\begin{aligned} 0 \leq i \leq N_\delta - 1, \\ 0 \leq j \leq N_\alpha - 1, \end{aligned} \quad (12)$$

and where $\Delta\delta = 0.25^\circ$ and $\Delta\alpha = 0.25^\circ$ are the grid spacings of the original fine resolution sky map. It turns out, however, that using the full resolution map leads to rather slow scattering calculations, taking approximately six seconds to compute one pair of scattered galactic brightness temperatures on a 1.5 GHz PC.

To avoid this problem, we perform the integration on a reduced resolution galactic map produced by applying an energy-conserving averaging operator $R(\cdot)$ to the original galactic map to produce a galactic noise map on a lower-resolution grid $\tilde{G}_{nm}(n(\Delta\delta), m(\Delta\alpha))$:

$$R: T(G_{ij}) \rightarrow \tilde{T}(\tilde{G}_{nm}). \quad (13)$$

On the coarse grid, the grid spacings in declination and right ascension are, respectively, $\overline{(\Delta\delta)} = (2N + 1)(\Delta\delta)$ and $\overline{(\Delta\alpha)} = (2N + 1)(\Delta\alpha)$. Here, N is a positive integer rescaling factor, which ranges from one through seven for our tests (seven is equivalent to a 15-fold increase in the grid spacing in declination and right ascension). The discrete indices of the

coarse grid have the ranges

$$\begin{aligned} 0 \leq n &\leq \frac{(N_\delta - 1)}{(2N + 1)}, \\ 0 \leq m &\leq \frac{(N_\alpha - 1)}{(2N + 1)}, \end{aligned} \quad (14)$$

and the averaging operator R takes the form

$$\tilde{T}_{nm} = \frac{1}{N} \sum_{i=i_0}^{i_1} \sum_{j=j_0}^{j_1} \sin(\delta_0 + i(\Delta\delta)) T_{ij}, \quad (15)$$

where \tilde{T}_{nm} is the discrete fine grid brightness temperature field, T_{ij} is the coarse grid field,

$$\begin{aligned} i_0 &= (2N + 1)n - N, \\ i_1 &= (2N + 1)n + N, \\ j_0 &= (2N + 1)m - N, \\ j_1 &= (2N + 1)m + N, \end{aligned} \quad (16)$$

and


$$N = \sum_{i=i_0}^{i_1} \sum_{j=j_0}^{j_1} \sin(\delta_0 + i(\Delta\delta)) \quad (17)$$

is a normalization factor for the averaging operator. The first cell in the reduced grid (in both latitude and longitude) is always aligned with the first cell in each dimension in the original grid, and the galactic noise values assigned to each of the reduced resolution grid cells is the weighted average of the noise in all original grid cells contained within the encompassing coarse grid cell. In the averaging procedure, the weight given to a particular fine grid cell is proportional to the solid angle subtended by that cell.

Once this reduced resolution galactic map has been generated, the computation of the scattered galactic signal at the Earth's surface is accomplished by summing the pointwise product of the discrete brightness temperature fields T_{mn} (in general one field for each of the H and V polarizations in the case of polarized maps) and the scattering cross sections interpolated from a lookup table (generated once for all possible wind conditions and scattering geometries) onto the same reduced resolution grid \tilde{G}_{nm} as detailed in the text.

2.2.7.2.1.2. Numerical Integration of Scattered Galactic Radiation

The integration over the upper hemisphere is thus performed in the celestial frame, on a discrete grid $\tilde{G}_{nm}(n(\Delta\delta), m(\Delta\alpha))$ that is a reduced resolution version of the grid on which the

	SMOS L2 OS Table Generation Requirements Document	Doc: SO-TN-ARG-GS-0014 Issue: 3 Rev: 18 Date: 16 March 2021 Page: 28
---	--	---

galactic map is originally provided, G_{ij} . Consider the computation of the scattered signal for one radiometer configuration, one set of geophysical conditions, and at some time t . Then t , θ_s and φ_s , α_{spec} , δ_{spec} , u_{10} , ϕ_w , and ψ_{uh} are fixed, and the problem is to integrate over all incoming directions θ_o and φ_o as discretized and projected into \tilde{G}_{nm} .

As a first step, the bistatic coefficient zeroth and second harmonics (including co-pol and cross-pol terms) are interpolated from a scattering coefficient lookup table onto the grid \tilde{G}_{nm} using a Hermite cubic interpolation operator H detailed in Appendix D of the ATBD. H takes as arguments a discrete function, the grid on which it is defined, and some new grid, and interpolates the function onto the new grid:

$$H = H(f(\tilde{G}_l), \tilde{G}_l, \tilde{G}_{nm}). \quad (18)$$

If we now let $\bar{\sigma}_p^0(\bar{G}_l)$ and $\bar{\sigma}_p^2(\bar{G}_l)$ denote the discretely defined scattering cross section harmonics on the upper hemisphere evaluated at a radiometer azimuth $\varphi_s = 0^\circ$, then we can compute the corresponding discrete cross sections on the celestial grid \tilde{G}_{nm} by applying H to obtain


$$\begin{aligned} \tilde{a}_p^{(0)}(\tilde{G}_{nm}) &= \frac{1}{4\pi \cos \theta_s} H(\bar{\sigma}_p^0(\bar{G}_l), \tilde{G}_l, \tilde{G}_{nm}), \\ \tilde{a}_p^{(2)}(\tilde{G}_{nm}) &= \frac{1}{4\pi \cos \theta_s} H(\bar{\sigma}_p^2(\bar{G}_l), \tilde{G}_l, \tilde{G}_{nm}) \cos(2\Phi_{si}^0), \\ \tilde{b}_p^{(2)}(\tilde{G}_{nm}) &= \frac{1}{4\pi \cos \theta_s} H(\bar{\sigma}_p^2(\bar{G}_l), \tilde{G}_l, \tilde{G}_{nm}) \sin(2\Phi_{si}^0), \end{aligned} \quad (19)$$

where we have pre-multiplied the coefficients by the factor in front of the scattered signal upper hemisphere integrals, except for the atmospheric attenuation factor that will depend on the target location.

In creating these discrete fields, we first perform the above calculations (19) for what we call reference conditions. We thus fix reference values for the target latitude and longitude of $(\vartheta_g^{ref}, \phi_g^{ref}) = (0^\circ, 0^\circ)$, the chosen reference radiometer azimuth angle $\varphi_s^{ref} = 0^\circ$ and date of acquisition t_{ref} , which, together with given radiometer incidence $\theta_{spec} = \theta_s$ angles, determine the reference specular right ascension and declination $(\alpha_{spec}^{ref}, \delta_{spec}^{ref})$ as well as the reference orientation angle ψ_{uh}^{ref} . (19) are then evaluated for ranges of $\theta_{spec} = \theta_s$ and surface wind speed values.

Then a complication arises, since we want to generate the LUTS at reference target and date for a range of desired specular location in the celestial sphere $(\alpha_{spec}^d, \delta_{spec}^d)$, with associated orientation angles ψ_{uh}^d . To solve this problem, we rotate the vectors associated with each gridpoint in \tilde{G}_{nm} so that the desired specular location is rotated into the reference specular location. This generates a new grid, say \tilde{G}'_{nm} , whose specular point is the reference specular

ARGANS Ltd.

	SMOS L2 OS Table Generation Requirements Document	Doc: SO-TN-ARG-GS-0014 Issue: 3 Rev: 18 Date: 16 March 2021 Page: 29
---	--	---

point for the scattering calculation. To accomplish this rotation, we begin by defining rotation operators in the celestial frame for rotations about each of the cartesian basis vectors, with \tilde{R}_y being a counterclockwise rotation of a vector about \hat{y}^c and \tilde{R}_z being a counterclockwise rotation of a vector about \hat{z}^c :

$$\tilde{R}_y(\varphi) = \begin{pmatrix} \cos\varphi & 0 & \sin\varphi \\ 0 & 1 & 0 \\ -\sin\varphi & 0 & \cos\varphi \end{pmatrix}; \tilde{R}_z(\varphi) = \begin{pmatrix} \cos\varphi & -\sin\varphi & 0 \\ \sin\varphi & \cos\varphi & 0 \\ 0 & 0 & 1 \end{pmatrix} \quad (20)$$

Now let the reference specular direction unit vector have cartesian components $(x_{ref}, y_{ref}, z_{ref})$ and let the desired specular direction unit vector have cartesian components (x_d, y_d, z_d) . With these definitions, the rotation from the desired to the reference specular point is

$$\begin{pmatrix} x_{ref} \\ y_{ref} \\ z_{ref} \end{pmatrix} = \tilde{R}_z(\alpha_{spec}^{ref}) \tilde{R}_y(\delta_{spec}^d - \delta_{spec}^{ref}) \tilde{R}_z(-\alpha_{spec}^d) \begin{pmatrix} x_d \\ y_d \\ z_d \end{pmatrix} \quad (21)$$

Similarly, the transformation of a vector \vec{V}_d to \vec{V}_{ref} under a rotation from the desired specular point to the reference specular point can be written as

$$\vec{V}_{ref} = \tilde{R}_z(\alpha_{spec}^{ref}) \tilde{R}_y(\delta_{spec}^d - \delta_{spec}^{ref}) \tilde{R}_z(-\alpha_{spec}^d) \vec{V}_d \quad (22)$$

This rotation is applied to every grid point in \tilde{G}_{nm} to generate \tilde{G}'_{nm} .


Then, we need to determine the orientation angle ψ_r of the upper hemisphere at the reference specular point relative to the rotated celestial grid \tilde{G}'_{nm} .

To do so, the line-of-sight alt-azimuth basis vectors in the Celestial frame are first computed at the desired specular point:

$$\begin{aligned} \hat{h}_c^d &= -\sin\alpha_{spec}^d \hat{x}^c + \cos\alpha_{spec}^d \hat{y}^c, \\ \hat{v}_c^d &= -\cos\alpha_{spec}^d \sin\delta_{spec}^d \hat{x}^c - \sin\alpha_{spec}^d \sin\delta_{spec}^d \hat{y}^d + \sin\delta_{spec}^d \hat{z}^c, \end{aligned} \quad (23)$$

These vectors are then transformed to the reference specular location by the above rotation that was applied to the galactic noise grid:

$$(24)$$

	SMOS L2 OS Table Generation Requirements Document	Doc: SO-TN-ARG-GS-0014 Issue: 3 Rev: 18 Date: 16 March 2021 Page: 30
---	--	---

$$\hat{v}_c^{ref} = \tilde{R}_z(\alpha_{spec}^{ref}) \tilde{R}_y(\delta_{spec}^d - \delta_{spec}^{ref}) \tilde{R}_z(-\alpha_{spec}^d) \hat{v}_c^d$$

Next, we compute the upper hemisphere alt-azimuth basis vectors at the reference specular point. Expressed in the upper hemisphere frame, these unit vectors are

$$\begin{aligned} \hat{h}^u &= -\sin \varphi_s^{ref} \hat{x}^u + \cos \varphi_s^{ref} \hat{y}^u, \\ \hat{v}^u &= -\cos \varphi_s^{ref} \sin \theta_s^{ref} \hat{x}^u - \sin \varphi_s^{ref} \sin \theta_s^{ref} \hat{y}^u + \sin \theta_s^{ref} \hat{z}^u, \end{aligned} \quad (25)$$

These basis vectors are then transformed to the celestial frame,

$$\begin{aligned} \tilde{h}^u &= T_{ac} \hat{h}^u, \\ \tilde{v}^u &= T_{ac} \hat{v}^u. \end{aligned} \quad (26)$$

where the transformation matrix T_{ac} is defined in Appendix B of the ATBD and is given by

$$T_{ac}(\vartheta_g^{ref}, \phi_g^{ref}, t_{ref}) = T_{ec}(H_{ref}) T_{ae}(\vartheta_g^{ref}, \phi_g^{ref}),$$

where T_{ec} and T_{ae} are transformations matrices from the Earth fixed frame to the Celestial frame and from the alt-azimuth frame to the Earth fixed frame, respectively. Both transformations are also completely defined as well in Appendix B of the ATBD . H_{ref} is the Earth rotation angle at reference conditions, which in turns is the sum of G_{ref} , the Greenwich sidereal angle at reference time t_{ref} and a nutation angle μ_{ref} . These transformation can be easily evaluated using Earth Explorer CFI.


Armed with these two sets of basis vectors at the reference specular point in the celestial frame, we compute the orientation angle ψ_r of the upper hemisphere at the reference specular point relative to the rotated celestial grid \tilde{G}_{nm}^{ref} ,

$$\psi_r = \tan^{-1} \left(\frac{\hat{h}_c^{ref} \cdot \tilde{v}^u}{\hat{h}_c^{ref} \cdot \tilde{h}^u} \right) \quad (27)$$

As defined, the angle ψ_r is the orientation of the upper hemisphere at the desired specular location in the celestial sphere after it has been rotated to bring the desired specular point to the reference specular point.

The next step is to rotate the grid \tilde{G}_{nm}' about the reference specular line of sight, so that the orientation angle ψ_r between the rotated upper hemisphere and the celestial sphere along the line of sight is the desired angle ψ_{uh}^d . This is accomplished with the following series of five rotations of the line-of-sight vector pointing towards the reference specular direction in the celestial frame:

ARGANS Ltd.

	SMOS L2 OS Table Generation Requirements Document	Doc: SO-TN-ARG-GS-0014 Issue: 3 Rev: 18 Date: 16 March 2021 Page: 31
---	--	---

- Rotate about the z-axis by $-\alpha_{spec}^{ref}$ to zero azimuth.
- Rotate about the y-axis by $\delta_{spec}^{ref} - \frac{\pi}{2}$ to the north pole.
- Rotate about the z-axis counterclockwise by the difference between the desired angle $-\psi_{uh}^d$ and the actual orientation angle after rotating the galactic noise grid into the actual specular direction, ψ_r . This is equivalent to a rotation by angle $-\psi_{uh}^d + \psi_r$.
- Rotate about the y-axis by $-\delta_{spec}^{ref} + \frac{\pi}{2}$ back to original altitude.
- Rotate about the z-axis by α_{spec}^{ref} back to the original azimuth.

Applying this series of rotations to every grid point in \tilde{G}'_{nm} , we generate a new rotated grid, say \tilde{G}''_{nm} . Given a vector \vec{V} in \tilde{G}'_{nm} , the rotated vector \vec{V}' in \tilde{G}''_{nm} is

$$\vec{V}' = \tilde{R}_z(\alpha_{spec}^{ref})\tilde{R}_y\left(\frac{\pi}{2} - \delta_{spec}^{ref}\right)\tilde{R}_z(-\psi_{uh}^d + \psi_r)\tilde{R}_y\left(\delta_{spec}^{ref} - \frac{\pi}{2}\right)\tilde{R}_z(-\alpha_{spec}^{ref})\vec{V} \quad (28)$$

where it is important to note that we have rotated the grid \tilde{G}'_{nm} by $-\psi_{uh}^d + \psi_r$ about the line-of-sight to produce \tilde{G}''_{nm} , so that the lookup table is expressed in terms of $-\psi_{uh}^d$ rather than ψ_{uh}^d .

Now we define two bilinear interpolation operators, B_1 and B_2 , which take as arguments a discrete function f , the original grid on which the function is defined, and some other grid, which in this case is the rotated grid \tilde{G}''_{nm} , so we have


$$\begin{aligned} B_1 &= B_1(f(\tilde{G}_{nm}), \tilde{G}_{nm}, \tilde{G}''_{nm}(\tilde{G}_{nm})), \\ B_2 &= B_2(f(\tilde{G}_{nm}), \tilde{G}_{nm}, \tilde{G}''_{nm}(\tilde{G}_{nm})), \end{aligned} \quad (29)$$

where the rotated grid is computed as just described. B_2 differs from B_1 in that it applies an additional rescaling after interpolation to preserve the discrete integral of the function f over the celestial sphere. Introducing the discrete celestial sphere integral operator

$$I(f, G) = \sum_{n,m} f_{nm}(G) \sin(\delta_{nm}(G)) \Delta\alpha_{nm} \Delta\delta_{nm} \quad (30)$$

we have that

$$B_2 = B_1 \left[\frac{I(f, \tilde{G}_{nm})}{I(B_1(f, \tilde{G}_{nm}, \tilde{G}''_{nm}), \tilde{G}_{nm})} \right] \quad (31)$$

	SMOS L2 OS Table Generation Requirements Document	Doc: SO-TN-ARG-GS-0014 Issue: 3 Rev: 18 Date: 16 March 2021 Page: 32
---	--	---

where the product operator (\cdot) is an element-by-element product. Applying these bilinear interpolation operators B_1 and B_2 to the rotated bistatic scattering cross section harmonic we obtain the following rotated harmonics

$$\begin{aligned}
\tilde{a}''^{(0)}(\tilde{G}_{nm}) &= B_2(\tilde{a}_p^{(0)}, \tilde{G}_{nm}, \tilde{G}''_{nm}(\tilde{G}_{nm})), \\
\tilde{a}''^{(2)}(\tilde{G}_{nm}) &= B_1(\tilde{a}_p^{(2)}, \tilde{G}_{nm}, \tilde{G}''_{nm}(\tilde{G}_{nm})), \\
\tilde{b}''^{(2)}(\tilde{G}_{nm}) &= B_1(\tilde{b}_p^{(2)}, \tilde{G}_{nm}, \tilde{G}''_{nm}(\tilde{G}_{nm})),
\end{aligned} \tag{32}$$

which are also defined on \tilde{G}_{nm} . Note that we only apply the integral preserving operator to the zeroth harmonic.

At this point, we have both the scattering cross sections and the galactic noise brightness temperatures $T(\tilde{G}_{nm})$ on the same uniform grid \tilde{G}_{nm} in the celestial sphere. We can now apply the integral operator to determine numerical approximations to the scattered signal harmonics directly on this same grid:

$$\begin{aligned}
\tilde{A}_p^{(0)}(\alpha_{spec}, \delta_{spec}, \theta_{spec}, \psi_{uh}, u_{10}) &= I(\tilde{a}''^{(0)}(\tilde{G}_{nm}) \cdot T(\tilde{G}_{nm}), \tilde{G}_{nm}), \\
\tilde{A}_p^{(2)}(\alpha_{spec}, \delta_{spec}, \theta_{spec}, \psi_{uh}, u_{10}) &= I(\tilde{a}''^{(2)}(\tilde{G}_{nm}) \cdot T(\tilde{G}_{nm}), \tilde{G}_{nm}), \\
\tilde{B}_p^{(2)}(\alpha_{spec}, \delta_{spec}, \theta_{spec}, \psi_{uh}, u_{10}) &= I(\tilde{b}''^{(2)}(\tilde{G}_{nm}) \cdot T(\tilde{G}_{nm}), \tilde{G}_{nm}).
\end{aligned} \tag{33}$$


where we use the \sim symbols to denote the numerical approximations of the actual harmonic coefficients from the model, and where the desired specular location in the celestial sphere $(\alpha_{spec}^d, \delta_{spec}^d)$, with associated orientation angles ψ_{uh}^d are now denoted $(\alpha_{spec}, \delta_{spec})$, and ψ_{uh} , respectively.

At this point it is worth reviewing what we have done. We rotated the celestial grid on which the galactic noise is defined such that the desired specular point is rotated into reference conditions defined by a specular point for a given time, target latitude, target longitude, radiometer incidence and azimuth angles. We then computed the orientation angle ψ_r of the upper hemisphere at the desired specular location, and we then rotated the galactic noise grid further by $-\psi_{uh}^d + \psi_r$ to bring the grid to the desired orientation angle ψ_{uh}^d . We then interpolated the scattering cross section harmonics onto this grid and then integrated products of these with the galactic noise to produce numerical approximations to the scattered signal harmonic coefficients.

2.2.7.3. Look up Tables Implementation

As described above, the scattered galactic noise signal can be expressed as a set of five-dimensional functions that provide zeroth and second harmonics as a function of wind direction. These functions are

ARGANS Ltd.

	SMOS L2 OS Table Generation Requirements Document	Doc: SO-TN-ARG-GS-0014 Issue: 3 Rev: 18 Date: 16 March 2021 Page: 33
---	--	---

$$\begin{aligned}
\tilde{A}_p^{(0)}(\alpha_{spec}, \delta_{spec}, \theta_{spec}, \psi_{uh}, u_{10}) &= I(\tilde{a}''^{(0)}(\tilde{G}_{nm}) \cdot T(\tilde{G}_{nm}), \tilde{G}_{nm}), \\
\tilde{A}_p^{(2)}(\alpha_{spec}, \delta_{spec}, \theta_{spec}, \psi_{uh}, u_{10}) &= I(\tilde{a}''^{(2)}(\tilde{G}_{nm}) \cdot T(\tilde{G}_{nm}), \tilde{G}_{nm}), \\
\tilde{B}_p^{(2)}(\alpha_{spec}, \delta_{spec}, \theta_{spec}, \psi_{uh}, u_{10}) &= I(\tilde{b}''^{(2)}(\tilde{G}_{nm}) \cdot T(\tilde{G}_{nm}), \tilde{G}_{nm}).
\end{aligned} \tag{34}$$

where the p subscript emphasizes the fact that there is one set of three five dimensional functions for each polarization p . To construct the lookup tables, we discretized all five dimensions $(\alpha_{spec}, \delta_{spec}, \theta_{spec}, \psi_{uh}, u_{10})$ of the coefficients. By analysing the dependence on each dimension, and weighing the accuracy constraint with constraints imposed by computational resources, we have determined that a reasonable discretization is the following:

$$\begin{aligned}
\{u_{10}\} &= \{3,5,7,10,15,25\} \quad m/s, \\
\{\theta_{spec}\} &= \{0^\circ, 10^\circ, 20^\circ, 25^\circ, 30^\circ, 35^\circ, 40^\circ, 45^\circ, 50^\circ, 55^\circ, 60^\circ, 70^\circ, 80^\circ\}.
\end{aligned}$$

The grid for ψ_{uh} is regular and defined (in degrees, mathematical convention) by the set

$$\{-\psi_{uh}\} = \{22.5n\},$$

where n is a integer ranging from 0 through 16. The grid for the specular right ascension α_{spec} is regular and defined (also in degrees) by the set

$$\{\alpha_{spec}\} = \{3.75n\},$$

where n is a integer ranging from 0 through 96. Finally, the grid for the specular declination δ_{spec} is regular and defined (in degrees) by the set

$$\{\delta_{spec}\} = \{3.75n\},$$

where n is an integer ranging from 0 through 96. It should be noted that the lookup table is defined in B1950 celestial coordinates, not the J2000 coordinate system. The lookup tables are stored in a MATLAB Version 7 file. The following table lists the correspondence between variable names and quantities described above.

Table 1: Mapping Between MATLAB Variable Names and Physical Quantities in the Lookup Tables

ARGANS Ltd.

Commercial in Confidence

Page 33

Use, duplication, or disclosure of this document or any information contained herein is subject to the restriction on the title page of this document.

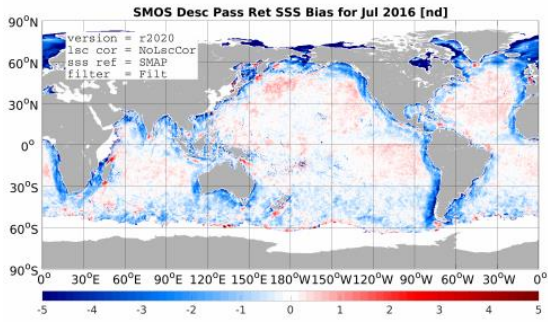
MATLAB Variable Name	Physical Quantity	Independent Variables
dec_b1950	B1950 declination δ_{spec} [deg]	δ_{spec}
ra_b1950	B1950 right ascension α_{spec} [deg]	α_{spec}
ws	10-m wind speed [m s ⁻¹]	u_{10}
eia	radiometer incidence angle [deg]	θ_{spec}
psi	Upper Hemisphere orientation angle $-\psi_{uh}$ [deg]	ψ_{uh}
th_symm	$\tilde{A}_h^{(0)}$: symmetric H-pol component [K]	$(\delta_{spec}, \alpha_{spec}, u_{10}, \theta_{spec}, \psi_{uh})$
tv_symm	$\tilde{A}_v^{(0)}$: symmetric V-pol component [K]	$(\delta_{spec}, \alpha_{spec}, u_{10}, \theta_{spec}, \psi_{uh})$
th_hc	$\tilde{A}_h^{(2)}$: $\cos(2\phi_w^r)$ harmonic amplitude H-pol [K]	$(\delta_{spec}, \alpha_{spec}, u_{10}, \theta_{spec}, \psi_{uh})$
th_vc	$\tilde{A}_v^{(2)}$: $\cos(2\phi_w^r)$ harmonic amplitude V-pol [K]	$(\delta_{spec}, \alpha_{spec}, u_{10}, \theta_{spec}, \psi_{uh})$
th_hs	$\tilde{B}_h^{(2)}$: $\sin(2\phi_w^r)$ harmonic amplitude H-pol [K]	$(\delta_{spec}, \alpha_{spec}, u_{10}, \theta_{spec}, \psi_{uh})$
th_vs	$\tilde{B}_v^{(2)}$: $\sin(2\phi_w^r)$ harmonic amplitude V-pol [K]	$(\delta_{spec}, \alpha_{spec}, u_{10}, \theta_{spec}, \psi_{uh})$

As noted above, prior to launch, lookup tables were derived for both the Kirchhoff and the SSA-1 scattering asymptotic models, since it was not known at the time which model might perform best. Within the first year after launch, however, it was realized that both the Kirchhoff and SSA-1 electromagnetic scattering models, together with the Kudryavtsev wave spectrum (see the ATBD for details), produce solutions that differ significantly from the scattered brightness inferred from the MIRAS brightness temperatures. Therefore, as discussed in the ATBD, a geometric optics model has been used to generate the lookup tables in the present version of the processor. This model is based upon an isotropic gaussian surface slope probability distribution function and has one free parameter, the slope variance, which is an empirically determined function of the ECMWF operational model 10-m wind speed. As described in the ATBD, the empirical relationship between slope variance and 10-m wind speed is significantly different for ascending and descending passes, and so the processor employs different lookup tables for ascending and descending passes.

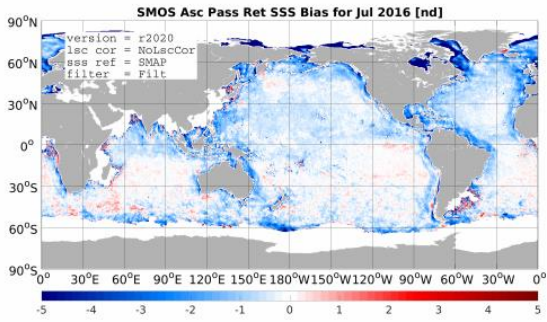
2.2.8. Land (Mixed Scene) Contamination

2.2.8.1. Brief introduction to land-sea contamination biases

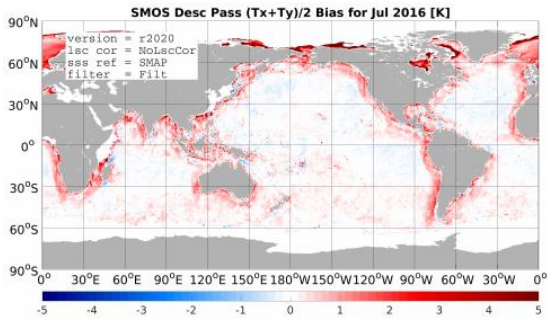
As discussed in detail in the ATBD, land-sea contamination is strong in MIRAS images over the ocean within several hundred kilometers from large land masses. Figure 3 shows an example of this bias for in both retrieved salinity (top panels) and first Stokes parameter (bottom panels) for both ascending and descending passes. Here the bias has been evaluated for July 2016 with respect to the 8-day running mean salinity from SMAP, as produced and distributed by Remote Sensing Systems [1]. Use of SMAP SSS as the reference avoids some biases present in WOA and ISAS SSS near river outflows, where little in-situ data are available. Note that the patterns of bias are qualitatively different for the two pass directions.



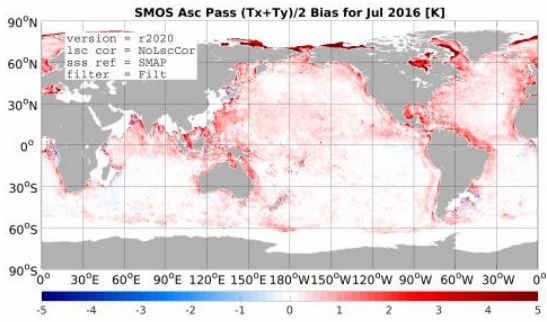
(a) SSS (desc)



(b) SSS (asc)



(c) T_p (desc)



(d) T_p (asc)

Figure 3: (a) and (b): Example dwell-line averaged bias between SMOS and SMAP (8-day running mean) retrieved SSS for July 2016 for descending and ascending passes, respectively. (c) and (d): Corresponding bias in first Stokes parameter divided by two T_p (K).

2.2.8.2. Brief Overview of the empirical land-sea contamination bias correction calculation

The land-sea contamination bias in polarization p may be expressed as

$$\Delta T_p^{(lsc)}(\xi, \eta, t) = \left[T_p^{(miras)}(\xi, \eta, t) - \Delta T_p^{OTT}(\xi, \eta) \right] - T_{tp}^{(full)}(\xi, \eta, t). \quad (1)$$

The preceding expression yields the land-sea contamination (LSC) for each scene. To obtain accurate estimates of the LSC, these biases must be averaged over many realizations with the same distribution of land in the front half-space (since LSC is scene-dependent). To accommodate this averaging, the LSC is expressed in the form of a four-dimensional array for each polarization p and each pass direction d:

$$\Delta \bar{T}_{pd}^{(lsc)} = \Delta \bar{T}_{pd}^{(lsc)}(\vartheta_g, \varphi_g, \xi, \eta) \quad (2)$$

where ϑ_g and φ_g are geodetic latitude and longitude, respectively. The discretization of these arrays is shown in Figure 4. The grid spacing in latitude and longitude is 0.5° and 0.025 director cosine units for ξ and η . This choice is a tradeoff between the ability to resolve variations in the LSC and the ability to perform the averaging with available computer resources.

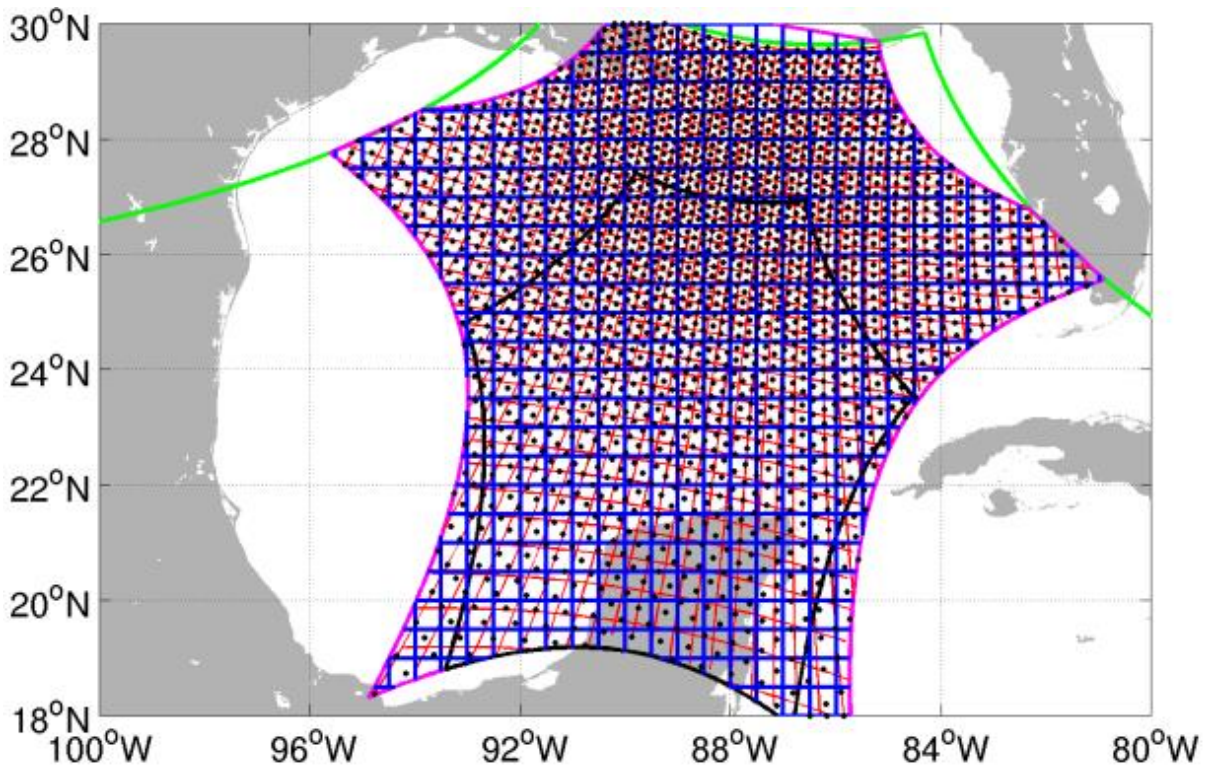


Figure 4: Example projection for the four-dimensional land-sea contamination lookup table (LSC LUT) grid lines onto earth for a particular scene. Blue lines are latitude-longitude grid cell boundaries and the red lines are director cosine grid cell boundaries. Black dots show the locations where the LSC biases are computed before interpolation to the LUT cells.

The basic steps involved in computing the LSC are shown in Figure 5. The first step is to establish the four dimensional arrays of the form $\Delta Tpd(\vartheta g, \varphi g, \xi, \eta)$ (where the superscript on the function has been dropped for 2 convenience). As mentioned above, there is one array for each polarization and each pass direction. Each array has dimensions $(N\varphi, N\vartheta, N\xi, N\eta) = (721, 321, 81, 81)$. The arrays vary fastest in longitude and slowest in η . For storage efficiency, the full arrays are not stored: only cells with at least one measurement are actually stored, and a separate indexing array is used to keep track of the mapping between stored cell and location in the full array.

The next step is to process (in parallel) all Level 1B products from 2012 through 2019 and accumulate the LSC biases into a single mini-lookup table (LSC LUT) for each product. As described below, the biases for each scene are weighted when placed into the LSC LUT. Powers of the weights and the first four (scaled) moments are actually stored in these mini-LUTs.

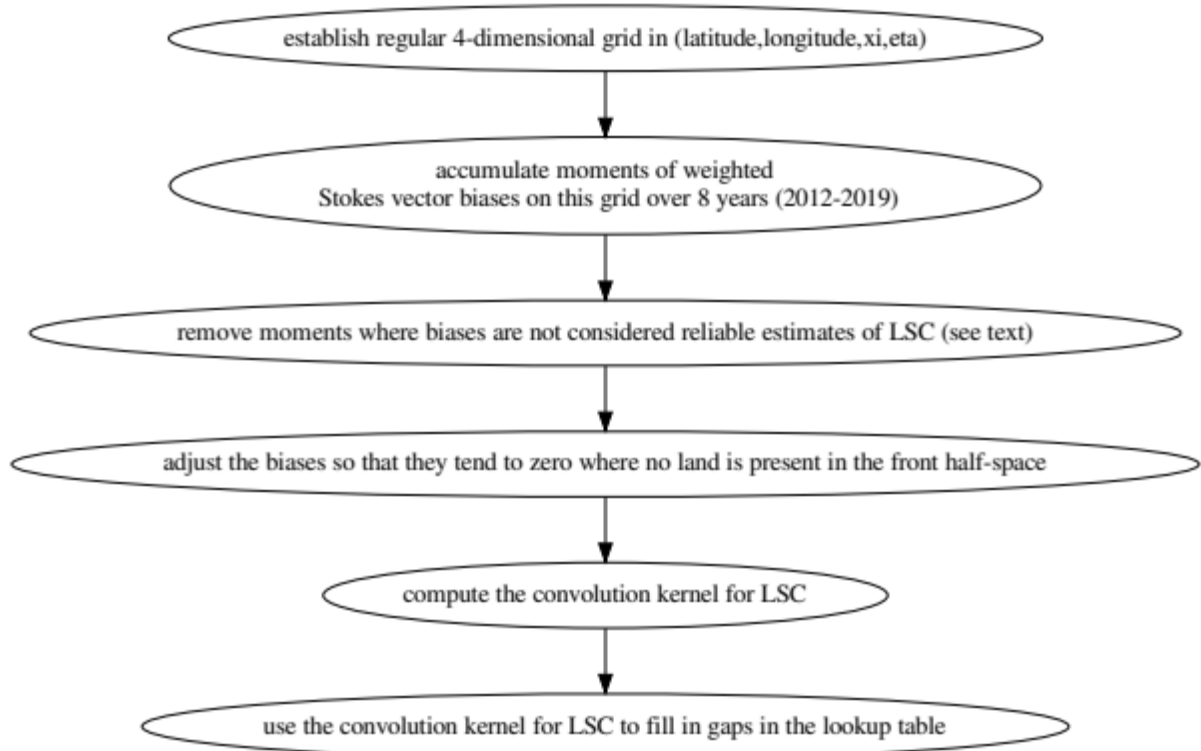



Figure 5: Flowchart showing the basic steps in producing the land-sea contamination lookup table.

Next, as described below, a multi-stage merging process is implemented in order to build the complete LUTs for 2012-2019, one for each pass direction. The resulting merged LUTs are then filtered to remove biases for which the standard deviations exceed a certain level (detailed below) or for which the temporal standard deviation of the reference monthly ISAS SSS exceeds 0.4.

	<p style="text-align: center;">SMOS L2 OS Table Generation Requirements Document</p>	<p>Doc: SO-TN-ARG-GS-0014 Issue: 3 Rev: 18 Date: 16 March 2021 Page: 38</p>
---	--	---

Next, the filtered LUTs are used together with many scenes with different distribution of land in the field of view to build a convolution kernel that may be used to reproduce an estimate of the LSC given the distribution of land in the field of view.

As a final step, this kernel is used to fill in the gaps in the empirical LUTs to produce complete LUTs.

2.2.8.3. Weighted moments of the land sea contamination

The biases entering into the lookup table are interpolated to exact LUT grid cell latitude and longitude. For any given scene, however, an exact cell center (latitude,longitude) does not correspond to a cell center director cosine location. Therefore, the interpolated biases are applied to all grid cells for the given (latitude,longitude) center and director cosine coordinates that lie within a window around the exact cell center director cosine coordinates. The biases are weighted by distance from a grid cell center in director cosine coordinates. The weighting function w is Gaussian of the form

$$d_h = 0.05 \quad (3)$$

$$d = \sqrt{(\xi' - \xi)^2 + (\eta' - \eta)^2} \quad (4)$$

$$w = \exp \{ \log(.5) d^2 / d_h^2 \} \quad (5)$$

The biases that comprise the empirical LSC LUT are weighted averages of the individual biases, with the weights given by w_i . The first four weighted central moments of these biases are stored. The calculation of these moments over the entire mission is computationally intensive and in what follows we describe the methodology.

2.2.8.3.1.1. Definition of the weighted moments

To fix the notation, define the sums of the first four integer powers of the weights as

$$V_1 = \sum_{i=1}^N w_i, \quad (6)$$

$$V_2 = \sum_{i=1}^N w_i^2, \quad (7)$$

$$V_3 = \sum_{i=1}^N w_i^3, \quad (8)$$

$$V_4 = \sum_{i=1}^N w_i^4. \quad (9)$$

The first four weighted central moments are defined as in [2],

$$m_1 = E_w[v_i] = \frac{1}{V_1} \sum_{i=1}^N w_i v_i = \bar{v}, \quad (10)$$

$$m_2 = E_w[(v_i - \bar{v})^2] = \frac{1}{V_1} \sum_{i=1}^N w_i (v_i - \bar{v})^2, \quad (11)$$

$$m_3 = E_w[(v_i - \bar{v})^3] = \frac{1}{V_1} \sum_{i=1}^N w_i (v_i - \bar{v})^3, \quad (12)$$

$$m_4 = E_w[(v_i - \bar{v})^4] = \frac{1}{V_1} \sum_{i=1}^N w_i (v_i - \bar{v})^4. \quad (13)$$

where we have introduced the expected value operator E_w , defined with respect to the weights w_i . In terms of the preceding variables, the biased weighted sample variance, skewness and kurtosis are defined as

$$\sigma_w^2 = E_w[(v_i - \bar{v})^2] = m_2, \quad (14)$$

$$S_w = \frac{1}{\sigma_w^3} E_w[(v_i - \bar{v})^3] = m_3 / (m_2^{3/2}), \quad (15)$$

$$K_w = \frac{1}{\sigma_w^4} E_w[(v_i - \bar{v})^4] = m_4 / (m_2^2) = m_4 / (\sigma_w^4). \quad (16)$$

In what follows it is convenient to introduce the following quantities,

$$M_1 = m_1 = \frac{1}{V_1} \sum_{i=1}^N w_i (v_i - \bar{v})^2, \quad (17)$$

$$M_2 = V_1 m_2 = \sum_{i=1}^N w_i (v_i - \bar{v})^2, \quad (18)$$

$$M_3 = V_1 m_3 = \sum_{i=1}^N w_i (v_i - \bar{v})^3, \quad (19)$$

$$M_4 = V_1 m_4 = \sum_{i=1}^N w_i (v_i - \bar{v})^4. \quad (20)$$

In terms of the preceding quantities, the weighted sample variance, skewness and kurtosis are

$$\sigma_w^2 = M_2 / V_1, \quad (21)$$

$$S_w = V_1^{1/2} M_3 / M_2^{3/2}, \quad (22)$$

$$K_w = V_1 M_4 / M_2^2. \quad (23)$$

The unbiased second, third and fourth weighted central moments are, respectively [2]

$$\hat{m}_2 = \frac{V_1^2}{V_1^2 - V_2} m_2, \quad (24)$$

$$\hat{m}_3 = \frac{V_1^3}{V_1^3 - 3V_1V_2 + 2V_3} m_3, \quad (25)$$

$$\hat{m}_4 = \frac{[V_1^2 (V_1^4 - 3V_1^2V_2 + 2V_1V_3 + V_2^2 - 3V_4)] m_4 - [3V_1^2 (2V_1^2V_2 - 2V_1V_3 - 3V_2^2 + 3V_4)] m_2^2}{(V_1^2 - V_2) (V_1^4 - 6V_1^2V_2 + 8V_1V_3 + 3V_2^2 - 6V_4)}. \quad (26)$$

Introducing the number of degrees of freedom

$$N_f = \frac{V_1^2}{V_2}, \quad (27)$$

The unbiased second central moment can be expressed as

$$\hat{m}_2 = \frac{1}{1 - 1/N_f} m_2. \quad (28)$$

2.2.8.3.1.2. Moment combining formulas

As mentioned above, the calculation of the preceding moments in a straightforward way would be prohibitive. Therefore, the approach adopted is to divide the complete moment calculation into many small moment calculations, and then to use moment combining formulas as provided in [3, 4, 5, 6, 7] to compute the moments for the complete dataset. The implementation is based upon code available in [7].

Consider two sets of samples with weights and first four (scaled) central moments

$$(V_1^{(1)}, V_2^{(1)}, V_3^{(1)}, V_4^{(1)}, M_1^{(1)}, M_2^{(1)}, M_3^{(1)}, M_4^{(1)}) \quad (29)$$

and

$$(V_1^{(2)}, V_2^{(2)}, V_3^{(2)}, V_4^{(2)}, M_1^{(2)}, M_2^{(2)}, M_3^{(2)}, M_4^{(2)}) \quad (30)$$

The combined weights and (scaled) central moments

$$(V'_1, V'_2, V'_3, V'_4, M'_1, M'_2, M'_3, M'_4) \quad (31)$$

can be shown to be

$$V'_1 = V_1^{(1)} + V_1^{(2)}, \tag{32}$$

$$V'_2 = V_2^{(1)} + V_2^{(2)}, \tag{33}$$

$$V'_3 = V_3^{(1)} + V_2^{(3)}, \tag{34}$$

$$V'_4 = V_4^{(1)} + V_2^{(4)}, \tag{35}$$

$$M'_1 = \frac{1}{V'_1} [V_1^{(1)} M_1^{(1)} + V_1^{(2)} M_1^{(2)}], \tag{36}$$

$$M'_2 = M_2^{(1)} + M_2^{(2)} + \Delta^2 \frac{V_1^{(1)} V_1^{(2)}}{V'_1}, \tag{37}$$

$$M'_3 = M_3^{(1)} + M_3^{(2)} + \frac{3\Delta}{V'_1} [V_1^{(1)} M_2^{(2)} - V_1^{(2)} M_2^{(1)}] + \frac{\Delta^3}{(V'_1)^2} [V_1^{(1)} V_1^{(2)} (V_1^{(1)} - V_1^{(2)})], \tag{38}$$

$$M'_4 = M_4^{(1)} + M_4^{(2)} + \frac{4\Delta}{V'_1} [V_1^{(1)} M_3^{(2)} - V_1^{(2)} M_3^{(1)}] + \frac{6\Delta^2}{(V'_1)^2} [(V_1^{(1)})^2 M_2^{(2)} + (V_1^{(2)})^2 M_2^{(1)}] + \Delta^4 \frac{V_1^{(1)} V_2^{(1)}}{(V'_1)^3} [(V_1^{(1)})^2 - V_1^{(1)} V_1^{(2)} + (V_1^{(2)})^2]. \tag{39}$$

where $\Delta = M_1^{(2)} - M_1^{(1)}$.

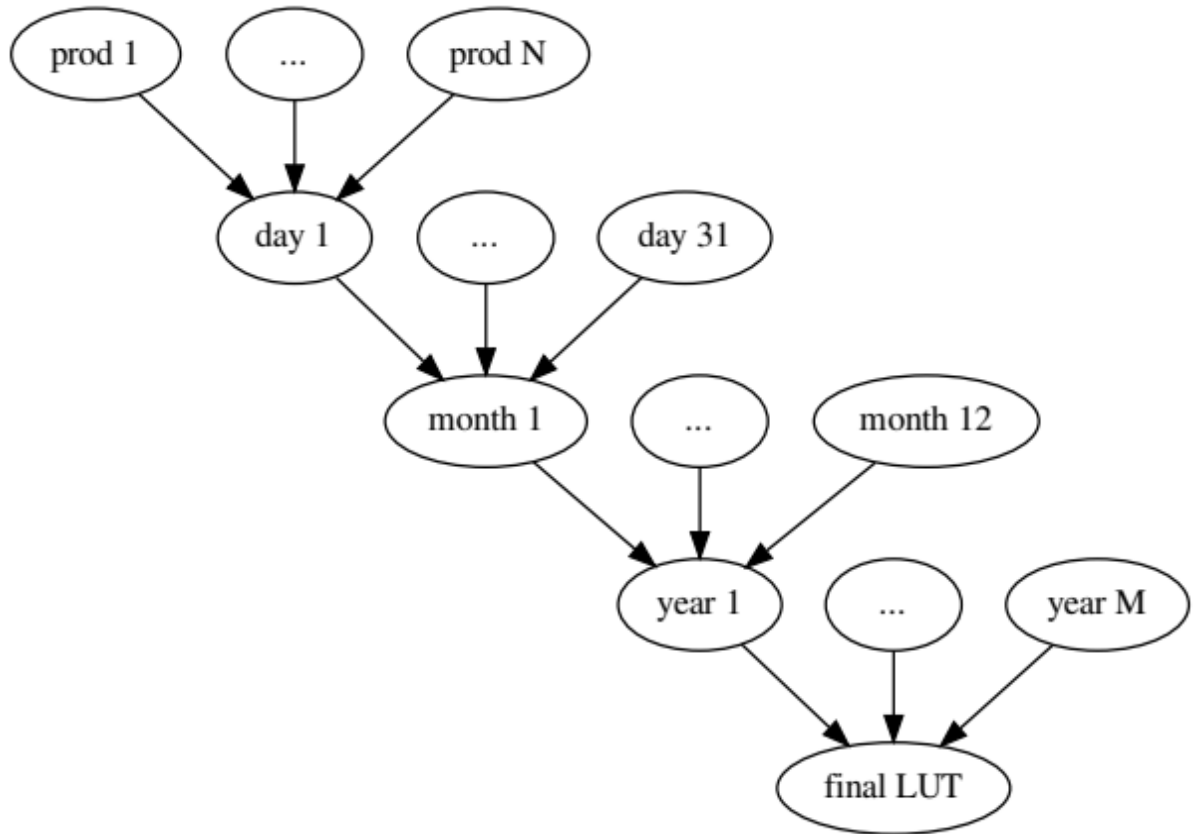


Figure 6: Flowchart showing stages of the process of merging the first four moments of the land sea contamination biases evaluated over the mission. At each stage the calculation is parallelized for efficiency.

The moment combining formulas allow the parallelization of the calculation of the overall LSC biases. Figure 6 illustrates the stages in the calculation. The parallelization is done at the daily, monthly, and yearly time scales.

2.2.8.3.1.3. Parallel computation of the lookup tables

The parallelization is done in several stages. First, individual Level 1B products from 2012 through 2019 are processed into mini-LUTs, one per product. Each mini-LUT contains the four scaled moments and sums of weights. Next, these products are merged into daily, then monthly, and then yearly LUTs. Finally, these yearly LUTs are merged into a single LUT for each pass direction. Figure 6 illustrates this process.

2.2.8.4. Weighted Filtering and adjusting the merged lookup table.

2.2.8.4.1.1. Filtering the biases

Although the individual scenes are removed from the averaging if a strong source of RFI is detected within the fundamental hexagon, some of the biases in the final merged LUTs are contaminated by residual low-level RFI. This is especially true in the northwest Atlantic Ocean. Also, although the reference salinity fields are obtained from monthly ISAS analyses, these fields are not reliable where there are few in-situ measurements, such as near river plumes.

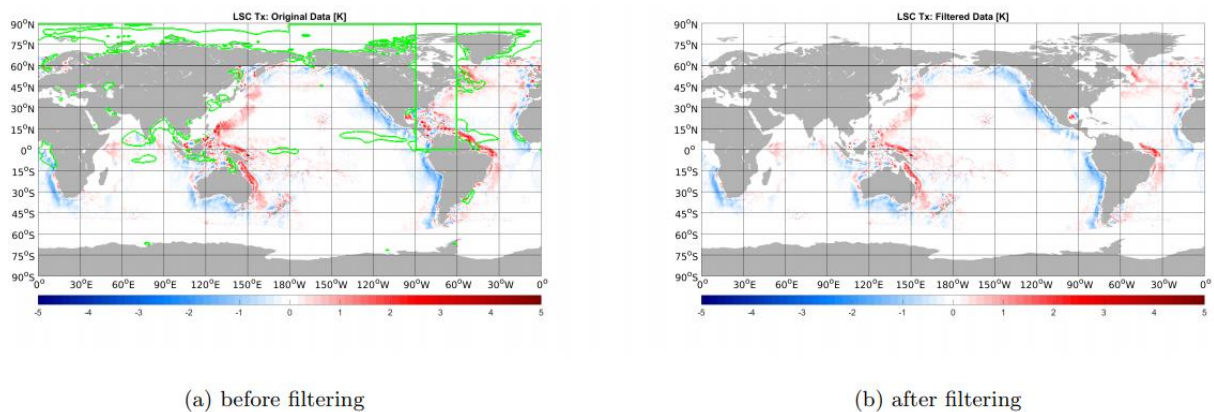


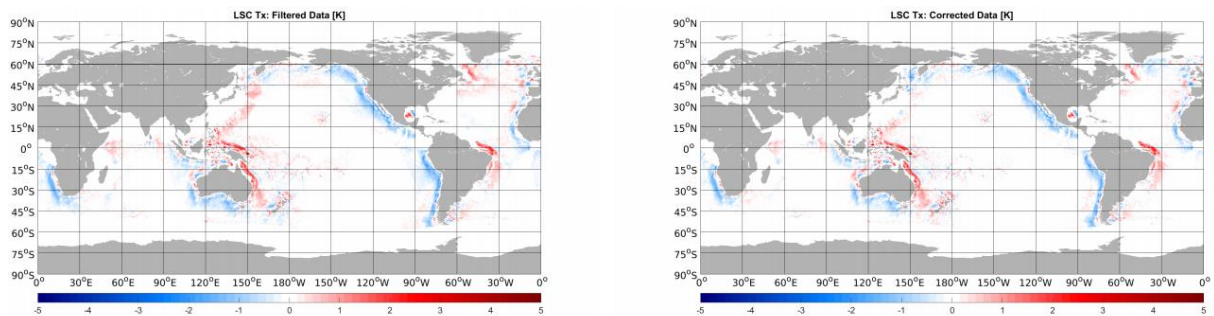
Figure 7: (a): Example slice through the unfiltered LSC LUT at grid cell $(i\xi, i\eta) = (41, 41)$ with the boundaries of filtered regions indicated by the green curves. The curves outline both a rectangular area in the northwest Atlantic Ocean (heavily affected by RFI) and areas where the temporal standard deviation of the monthly 25 km ISAS SSS from 2013-2016 exceeds 0.4. (b): The same as in (a) except filtered to remove all biases inside the green curves as well as biases for which the sum of the weights is below 0.1, the fraction of land in the front half-space is below 0.005, or the standard deviation of the bias exceeds the 95th percentile for the given polarization and $(i\xi, i\eta)$ location.

Therefore, biases in these areas are removed from the LUTs. The following lists the filtering criteria:

ARGANS Ltd.

- biases for which $\vartheta_g > 0^\circ$ and $270^\circ < \varphi_g < 300^\circ$ are removed;
- biases for which the corresponding standard deviation exceeds the 95th percentile for the given latitude/longitude slice at any fixed position in the field of view;
- biases for which the temporal standard deviation of monthly ISAS SSS exceeds 0.4 are removed.

The green curves in Figure 7(a) show the areas where biases are removed on a particular slice through the LUT (near the center of the field of view), and Figure 7(b) shows the slice after filtering.



(a) before bias correction


(b) after bias correction

Figure 8: Same slice as in Figure 7 through the LSC correction (a) before and (b) after correcting for open ocean (far from land) biases.

2.2.8.4.1.2. Filtering Correcting for open ocean biases

After filtering one more issue remains, which is that the biases do not generally tend to zero in the limit of zero land fraction in the field of view. Therefore, an adjustment is made to force the biases to tend to zero as the land fraction approached zero. This is achieved in the following steps for each (ξ, η) position:

- A set of 'boundary biases' is produced, consisting only of the biases for which the FHS land fraction does not exceed 0.02.
- These boundary biases are averaged using a running window of width 4° in longitude and 2° in latitude.
- A gap-filling procedure is applied to fill in the gaps in the boundary bias maps. This procedure involves iteratively finding the grid cells without biases that are adjacent to non-missing cells and replacing the missing values with the average of the surrounding non-missing biases. Surrounding non-missing values are averaged, with values at the same latitude as the missing value given four times the weight of those at different latitudes. This gap-filling procedure is repeated until no gaps remain.

	SMOS L2 OS Table Generation Requirements Document	Doc: SO-TN-ARG-GS-0014 Issue: 3 Rev: 18 Date: 16 March 2021 Page: 44
---	--	---

- The resulting gap-filled bias maps are averaged using a running window of width 8° in longitude and 4° in latitude;
- These offset fields are then subtracted from the LUT biases to produce the final bias-corrected maps that tend to zero as the land fraction in the FoV approaches zero.

Figure 8 shows an example slice through the LUT showing both the (filtered) uncorrected and corrected biases in Tx. Differences are most obvious in the Northwest Pacific Ocean.

2.2.8.5. Using the convolution kernel to fill gaps in the filtered lookup table

2.2.8.5.1.1. Building the convolution kernel

After filtering the merged LSC LUTs, large gaps exist over the ocean where no correction is available. In order to fill in these gaps, a kernel function is developed that is able to reproduce accurately the LSC biases given only a land sea mask for each scene. To build this kernel, a large number of scenes are generated by shifting the field of view over the globe in order to sample diverse distributions of land in the field of view. The result is the following matrix equation, where each line in the first matrix corresponds to the land-sea mask for a given scene. The vector c^p_n is the desired kernel, or weighting function, that produces the LSC biases B^p_k on the RHS of the equation.

$$\begin{pmatrix} L_1(\xi_1, \eta_1) & L_1(\xi_2, \eta_2) & L_1(\xi_3, \eta_3) & \dots & L_1(\xi_N, \eta_N) \\ L_2(\xi_1, \eta_1) & L_2(\xi_2, \eta_2) & L_2(\xi_3, \eta_3) & \dots & L_2(\xi_N, \eta_N) \\ L_3(\xi_1, \eta_1) & L_3(\xi_2, \eta_2) & L_3(\xi_3, \eta_3) & \dots & L_3(\xi_N, \eta_N) \\ \vdots & \vdots & \vdots & \ddots & \vdots \\ L_M(\xi_1, \eta_1) & L_M(\xi_2, \eta_2) & L_M(\xi_3, \eta_3) & \dots & L_M(\xi_N, \eta_N) \end{pmatrix} \begin{pmatrix} c^p_1(\xi_k, \eta_k, \xi_1, \eta_1) \\ c^p_2(\xi_k, \eta_k, \xi_2, \eta_2) \\ c^p_3(\xi_k, \eta_k, \xi_3, \eta_3) \\ \vdots \\ c^p_N(\xi_k, \eta_k, \xi_N, \eta_N) \end{pmatrix} = \begin{pmatrix} B^p_1(\xi_k, \eta_k) \\ B^p_2(\xi_k, \eta_k) \\ B^p_3(\xi_k, \eta_k) \\ \vdots \\ B^p_M(\xi_k, \eta_k) \end{pmatrix} + \mathcal{E}$$

This equation may be developed for all possible gridpoints (ξ_k, η_k) . In what follows (ξ_k, η_k) is fixed and c^p reduces to a vector. The preceding can then be written compactly as


$$\mathbf{L}c^p = \mathbf{b}^p + \mathcal{E} \tag{40}$$

We seek a solution that satisfies

$$\min_{c^p \in \mathbb{R}^N} \|\mathbf{L}c^p - \mathbf{b}^p\|_2^2 \tag{41}$$

whose solution satisfies the normal equation

$$\mathbf{L}^T \mathbf{L} \hat{c} = \mathbf{L}^T \mathbf{b}^p \tag{42}$$

	<p style="text-align: center;">SMOS L2 OS Table Generation Requirements Document</p>	<p>Doc: SO-TN-ARG-GS-0014 Issue: 3 Rev: 18 Date: 16 March 2021 Page: 45</p>
---	--	---

The solution of which is

$$\hat{\mathbf{c}} = (\mathbf{L}^T \mathbf{L})^{-1} \mathbf{L}^T \mathbf{b}^P = \mathbf{L}^+ \mathbf{b}^P \quad (43)$$

As the inverse problem is not well-posed, the inversion must be stabilised. One possibility is to solve instead the problem

$$\min_{\mathbf{c}^P \in \mathbb{R}^N} \{ \|\mathbf{L} \mathbf{c}^P - \mathbf{b}^P\|_2^2 + \|\mathbf{L}_\mu \mathbf{c}^P\|_2^2 \} \quad (44)$$

where \mathbf{L}_μ is chosen appropriately to stabilise the inversion without degrading accuracy excessively. One choice is to constrain the magnitude of the vector

$$\min_{\mathbf{c}^P \in \mathbb{R}^N} \{ \|\mathbf{L} \mathbf{c}^P - \mathbf{b}^P\|_2^2 + \|\mu \mathbf{I} \mathbf{c}^P\|_2^2 \} \quad (45)$$

Another is to constrain the curvature of the vector with respect to slope

$$\min_{\mathbf{c}^P \in \mathbb{R}^N} \{ \|\mathbf{L} \mathbf{c}^P - \mathbf{b}^P\|_2^2 + \|\mu \mathbf{D}_2 \mathbf{c}^P\|_2^2 \} \quad (46)$$

In any case the normal equations become

$$(\mathbf{L}^T \mathbf{L} + \mathbf{L}_\mu^T \mathbf{L}_\mu) \hat{\mathbf{c}}_\mu = \mathbf{L}^T \mathbf{b}^P \quad (47)$$

whose solution is

$$\hat{\mathbf{c}}_\mu = (\mathbf{L}^T \mathbf{L} + \mathbf{L}_\mu^T \mathbf{L}_\mu)^{-1} \mathbf{L}^T \mathbf{b}^P \quad (48)$$

For the standard constraint this becomes

$$(\mathbf{L}^T \mathbf{L} + \mu^2 \mathbf{I}) \hat{\mathbf{c}}_\mu = \mathbf{L}^T \mathbf{b}^P \quad (49)$$

Another method of stabilising the inversion is to employ singular value decomposition. Returning to the inverse problem,

$$\hat{\mathbf{c}} = (\mathbf{L}^T \mathbf{L})^{-1} \mathbf{L}^T \mathbf{b}^P = \mathbf{L}^+ \mathbf{b}^P. \quad (50)$$

Compute the SVD of L,

$$\mathbf{L} = \mathbf{U} \mathbf{S} \mathbf{V}^T \quad (51)$$

where U and V are orthogonal matrices and S is a diagonal matrix whose entries are the singular values of L. Then

$$\mathbf{L}^T \mathbf{L} = (\mathbf{V} \mathbf{S} \mathbf{U}^T) (\mathbf{U} \mathbf{S} \mathbf{V}^T) = \mathbf{V} \mathbf{S}^2 \mathbf{V}^T \quad (52)$$

and so

$$(\mathbf{L}^T \mathbf{L})^{-1} = \mathbf{V} \mathbf{S}^{-2} \mathbf{V}^T \quad (53)$$

Thus,

$$(\mathbf{L}^T \mathbf{L})^{-1} \mathbf{L}^T = (\mathbf{V} \mathbf{S}^{-2} \mathbf{V}^T) (\mathbf{V} \mathbf{S} \mathbf{U}^T) = \mathbf{V} \mathbf{S}^{-1} \mathbf{U}^T \quad (54)$$

and so

$$\hat{\mathbf{c}} = (\mathbf{L}^T \mathbf{L})^{-1} \mathbf{L}^T \mathbf{b}^p = \mathbf{V} \mathbf{S}^{-1} \mathbf{U}^T \mathbf{b}^p. \quad (55)$$

We actually compute the SVD of $\mathbf{L}^T \mathbf{L}$,

$$\mathbf{L}^T \mathbf{L} = \tilde{\mathbf{U}} \tilde{\mathbf{S}} \tilde{\mathbf{V}}^T = \tilde{\mathbf{V}} \tilde{\mathbf{S}} \tilde{\mathbf{V}}^T, \quad (56)$$

where $\tilde{\mathbf{U}}$ and $\tilde{\mathbf{V}}$ are orthogonal matrices and $\tilde{\mathbf{S}}$ is a diagonal matrix whose entries are the singular values of $\mathbf{L}^T \mathbf{L}$. The inverse may then be expressed as

$$(\mathbf{L}^T \mathbf{L})^{-1} = \tilde{\mathbf{V}} \tilde{\mathbf{S}}^{-1} \tilde{\mathbf{U}}^T = \tilde{\mathbf{V}} \tilde{\mathbf{S}}^{-1} \tilde{\mathbf{V}}^T, \quad (57)$$

and so

$$(\mathbf{L}^T \mathbf{L})^{-1} \mathbf{L}^T = \tilde{\mathbf{V}} \tilde{\mathbf{S}}^{-1} \tilde{\mathbf{U}}^T \mathbf{L}^T = \tilde{\mathbf{V}} \tilde{\mathbf{S}}^{-1} \tilde{\mathbf{V}}^T \mathbf{L}^T. \quad (58)$$

Note that

$$\mathbf{L}^T \mathbf{L} = (\mathbf{V} \mathbf{S} \mathbf{U}^T) (\mathbf{U} \mathbf{S} \mathbf{V}^T) = \mathbf{V} \mathbf{S}^2 \mathbf{V}^T = \tilde{\mathbf{U}} \tilde{\mathbf{S}} \tilde{\mathbf{V}}^T, \quad (59)$$

so that

$$\tilde{\mathbf{U}} = \mathbf{V}, \quad (60)$$

$$\tilde{\mathbf{V}} = \mathbf{V}, \quad (61)$$

$$\tilde{\mathbf{S}} = \mathbf{S}^2. \quad (62)$$

Using these relations,

$$(\mathbf{L}^T \mathbf{L})^{-1} \mathbf{L}^T = \tilde{\mathbf{V}} \tilde{\mathbf{S}}^{-1} \tilde{\mathbf{U}}^T \mathbf{L}^T = \mathbf{V} \mathbf{S}^{-2} \tilde{\mathbf{U}}^T \mathbf{L}^T. \quad (63)$$

Note also that since

$$\mathbf{L} = \mathbf{U} \mathbf{S} \mathbf{V}^T, \quad (64)$$

we have

$$\mathbf{U} = \mathbf{L} \mathbf{V} \mathbf{S}^{-1} = \mathbf{L} \tilde{\mathbf{V}} \tilde{\mathbf{S}}^{-1/2}. \quad (65)$$

In terms of column vectors, this equation may be written as

$$\mathbf{U}_i = \frac{1}{\sqrt{\tilde{S}_i}} \mathbf{L} \tilde{\mathbf{V}}_i. \quad (66)$$

The solution for the weighting function vector may then be expressed as

$$\hat{\mathbf{c}} = (\mathbf{L}^T \mathbf{L})^{-1} \mathbf{L}^T \mathbf{b}^p = \tilde{\mathbf{V}} \tilde{\mathbf{S}}^{-1} \tilde{\mathbf{U}}^T \mathbf{L}^T \mathbf{b}^p. \quad (67)$$

or

$$\hat{\mathbf{c}} = \mathbf{V} \mathbf{S}^{-2} \mathbf{V}^T \mathbf{L}^T \mathbf{b}^p. \quad (68)$$

Explicitly, the equation

$$\hat{\mathbf{c}} = \mathbf{V} \mathbf{S}^{-1} \mathbf{U}^T \mathbf{b}^p. \quad (69)$$

may be written more explicitly as the sum

$$\hat{\mathbf{c}} = \sum_{i=1}^N \left(\frac{\mathbf{U}_i \cdot \mathbf{b}^p}{S_i} \right) \mathbf{V}_i. \quad (70)$$

Taking only the first K singular values we obtain

$$\hat{\mathbf{c}} = \sum_{i=1}^K \left(\frac{\mathbf{U}_i \cdot \mathbf{b}^p}{S_i} \right) \mathbf{V}_i. \quad (71)$$

In terms of the eigendecomposition of $\mathbf{L}^T \mathbf{L}$ this may be written as

$$\hat{\mathbf{c}}_K = \sum_{i=1}^K \left(\frac{(\mathbf{L} \tilde{\mathbf{V}}_i) \cdot \mathbf{b}^p}{\tilde{S}_i} \right) \tilde{\mathbf{V}}_i. \quad (72)$$

The final weighting functions are obtained by keeping the first 300 singular vectors. Having found the coefficients for every position in the field of view, we can correct any image for the presence of land, since the bias in polarization p at position (ξ_i, η_i) is

$$B^p(\xi_i, \eta_i) = \begin{pmatrix} c_1^p(\xi_i, \eta_i) & c_2^p(\xi_i, \eta_i) & c_3^p(\xi_i, \eta_i) & \dots & c_N^p(\xi_i, \eta_i) \\ L(\xi_1, \eta_1) \\ L(\xi_2, \eta_2) \\ L(\xi_3, \eta_3) \\ \vdots \\ L(\xi_N, \eta_N) \end{pmatrix}$$

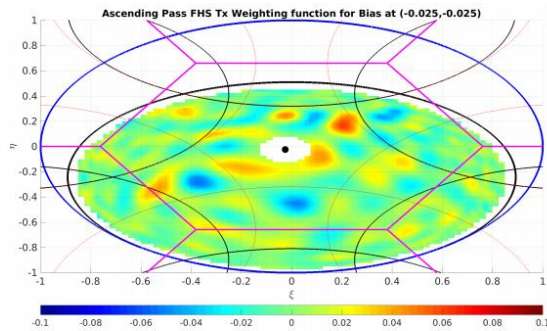
Combining the corrections for all points in the field of view, we obtain

$$\mathbf{B}^p = \begin{pmatrix} c_1^p(\xi_1, \eta_1) & c_2^p(\xi_1, \eta_1) & c_3^p(\xi_1, \eta_1) & \dots & c_N^p(\xi_1, \eta_1) \\ c_1^p(\xi_2, \eta_2) & c_2^p(\xi_2, \eta_2) & c_3^p(\xi_2, \eta_2) & \dots & c_N^p(\xi_2, \eta_2) \\ c_1^p(\xi_3, \eta_3) & c_2^p(\xi_3, \eta_3) & c_3^p(\xi_3, \eta_3) & \dots & c_N^p(\xi_3, \eta_3) \\ \vdots & \vdots & \vdots & \ddots & \vdots \\ c_1^p(\xi_N, \eta_N) & c_2^p(\xi_N, \eta_N) & c_3^p(\xi_N, \eta_N) & \dots & c_N^p(\xi_N, \eta_N) \end{pmatrix} \begin{pmatrix} L(\xi_1, \eta_1) \\ L(\xi_2, \eta_2) \\ L(\xi_3, \eta_3) \\ \vdots \\ L(\xi_N, \eta_N) \end{pmatrix}$$

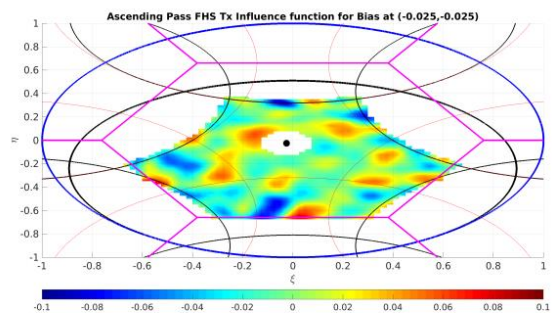
or more explicitly we have for polarization p

$$\mathbf{B}^p = \begin{pmatrix} C^p(\xi_1, \eta_1; \xi_1, \eta_1) & C^p(\xi_1, \eta_1; \xi_2, \eta_2) & C^p(\xi_1, \eta_1; \xi_3, \eta_3) & \dots & C^p(\xi_1, \eta_1; \xi_N, \eta_N) \\ C^p(\xi_2, \eta_2; \xi_1, \eta_1) & C^p(\xi_2, \eta_2; \xi_2, \eta_2) & C^p(\xi_2, \eta_2; \xi_3, \eta_3) & \dots & C^p(\xi_2, \eta_2; \xi_N, \eta_N) \\ C^p(\xi_3, \eta_3; \xi_1, \eta_1) & C^p(\xi_3, \eta_3; \xi_2, \eta_2) & C^p(\xi_3, \eta_3; \xi_3, \eta_3) & \dots & C^p(\xi_3, \eta_3; \xi_N, \eta_N) \\ \vdots & \vdots & \vdots & \ddots & \vdots \\ C^p(\xi_N, \eta_N; \xi_1, \eta_1) & C^p(\xi_N, \eta_N; \xi_2, \eta_2) & C^p(\xi_N, \eta_N; \xi_3, \eta_3) & \dots & C^p(\xi_N, \eta_N; \xi_N, \eta_N) \end{pmatrix} \begin{pmatrix} L(\xi_1, \eta_1) \\ L(\xi_2, \eta_2) \\ L(\xi_3, \eta_3) \\ \vdots \\ L(\xi_N, \eta_N) \end{pmatrix}$$

Example slices through this four-dimensional kernel are shown in Figure 9. An example bias map for a gridpoint (near the center of the field of view) produced with only the kernel function applied to a land-sea mask is shown in Figure 10(a), and the difference between this maps and one produced with only the empirical LSC LUT is shown in Figure 10(b). As shown, the difference between the maps is a small fraction of the biases, indicating that the PSF accurately reproduces the LSC biases at least where the biases are known from the original LUT.

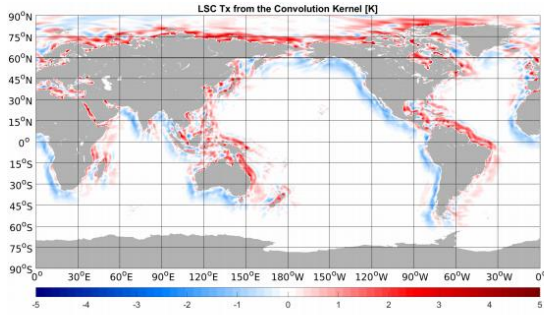


(a) weighting function at $(i_\xi, i_\eta) = (40, 40)$

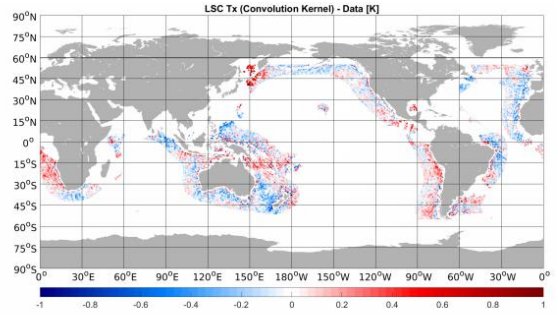


(b) influence function at $(i_\xi, i_\eta) = (40, 40)$

Figure 9: Convolution kernel (a) weighting and (b) influence functions for land occupying an LSC LUT cell with center at director cosine position index $(i_\xi, i_\eta) = (40, 40)$. Integration of the product of the weighting function $C^p(\xi_k, \eta_k; \xi, \eta)$ (with k fixed) and the land-sea mask over the entire FoV yields the total LSC at position (ξ_k, η_k) . By contrast, the influence function $C^p(\xi, \eta; \xi_i, \eta_i)$ (with i fixed) is the bias over the EAF-FoV associated with the presence of land at position (ξ_i, η_i) . Hence these two functions are different slices through the same four-dimensional function $C^p(\xi_k, \eta_k; \xi_i, \eta_i)$. Units are kelvin.



(a) convolution kernel bias at $(i_\xi, i_\eta) = (41, 41)$



(b) convolution kernel - original at $(i_\xi, i_\eta) = (41, 41)$

Figure 10: (a): Ascending pass LSC at grid cell $(i_\xi, i_\eta) = (41, 41)$ computed using only the convolution kernel method. (b): Difference between convolution kernel solution and the bias-corrected LSC LUT solution. Units are kelvin.

2.2.8.5.1.2. Filling the gaps in the LSC LUTs

The kernel-based solutions are combined with the filtered and bias-corrected LUT solutions to produce a gap free LUT to be used by the L2OS processor. As a first step, gaps in the LUT are filled with the biases computed using the kernel. Next, a linear combination of the LUT and kernel solutions is computed as follows. If F is the average fraction of gridpoints in the front half-space occupied by land, then the weighting function applied to the kernel solutions is following limits

$$w_f = \max\left(0, \min\left(1, \frac{F - F_0}{F_1 - F_0}\right)\right), \quad (73)$$

$$F_0 = 0.05, \quad (74)$$


$$F_1 = 0.1. \quad (75)$$

The weighted solutions are then

$$\bar{T}'_{pd}(\vartheta_g, \varphi_g, \xi, \eta) = (1 - w_f)\bar{T}^{(L)}_{pd}(\vartheta_g, \varphi_g, \xi, \eta) + w_f\bar{T}^{(K)}_{pd}(\vartheta_g, \varphi_g, \xi, \eta), \quad (76)$$

where $\bar{T}^{(K)}_{pd}$ is the kernel solution and the $\bar{T}^{(L)}_{pd}$ is the original LUT solution (where it exists). Finally, between 60° and 75° from the equator a weighting function is applied to ramp all biases from the full values to zero 75° from the equator:

$$\bar{T}''_{pd}(\vartheta_g, \varphi_g, \xi, \eta) = w_\vartheta\bar{T}'_{pd}(\vartheta_g, \varphi_g, \xi, \eta), \quad (77)$$

	<p style="text-align: center;">SMOS L2 OS Table Generation Requirements Document</p>	<p>Doc: SO-TN-ARG-GS-0014 Issue: 3 Rev: 18 Date: 16 March 2021 Page: 50</p>
---	--	---

where

$$w_{\vartheta} = \max \left(0, \min \left(1, \left[1 - \frac{(|\vartheta_g| - 60^\circ)}{(75^\circ - 60^\circ)} \right] \right) \right). \quad (78)$$

These are the final biases stored in the LUT for the L2OS processor.

2.2.8.6. Contents of the MATLAB LSC LUT files

Table 2 summarizes the contents of an LSC LUT MALAB file. There is a single file for each pass direction (see next page).

2.2.8.7. Example C++ code to compute dimension and global indices

Example C++ code to calculate the global lookup table index (MATLAB convention) from physical dimension coordinates is

```
int smosLscUnstructuredMatlab::coord to globalIndex(const double
lat, const double lon, const double xi, const double eta) const
{
    double tlon = JetMisc::normalizeAngle(lon);
    // Here in order of dimensions in matlab.
    int oilon = floor((eps+tlon - lon0) / dlon);
    int oilat = floor((eps+lat - lat0) / dlat);
    int oixi = floor((eps+xi - xi0) / dxi);
    int oieta = floor((eps+eta - eta0) / deta);
    int gind = oilon + nlon*oilat + nlon*nlat*oixi +
nlon*nlat*nxi*oieta;

    // Matlab convention here.
    return(gind+1);
}
```

Example C++ code to calculate the global lookup table index from dimension indices (starting at 1 in MATLAB) is:

```
int smosLscUnstructuredMatlab::coordIndices to globalIndex(const
int ilat, const int ilon, const int ixi, const int ieta) const
{
    int gind = ilon + nlon*ilat + nlon*nlat*ixi + nlon*nlat*nxi*ieta;

    //Switch to Matlab convention by adding 1 to the global index.

    return(gind+1);
}
```

ARGANS Ltd.


Commercial in Confidence

Page 50

Use, duplication, or disclosure of this document or any information contained herein is subject to the restriction on the title page of this document.

Table 2: Variables in the MATLAB LSC Lookup Table Files

Variable	Dimensions or Value	Meaning
cnt	[1175335382 single]	V_1 (sum of weights)
cnt2	[1175335382 single]	V_2 (sum of square of weights)
dTx_ott	[1175335382 single]	first moment M_1 of T_x bias [K]
dTx_mom2	[1175335382 single]	second moment M_2 of T_x bias [K ²]
dTx_mom3	[1175335382 single]	third moment M_3 of T_x bias [K ³]
dTx_mom4	[1175335382 single]	fourth moment M_4 of T_x bias [K ⁴]
dTy_ott	[1175335382 single]	first moment M_1 of T_y bias [K]
dTy_mom2	[1175335382 single]	second moment M_2 of T_y bias [K ²]
dTy_mom3	[1175335382 single]	third moment M_3 of T_y bias [K ³]
dTy_mom4	[1175335382 single]	fourth moment M_4 of T_y bias [K ⁴]
dT3_ott	[1175335382 single]	first moment M_1 of T_3 bias [K]
dT3_mom2	[1175335382 single]	second moment M_2 of T_3 bias [K ²]
dT3_mom3	[1175335382 single]	third moment M_3 of T_3 bias [K ³]
dT3_mom4	[1175335382 single]	fourth moment M_4 of T_4 bias [K ⁴]
dT4_ott	[1175335382 single]	first moment M_1 of T_4 bias [K]
dT4_mom2	[1175335382 single]	second moment M_2 of T_4 bias [K ²]
dT4_mom3	[1175335382 single]	third moment M_3 of T_4 bias [K ³]
dT4_mom4	[1175335382 single]	fourth moment M_4 of T_4 bias [K ⁴]
fhs_land_frac	[1175335382 single]	average fraction of gridpoints in front half-space occupied by land
ind_sorted_unique	[1175335382 int32]	global index (starting at 1) into complete 4-D LUT grid
dims	[721 361 81 81]	lookup table dimensions (first dimension varies fastest)
lat0	-90	starting latitude cell center [deg]
lat1	90	ending latitude cell center [deg]
dlat	0.5000	latitude grid spacing [deg]
lon0	0	starting longitude cell center [deg]
lon1	360	ending longitude cell center [deg]
dlon	0.5000	longitude grid spacing [deg]
xi0	-1	grid starting director cosine ξ value (cell center)
xi1	1	grid ending director cosine ξ value (cell center)
dxi	0.0250	director cosine ξ grid spacing
eta0	-1	grid starting director cosine η value (cell center)
eta1	1	grid ending director cosine η value (cell center)
deta	0.0250	director cosine η grid spacing
nlon	721	number of longitude (first MATLAB dimension) coordinates
nlat	361	number of latitude (second MATLAB dimension) coordinates
nxi	81	number of ξ (third MATLAB dimension) coordinates
neta	81	number of η (fourth MATLAB dimension) coordinates
lon	[1721 double]	first array dimension in MATLAB (varies fastest)
lat	[1361 double]	second array dimension in MATLAB
xi	[181 double]	third array dimension in MATLAB (ξ cell center values)
eta	[181 double]	fourth array dimension in MATLAB (η cell center values)

	<p style="text-align: center;">SMOS L2 OS Table Generation Requirements Document</p>	<p>Doc: SO-TN-ARG-GS-0014 Issue: 3 Rev: 18 Date: 16 March 2021 Page: 52</p>
---	--	---

The inverse, from global index (MATLAB convention starting at 1) to coordinate indices, can be computed as follows:

```
int smosLscUnstructuredMatlab::globalIndex to coordIndices(const
int agind, int &ilat, int &ilon, int &ixi, int &ieta) const
{
    // From MATLAB to C index convention.
    int gind = agind-1;
    ieta = floor(gind/(nlon*nlat*nxi));
    gind -= ieta*(nlon*nlat*nxi);
    ixi = floor(gind/(nlon*nlat));
    gind -= ixi*(nlon*nlat);
    ilat = floor(gind/nlon);
    gind -= ilat*nlon;
    ilon = gind;

    return(1);
}
```

An example to compute physical coordinates from the global index,

```
int smosLscUnstructuredMatlab::globalIndex to coord(const int
agind, double &lat, double &lon, double &xi, double &eta) const
{
    int ilat, ilon, ixi, ieta;
    globalIndex to coordIndices(agind, ilat, ilon, ixi, ieta);
    lat = lat0 + dlat*ilat;
    lon = lon0 + dlon*ilon;
    xi = xi0 + dxi*ixi;
    eta = eta0 + deta*ieta;
    return(1);
}
```

2.2.8.8. The total model solution

This section reviews the complete ocean scene brightness model used to derive the land-sea contamination biases. Considering all of the components of the scene brightness at L-band, the complete model solution for the upwelling brightness temperatures above the atmosphere but below the ionosphere (before Faraday rotation) in the surface polarization basis is, in horizontal polarization,

$$T_{th}^{(full)} = (\tau_d \tau_v) [T_{esh} + T_{sch} + T_{ssh} + R_h T_{ea}] + T_{ea} + (\tau_d \tau_v) [(1 - F_f) T_{erh} - F_f T_{esh} - e_{rh} T_{ea}] \quad (79)$$

and in vertical polarization

$$T_{tv}^{(\text{full})} = (\tau_d \tau_v) [T_{esv} + T_{scv} + T_{ssv} + R_v T_{ea}] + T_{ea} + (\tau_d \tau_v) [(1 - F_f) T_{crv} - F_f T_{esv} - e_{rv} T_{ea}] \quad (80)$$

where the variables are listed in Table 3 (next page). The dominant contribution to the total scene brightness is specular emission. The dielectric constant model of [8] and the ISAS NRT monthly mean surface salinity fields are used to compute the specular emission. Sea surface temperature is obtained from the ECMWF. The third and fourth Stokes parameters are assumed to be identically zero in the surface polarization basis below the ionosphere. After passage of the radiation upward through the ionosphere and after transformation into the Ludwig-3 [9] instrument polarization basis, the Stokes vector elements of the total and non-sunglint model solution are

$$\begin{pmatrix} T_{tx}^{(\text{full})} \\ T_{ty}^{(\text{full})} \\ T_{t3}^{(\text{full})} \\ T_{t4}^{(\text{full})} \end{pmatrix} = \begin{pmatrix} \cos^2 \beta & \sin^2 \beta & -\cos \beta \sin \beta & 0 \\ \sin^2 \beta & \cos^2 \beta & \cos \beta \sin \beta & 0 \\ \sin(2\beta) & -\sin(2\beta) & \cos(2\beta) & 0 \\ 0 & 0 & 0 & 1 \end{pmatrix} \begin{pmatrix} T_{th}^{(\text{full})} \\ T_{tv}^{(\text{full})} \\ T_{tu}^{(\text{full})} \\ T_{tv}^{(\text{full})} \end{pmatrix}, \quad (81)$$

where the angle β accounts for both rotation of the polarization plane during passage through the ionosphere and rotation of the polarization basis from the surface basis to the Ludwig-3 basis. Faraday rotation is computed using consolidated global maps of total electron content reduced by a factor to account for the SMOS satellite altitude.

The difference between the brightness temperatures from SMOS and the forward model in (instrument basis) polarization p is

$$\Delta T_p(\xi, \eta, t) = T_p^{(\text{miras})}(\xi, \eta, t) - T_{tp}^{(\text{full})}. \quad (82)$$

and the corresponding OTT is


$$\Delta T_p^{\text{OTT}}(\xi, \eta) = \langle \Delta T_p \rangle_t(\xi, \eta, t). \quad (83)$$

where the average is taken over some long time interval (more than one day). To ensure that that land-sea contamination biases do not enter into the OTTs, only scenes for which the fraction of the FHS occupied by land or ice is less than 0.01 are included in the averages. Using the preceding notation, the land-sea contamination in polarization p can be computed from the OTT-corrected measurements and the total forward model as

$$\Delta T_p^{(\text{lsc})}(\xi, \eta, t) = \left[T_p^{(\text{miras})}(\xi, \eta, t) - \Delta T_p^{\text{OTT}}(\xi, \eta) \right] - T_{tp}^{(\text{full})}(\xi, \eta, t). \quad (84)$$

Table 3: Quantities in the total Scene Brightness Model

Variable	Physical Quantity
$T_{th}^{(full)}$	H-pol total brightness temp. in the surface pol. basis [K]
$T_{tv}^{(full)}$	V-pol total brightness temp. in the surface pol. basis [K]
$T_{tU}^{(full)}$	third Stokes parameter total brightness temp. in the surface pol. basis [K]
$T_{tV}^{(full)}$	fourth Stokes parameter total brightness temp. [K]
$T_{tx}^{(full)}$	H-pol total brightness temp. in the instrument pol. basis [K]
$T_{ty}^{(full)}$	V-pol total brightness temp. in the instrument pol. basis [K]
$T_{t3}^{(full)}$	third Stokes parameter total brightness temp. in the instrument pol. basis [K]
$T_{t4}^{(full)}$	fourth Stokes parameter total brightness temp. [K]
τ_d	1-way atmospheric transmittance associated with molecular oxygen absorption [nd]
τ_v	1-way atmospheric transmittance associated with water vapor absorption [nd]
T_{esh}	H-pol brightness temp. of specular emission H-pol (surface pol. basis) [K]
T_{erh}	H-pol brightness temp. of rough surface emission H-pol (surface pol. basis) [K]
T_{sch}	H-pol brightness temp. of scattered celestial sky radiation (surface pol. basis) [K]
T_{esv}	V-pol brightness temp. of specular emission H-pol (surface pol. basis) [K]
T_{erv}	V-pol brightness temp. of rough surface emission H-pol (surface pol. basis) [K]
T_{scv}	V-pol brightness temp. of scattered celestial sky radiation (surface pol. basis) [K]
T_{ea}	brightness temp. of (unpolarized) atmospheric 1-way emission [K]
R_h	H-pol surface power reflection coefficient (surface pol. basis) [K]
R_v	V-pol surface power reflection coefficient (surface pol. basis) [K]
e_{rh}	H-pol rough surface emissivity [K]
e_{rv}	V-pol rough surface emissivity [K]
F_f	foam fraction from rough surface emission model [nd, range: 0-1]
T_{ssh}	H-pol brightness temp. of scattered solar radiation (sun glint) (surface pol. basis) [K]
T_{ssv}	V-pol brightness temp. of scattered solar radiation (sun glint) (surface pol. basis) [K]

	<p style="text-align: center;">SMOS L2 OS Table Generation Requirements Document</p>	<p>Doc: SO-TN-ARG-GS-0014 Issue: 3 Rev: 18 Date: 16 March 2021 Page: 55</p>
---	--	---

2.2.8.9. Notes

SMAP salinity data are produced by Remote Sensing Systems and sponsored by the NASA Ocean Salinity Science Team. Data are available at www.remss.com.

2.2.8.10. References

- [1] T. Meissner, F. J. Wentz, A. Manaster, and R. Lindsley, "Remote Sensing Systems SMAP Ocean Surface Salinities [Level 2C, Level 3 Running 8-day, Level 3 Monthly], Version 4.0 validated release," Available online at www.remss.com/missions/smap, 2019.
- [2] L. Rimoldini, "Weighted skewness and kurtosis unbiased by sample size and Gaussian uncertainties," *Astronomy and Computing*, vol. 5, pp. 1–8, July 2014.
- [3] T. F. Chan, G. H. Golub, and R. J. Leveque, "Algorithms for computing the sample variance: Analysis and recommendations," *The American Statistician*, vol. 37, no. 3, pp. 242–247, 1983.
- [4] —, "Updating formulae and a pairwise algorithm for computing sample variances," Stanford, Tech. Rep., Nov. 1979.
- [5] P. P'ebay, "Formulas for robust, one-pass parallel computation of covariances and arbitrary-order statistical moments," Sandia National Laboratories, Tech. Rep., Sept. 2008.
- [6] P. P'ebay, T. Terriberry, H. Kolla, and J. Bennett, "Numerically stable, scalable formulas for parallel and online computation of higher-order multivariate central moments with arbitrary weights," *Computational Statistics*, vol. 31, pp. 1305–1325, Mar. 2016.
- [7] "Computing skewness and kurtosis in one pass," <https://www.johndcook.com/blog/2013/06/11/computing-skewness-and-kurtosis-in-one-pass/>, accessed: 2020-10-13.
- [8] L. A. Klein and C. T. Swift, "An Improved model of the dielectric constant of sea water at microwave frequencies," *IEEE Trans. Antennas Propag.*, vol. 25, pp. 104–111, 1977.
- [9] A. C. Ludwig, "The definition of cross polarization," *IEEE Trans. Antennas Propag.*, vol. AP-21, no. 1, pp. 116–119, Jan. 1973.

2.2.9. SMOS-based climatology LUT for SSS anomaly computation

2.2.9.1. Purpose

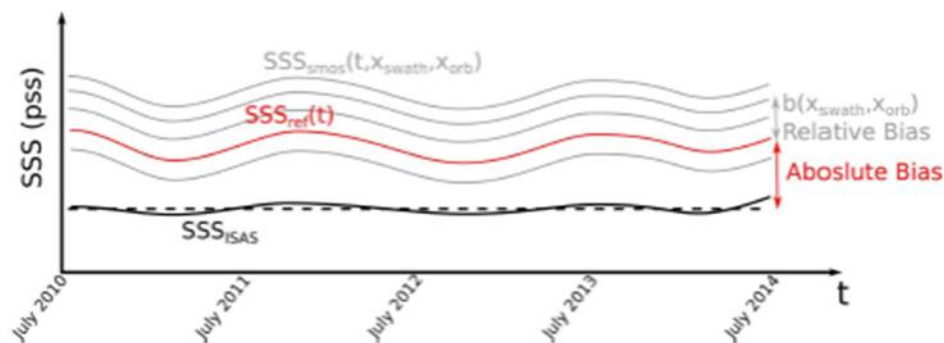
The SMOS derived climatology LUT, AUX_SSSCLI is to be used for generation of the SSS_anomaly field in the UDP.

2.2.9.2. Mathematical Formulation

The climatology is derived using a methodology described in Kolodziejczyk et al., 2016 [REF] (K2016). The K2016 approach removes systematic biases by considering the SSS as a function of distance from the centre of the swath. The anomaly is evaluated in two steps, including a relative correction that is evaluated per dwell lines, and then an absolute correction is evaluated with respect the ISAS 7 years mean (2013-2019, both included). These steps shall now be discussed in more detail.

Step 1:

The three years mean bias is estimated between the dwell lines signal at a fixed across swath location, X_{swath} and a reference salinity S_{ref} .




$$S_{smos}(t, r(X_{swath}), X_{orb}) = S_{ref}(t) - \overline{b(X_{swath}, X_{orb})}$$

Figure 11: Example of SMOS absolute bias determination

S_{smos} is the instantaneous (daily) salinity at each time, t , at each across-track distance to the satellite track, X_{swath} , and for each orbit, X_{orb} . S_{ref} is the temporal variation (in relative value) of SSS, and b the relative bias estimated for each distance to the satellite track and each orbit orientation (independent of time).

This equation is solved using a Bayesian least square minimization with an a priori value computed from the median value of SMOS SSS of the central dwell computed at each grid point over the entire period. SSS in this central dwell is chosen as prior because this dwell-line contains the largest number of TB pertaining to the alias free field of view and because the spatial extension of the coast bias is reduced in this FOV region (Vergely et al., 2013).

ARGANS Ltd.

	<p style="text-align: center;">SMOS L2 OS Table Generation Requirements Document</p>	<p>Doc: SO-TN-ARG-GS-0014 Issue: 3 Rev: 18 Date: 16 March 2021 Page: 57</p>
---	--	---

The method does not only correct biases but also looked at the dwell line closer to ISAS, as a metric. Results showed that the so-obtained anomalies are substantially better than without performing any debiasing. However, biases are not stable, so outside the period used to generate the climatology, the correction loses performance. The study was done considering a range between 45°N and 45°S in latitude and adding together ascending and descending. The anomalies showed better standard deviation of differences than when comparing directly SMOS with ISAS.

Step 2:

The estimated Sref is a relative estimate of the SSS temporal variability at each grid point, filtered out from outliers and corrected from a relative systematic inter-dwell and inter-orbit biases, b. The final step consists in the adjustment of the 7-year mean SSS ref on a 7-year mean SSS climatology. The climatology is taken from seven years (January 2013 to December 2019) median average of ISAS SSS fields interpolated at each SMOS L3 grid point. For each grid point, the correction b_{abs} is applied on each individual SSS from SSS time series:

$$b_{abs} = \langle SISAS \rangle - \langle SREF \rangle$$

where $\langle . \rangle$ is the median operator over 7 years of SMOS observations. This approach preserves the temporal dynamics of SMOS SSS.


2.2.9.3. Calculation of LUT

The SSSCLI LUT is calculated using the above methodology. Given the 18-day sub-cycle of SMOS, a given location over the ocean is observed with the same SMOS measurement geometry every ~18 days; within 18 days, it is sampled by several SMOS SSS measurements which are located at various locations across the swath, X_{swath} . The K2016 methodology considers that the long term (2013-2019) SSS variability observed by SMOS must be rather similar whatever **X_{swath}** and the orbit orientation **X_{orb}** . Relative biases, b_{land} , with respect to a reference SSS, SSS_{ref} , are derived from SMOS SSS through a least square minimization approach, and through a series of iterations that will be described below. A consistent set of SMOS SSS, $SSSK_{2016}$, is obtained as:

$$SSSK_{2016}(t, \phi, \lambda, X_{swath}, X_{orb}) = SSS_{ref}(t, \phi, \lambda) - b_{land}(\phi, \lambda, X_{swath}, X_{orb})$$

where t is the time of the measurement ϕ and λ are respectively the latitude and longitude of the considered location over the ocean. X_{swath} is sampled in 25km wide bins. b_{land} and SSS_{ref} are derived as follows. Defining $p=(SSS_{ref}, b_{land})^T$, p_0 the a priori values of p , y_0 the SMOS SSS, the estimated values of p , p_{est} , are derived as:

$$p_{est} = p_0 + C_p \cdot G^T \cdot (G \cdot C_p \cdot G^T + R)^{-1} \cdot [y_0 - f(p_0)]$$

	<p style="text-align: center;">SMOS L2 OS Table Generation Requirements Document</p>	<p>Doc: SO-TN-ARG-GS-0014 Issue: 3 Rev: 18 Date: 16 March 2021 Page: 58</p>
---	--	---

where G is the matrix of derivatives of observations with respect to the parameters (also called observational operator), R is the covariance matrix for the observation error, Cp is the covariance matrix for the a priori error on the parameters p. Cp is parametrized as a function of an acceptable standard deviation of SSS, σ_{SSSref} , over a correlation timescale τ .

The minimization is repeated four times, twice with $\tau=16$ days (corresponding to an 18-day Gaussian smoothing window), then twice with $\tau=8$ days (corresponding to a 9-day Gaussian smoothing window). At each iteration, a new set of a priori values for p and for σ_{SSSref} are computed.

During the first iteration, the a priori values of SSSref, SSSref0, are taken as the median of SMOS SSS at the centre of its swath over the 2013-2019 period, the a priori value of bland is equal to 0, σ_{SSSref} is taken equal to 0.3 pss, and the observation errors are taken equal to the theoretical error associated with the L2 SMOS SSS retrieval, ESSS_L2. SSSref1 and bland1 are computed from the p and σ_{SSSref} solutions of the first iteration.

During the second iteration, SSS outliers, linked primarily to RFI contamination, are detected using a 3- sigma outlier detection: if the difference between the L2 SMOS SSS and (SSSref1-bland1) is larger than 3 times ESSS_L2, the error on the measurement indicated in the matrix R is artificially increased. SSSref2 and bland2, estimated at the end of step 2, are used to produce the 18-day SSSK2016 fields. The third and fourth iterations aims at optimizing SSSref and bland at 9-day resolution. During the third iteration, SSSref2 and bland2 are taken as a priori parameters, τ is reduced to 8 days and σ_{SSSref} is increased to 0.5 pss resulting in SSSref3 and bland3. The fourth step leading to SSSref4 and bland4 is like the second one using the same a priori values as in step 3. At the end, an additional term is added to the estimated bias, to ensure that the 7-year (2013-2019) median average of SSSK2016 equals the 7-year median average of ISAS SSS for each latitude and longitude:

$$b_{land}(\phi, \lambda, X_{swath}, X_{orb}) = b_{landx}(\phi, \lambda, X_{swath}, X_{orb}) - (med(SSSref(t, \phi, \lambda)) - med(SSSISAS(t, \phi, \lambda)))$$


with b_{landx} equals to b_{land2} in the case of 18-day corrected field estimates, or to bland4 in the case of 9-day corrected fields. Note that the last term of the equation above is the only external information used in the entire correction process and does not modify the temporal variability of the observed fields. This method is applied to correct SSS before L3 averaging at CATDS (CEC LOCEAN and C-PDC processing). The correction is purely static (no time dependency). Contrary to the CATDS, no latitudinal correction is applied.

Filtering of data:

Geophysical filters:

- No filtering is used at this level. We consider potentially that the biases coming from RFI or other sources can be totally or partially corrected. The idea is that, in some cases,

ARGANS Ltd.

	<p style="text-align: center;">SMOS L2 OS Table Generation Requirements Document</p>	<p>Doc: SO-TN-ARG-GS-0014 Issue: 3 Rev: 18 Date: 16 March 2021 Page: 59</p>
---	--	---

even if the biases are important, the expected signal could be meaningful (for instance, if we expect a SSS anomaly of 10 psu, a 1 or 2 psu bias could be acceptable).

- No average is done with closest neighbours. Retrieval is applied strictly at each ISEA grid point.

Retrieval filters:

- The filtering is done dynamically in 2 steps. A first SSS and inter-dwell bias retrieval is done over a 18 days slipping windows (applied in a least square context). A 3-sigma detection is applied allowing to remove the influence of the L2 SSS which are too far from the expected SSS (SSS are not completely removed but associated errors are increased). A second SSS and inter-dwell bias estimation is performed.

Geometrical filter:

- Selection of data close to the track with $\text{abs}(X_{\text{swath}}) < 400\text{km}$
- The X_{swath} sampling is 25km.

2.2.9.4. Generation of LUT

Two files are provided to ARGANS by LOCEAN/ACRI, SMOSmean_nocorrTB_A_001.nc and SMOSmean_nocorrTB_D_001.nc. Which contain the Ascending and Descending climatology, respectively. The uncorrected salinity was used to generate this climatology.

The netCDF files have variables, lat, long, xswath, GPID (grid point ID) and SSSmean which are used to create the AUX_SSSCLI.

The values are filtered to remove any grid points with no data. Then the SSSmean values are multiplied by 1000 and converted to unsigned short from float. Then for each grid point the 33 SSSmean values are written out to the binary file, AUX_SSSCLI.

As a sanity check, resulting climatologic values that were too low to have physical meaning are set to NaNs, along with any other grid point resulting in non-valid values.

2.2.9.5. Contents of LUT

The LUT contains two sections, one for Ascending orbits and one for Descending orbits. Each section contains all the Grid point IDs with data. For each Grid point ID, there are 33 SSSanom values. One for each Xswath bin.

The Xswath bin is calculated from Xswath as follows:

$$\text{bin} = (X_{\text{Swath}} + X_{\text{swathMax}}) / X_{\text{swathStep}}$$

where X_{swath} is the value of the Xswath for that grid point, $X_{\text{swathMax}} = 412.5$ and $X_{\text{swathStep}} = 25$.

ARGANS Ltd.

2.3. TIME VARYING TABLES

2.3.1. Auxiliary Geophysical Data Processor Tables

2.3.1.1. Physical constants

Several components of the AGDP require physical constants, which are specified in the following table.

Table: Physical Constants and Coefficients Used in the AGDP

Name	Definition	Units	Value
α	Coefficient in denominator of formula for inverse wave age	dl	1.1
g	Gravitational constant	ms ⁻²	9.81
κ	Von Karman constant	dl	0.4

Note: α is noted Fac_omega in DPM

As discussed in the ATBD, the AGDP must compute the height of the lowest model level, and the formula for doing this involved the constants specified in the following table.

Table: a and b Coefficients for Computing Pressure at Lowest Model Level

# of levels	a	b
60	0.000000	.99763012
91	0.003160	.99763000

2.3.1.2. First guess, uncertainty on priors and bias correction

The AGDP will provide to the rest of the processor values of geophysical fields to be used as priors, first guess, and error standard deviation in the iterative retrieval scheme. It is anticipated that during the iterative retrieval the first guess values will be set equal to the prior values. Bias correction will be applied using lookup tables described below. Initially, however, the correction scale factor will be set to 1 and the offset to 0.

2.3.1.3. Scale factor and offset correction for the geophysical parameters used in the iterative retrieval.

It is anticipated that the processor may perform bias removal for the geophysical parameters used in the iterative retrieval. Bias removal consists of first subtracting an offset from the original the data and then dividing the result by a scale factor. Both scale factor and offset may vary in space and time of year and are provided in lookup tables.

For all parameters, the scale factor and offset LUT is dimensioned as summarized in the following table. Each geophysical parameter will have its own instance of an AGDPT, with the parameter name in the first field. The operational processor will ignore any AGDPT's in the job order. The prototype processor will read a hidden switch (Ignore_AGDP) which can be used to disable reading of the AUX_AGDPT_ tables. The table below lists the start & end values for selected geophysical parameters that may be used to create AGDPTs.

Table: Lookup Tables for Bias Removal

LUT Dimension	Starting Value	Ending Value	Interval	Number of Values
Latitude	-90°N	90°N	1°	181
Longitude	0°E	360°E	1°	361
Time of year	January	December	1 month	12
MSQS (Mean square slope)	0	0.05	variable	16
omega (Inverse wave age)	1	12	variable	16
phi_WSn (Wind direction)	0°	360°	5°	16
SSS	30 psu	40 psu	variable	16
SST	0°C	30 °C	variable	16
U* (Friction velocity from surface layer module)	0 m/s	1 m/s	0.1	16
WSn (10 m NE wind speed prior to adjustment)	0 m/s	30 m/s	variable	16
UN10 (10 metre neutral equivalent wind – zonal component)	0 m/s	30 m/s	variable	16

VN10 (10 metre neutral equivalent wind – meridional component)	0 m/s	30 m/s	variable	16
TEC	0 TECu	80 TECu	variable	16
HS (Wave Height)	0	15m	1m	16
Acard	0	70	variable	16

LUTs for bias removal will be provided in MATLAB files with the following contents:

MATLAB variable name	Definition	Units	Number of values	Number of bytes per value	Total number of bytes
lat	Latitude	degN	181	4	724
lon	Longitude	degE	361	4	1444
month	Month of year: 1=January, 12=december	dl	12	4	48
parameter	Original parameter values	dl	16	4	64
scale_factor	Data scale factor relative to true value	dl	12545472	4	50181888
offset	Data offset relative to true value	dl	12545472	4	50181888
sigma_abs	Absolute error standard deviation	dl	12545472	4	50181888
sigma_rel	Relative error standard deviation	dl	12545472	4	50181888
first	First guess	dl	12545472	4	50181888

The scale factor values in these LUTs will be initially set to 1 everywhere, and the offset will be set to 0 everywhere. It is anticipated that these values may change during commissioning.

2.3.2. Ocean Target Transformation Tables

ESL analysis of L1c and L2OS during commissioning showed that TBs from L2 forward models do not match those from L1c input products. The mismatch appears to be systematic in the xi-eta antenna frame, at least in regions far from land, such as the Pacific Ocean. To correct for these errors for the L2OS processor to retrieve salinity, ESL proposed, and ESA agreed that **ARGANS Ltd.**

an Ocean Target Transformation should be generated and applied to L1c TBs during L2OS processing. Each OTT contains TB offsets in a 2D array in xi/eta: during processing the L1c TBs are transformed into the xi/eta frame and the offset applied:

$$Tb \text{ used for retrieval} = L1c \text{ Tb} - OTT \text{ offset}$$

As described in Annex 4 of the ATBD, OTT are generated by running the OTT post-processor (OSCOTT) on a set of current deltaTBs (from AUX_DTBCUR) and new deltaTB ADFs (AUX_DTBXY_). Details of the format for AUX_OTTxF_ (and AUX_DTBXY_/AUX_DTBCUR) are given in the IODD. The L2OS processor and OTT post-processor selects data for OTT computation according to parameters in the following table:


Name	Value	Units	Comments
Max_OTT_orbits	10	dl	Maximum number of orbits used by OSCOTT to compute OTTs per orbit direction
Min_Snapshots	10	dl	Minimum number of valid snapshots below which deltaTBs from AUX_DTBXY_ are ignored
L1_Software_Errors_Max_Percent	2	%	Maximum % of valid snapshots flagged by L1 with software errors above which deltaTBs from AUX_DTBXY_ are ignored
L1_Instrument_Errors_Max_Percent	2	%	Maximum % of valid snapshots flagged by L1 with instrument errors above which deltaTBs from AUX_DTBXY_ are ignored
L1_ADF_Errors_Max_Percent	2	%	Maximum % of valid snapshots flagged by L1 with ADF errors above which deltaTBs from AUX_DTBXY_ are ignored
L1_Calibration_Errors_Max_Percent	2	%	Maximum % of valid snapshots flagged by L1 with calibration errors above which deltaTBs from AUX_DTBXY_ are ignored
TBs_Out_Of_Range_Max_Percent	5	%	Maximum % of valid snapshots flagged by L2 with TBs out-of-range above which deltaTBs from AUX_DTBXY_ are ignored

ARGANS Ltd.

Commercial in Confidence

Page 63

Use, duplication, or disclosure of this document or any information contained herein is subject to the restriction on the title page of this document.

	<p style="text-align: center;">SMOS L2 OS Table Generation Requirements Document</p>	<p>Doc: SO-TN-ARG-GS-0014 Issue: 3 Rev: 18 Date: 16 March 2021 Page: 64</p>
---	--	---

High_Std_Max_Percent	30	%	Maximum % of valid snapshots flagged by L2 as high std above which deltaTBs from AUX_DTBXY_ are ignored
High_Std_Stokes3_Max_Percent	60	%	Maximum % of valid snapshots flagged by L2 as high std Stokes 3 above which deltaTBs from AUX_DTBXY_ are ignored
High_Std_Stokes4_Max_Percent	15	%	Maximum % of valid snapshots flagged by L2 as high std Stokes 4 above which deltaTBs from AUX_DTBXY_ are ignored
Min_Measurements	1000	dl	Minimum number of valid measurements below which deltaTBs from AUX_DTBXY_ are ignored
L1_Sun_Tails_Max_Percent	40	%	Maximum % of valid measurements flagged by L1 as sun tails above which deltaTBs from AUX_DTBXY_ are ignored
Sun_Glint_Max_Percent	35	%	Maximum % of valid measurements flagged by L1 or L2 as sun glint above which deltaTBs from AUX_DTBXY_ are ignored
Moon_Glint_Max_Percent	1	%	Maximum % of valid measurements flagged by L2 as moon glint above which deltaTBs from AUX_DTBXY_ are ignored
L2_Gal_Noise_Max_Percent	50	%	Maximum % of valid measurements flagged by L2 as galactic noise above which deltaTBs from AUX_DTBXY_ are ignored
L1_RFI_Max_Percent	1	%	Maximum % of valid measurements flagged by L1 as RFI above which deltaTBs from AUX_DTBXY_ are ignored
L2_RFI_Max_Percent	1	%	Maximum % of valid measurements flagged by L2 as

ARGANS Ltd.

Commercial in Confidence

Page 64

Use, duplication, or disclosure of this document or any information contained herein is subject to the restriction on the title page of this document.

			RFI above which deltaTBs from AUX_DTBXY_ are ignored
Max_XX_AFFOV_StdRa	2.5	dl	Maximum std/ra in AFFOV XX pol above which deltaTBs from AUX_DTBXY_ are ignored
Max_XX_EAFFOV_StdRa	3.5	dl	Maximum std/ra in EAFFOV XX pol above which deltaTBs from AUX_DTBXY_ are ignored
Max_YY_AFFOV_StdRa	2.5	dl	Maximum std/ra in AFFOV YY pol above which deltaTBs from AUX_DTBXY_ are ignored
Max_YY_EAFFOV_StdRa	4.0	dl	Maximum std/ra in EAFFOV YY pol above which deltaTBs from AUX_DTBXY_ are ignored
Max_Stokes3_AFFOV_StdRa	2.0	dl	Maximum std/ra in AFFOV Stokes3 above which deltaTBs from AUX_DTBXY_ are ignored
Max_Stokes3_EAFFOV_StdRa	3.5	dl	Maximum std/ra in EAFFOV Stokes3 above which deltaTBs from AUX_DTBXY_ are ignored
Max_Stokes4_AFFOV_StdRa	1.5	dl	Maximum std/ra in AFFOV Stokes4 above which deltaTBs from AUX_DTBXY_ are ignored
Max_Stokes4_EAFFOV_StdRa	2.5	dl	Maximum std/ra in EAFFOV Stokes4 above which deltaTBs from AUX_DTBXY_ are ignored
Merge_weight	0.625	dl	Weight to use when merging short XX/YY with long integration time XX/YY OTTs

Two regions are defined for OTT extraction: one for ascending orbit OTTs, and one for descending orbit OTTs. For ascending orbit OTTs:


Name	Value	Units	Comments
ID	9001	dl	Unique region ID
Start_Lat	-45.0	degrees	Region start latitude
End_Lat	-5.0	degrees	Region end latitude
Centre_Long_At_Start_Lat	-116.0	degrees	Region centre longitude at start latitude
Centre_Long_At_End_Lat	-126.0	degrees	Region centre longitude at end latitude

ARGANS Ltd.

Commercial in Confidence

Page 65

Use, duplication, or disclosure of this document or any information contained herein is subject to the restriction on the title page of this document.

	SMOS L2 OS Table Generation Requirements Document	Doc: SO-TN-ARG-GS-0014 Issue: 3 Rev: 18 Date: 16 March 2021 Page: 66
---	--	---

Long_Width	42.0	degrees	Region longitude width
Min_Snapshots	200	dl	Minimum number of snapshots to trigger writing region to AUX_DTBXY_
Min_Percent_Snapshot_Measurements	50	%	Minimum percentage of measurements in a snapshot to trigger writing region to AUX_DTBXY_
Min_Percent_Valid_Snapshots	25	%	Minimum percentage of valid snapshots to trigger writing region to AUX_DTBXY_
Min_Grid_Points	2500	dl	Minimum number of grid points to trigger writing region to AUX_DTBXY_
Min_Percent_Valid_Grid_Points	25	%	Minimum percentage of valid grid points to trigger writing region to AUX_DTBXY_

For descending orbit OTTs:


Name	Value	Units	Comments
ID	9002	dl	Unique region ID
Start_Lat	-45.0	degrees	Region start latitude
End_Lat	-5.0	degrees	Region end latitude
Centre_Long_At_Start_Lat	-128.0	degrees	Region centre longitude at start latitude
Centre_Long_At_End_Lat	-117.0	degrees	Region centre longitude at end latitude
Long_Width	42.0	degrees	Region longitude width
Min_Snapshots	200	dl	Minimum number of snapshots to trigger writing region to AUX_DTBXY_
Min_Percent_Snapshot_Measurements	50	%	Minimum percentage of measurements in a snapshots to trigger writing region to AUX_DTBXY_
Min_Percent_Valid_Snapshots	25	%	Minimum percentage of valid snapshots to trigger

ARGANS Ltd.

Commercial in Confidence

Page 66

Use, duplication, or disclosure of this document or any information contained herein is subject to the restriction on the title page of this document.

	<p style="text-align: center;">SMOS L2 OS Table Generation Requirements Document</p>	<p>Doc: SO-TN-ARG-GS-0014 Issue: 3 Rev: 18 Date: 16 March 2021 Page: 67</p>
---	--	---

			writing region to AUX_DTBXY_
Min_Grid_Points	2500	dl	Minimum number of grid points to trigger writing region to AUX_DTBXY_
Min_Percent_Valid_Grid_Points	25	%	Minimum percentage of valid grid points to trigger writing region to AUX_DTBXY_

2.4. USER PARAMETERS TABLES

2.4.1. Physical constants


Name	Value	Units	Comments	ATBD ref
π	3.14159	dl	Pi	
k_{BC}	$5.67 \cdot 10^{-8}$	Watt.m ⁻² .K ⁻⁴	Stefan-Boltzmann constant	
c	$2.99792 \cdot 10^8$		Speed of light in vacuum	
T0	273.15	K	0 °C expressed in K	
ϵ_0	$8.85419 \cdot 10^{-12}$	F m ⁻¹	Permittivity of vacuum	4.1
ϵ_∞	4.9		High frequency limit of static water dielectric constant	4.1
Omega_sun	$8.2 \cdot 10^{-5}$	strad	Apparent solid angle of the Sun for Sun glint	Omega_sun
TB_gal_mean	3.7	K	Sky background Tb for Galactic Noise model 0	TB_gal_mean
Specific for SMOS				
freq_smos	1.4135	GHz	Central frequency of microwave sensor	
Ω_{smos}	$8.878 \cdot 10^9$	rad/s	Angular frequency of microwave sensor	
λ	0.21	m	Wavelength of microwave sensor	
BD_S	19	MHz	Equivalent SMOS bandwidth	

ARGANS Ltd.

Commercial in Confidence

Page 67

Use, duplication, or disclosure of this document or any information contained herein is subject to the restriction on the title page of this document.

	SMOS L2 OS	Doc: SO-TN-ARG-GS-0014
	Table Generation Requirements Document	Issue: 3 Rev: 18 Date: 16 March 2021 Page: 68

Tilt	33	°	Elevation angle of antenna plane	
δ_{sn}	1.2	s	Acquisition time in dual pol	
g	9.8039	m/s ²	Acceleration of free fall	

2.4.2. Measurement discrimination

Name of parameter	Value	Units	Range	Comments	ATDB ref.
Tg_ice_concentration	30%	dl			3.1
Tg_low_SST_ice	275.15	K			3.1
Tg_suspect_ice%	50%	dl			3.1
Tg_max_rainfall	0.002	m/h			3.1
Tg_high_wind	12	m/s			3.1
Tg_medium_wind	7	m/s			3.1
Tg_low_wind	3	m/s			3.1
Tg_high_SST	298	K			3.1
Tg_medium_SST	291	K			3.1
Tg_low_SST	283	K			3.1
Tg_high_SSS	37	psu			3.1
Tg_medium_SSS	34	psu			3.1
Tg_low_SSS	31	psu			3.1
Tg_swell	0.5	dl			3.1, 3.6
Tg_old_sea	0.8	dl			3.1, 3.6
Tg_young_sea	2.5	dl			3.1, 3.6
Radius_front	35	km			3.1, 3.7
Tg_SST_front	0.02	K/km			3.1, 3.7
Tg_SSS_front	0.02	psu/km			3.1, 3.7
Tg_num_meas_valid	30	dl			3.1
Tg_num_meas_min	16	dl			3.1
Tg_num_meas_outliers_min	16	dl			3.5.1
Tg_num_meas_RFI_outliers_min	16	dl			3.5.2

ARGANS Ltd.

Commercial in Confidence

Page 68


Use, duplication, or disclosure of this document or any information contained herein is subject to the restriction on the title page of this document.



Tg_num_outliers_max%	50%	dl			3.5.1
Tg_num_RFI_max%	33%	dl			3.5.2
Tg_num_RFI_outlier_max%	3%	dl			3.5.2
Tg_current_RFI_max_X%	1%	dl			3.5.2
Tg_current_RFI_max_Y%	1%	dl			3.5.2
Tg_sunlint_max%	10%	dl			3.1
Tg_moonglint_max%	10%	dl			3.1
Tg_gal_noise_max%	10%	dl			3.1
Tm_out_of_range_affov	50	K			3.5
Tm_out_of_range_eaffov	100	K			3.5
Tm_out_of_range_stokes3_affov	50	K			3.5
Tm_out_of_range_stokes3_eaffov	100	K			3.5
Tm_out_of_range_stokes4_affov	50	K			3.5
Tm_out_of_range_stokes4_eaffov	100	K			3.5
Ts_snapshot_out_of_range	20	%			3.5
Ts_meas_min	35	%			3.5
Ts_std	2.5	K			3.5
Ts_std_stokes3	2.5	K			3.5
Ts_std_stokes4	2.5	K			3.5
Tg_resol_max_ocean	100	km			3.2
Tm_DT_ice	20	K			3.2
Tm_high_sun_glint	2	K			3.2
Tm_medium_sun_glint	0.5	K			3.2
Tm_low_sun_glint	0.2	K			3.2
Tm_sun_limit	0.5	K			3.2
Tm_angle_moon	1.5	deg			3.2
Tm_max_gal_noise_error	0.1	K			3.2
Tm_high_gal_noise	4	K			3.2
Tg_WS_gal	2	m/s			3.2
nsig	5	dl			3.4.1
σ Th_model1	0.5	K			3.4.1
σ Tv_model1	0.5	K			3.4.1
σ T3_model1	0.1	K			3.4.1
σ T4_model1	0.1	K			3.4.1
σ Th_model2	0.5	K			3.4.1
σ Tv_model2	0.5	K			3.4.1
σ T3_model2	0.1	K			3.4.1
σ T4_model2	0.1	K			3.4.1
σ Th_model3	0.5	K			3.4.1
σ Tv_model3	0.5	K			3.5.1

ARGANS Ltd.

Commercial in Confidence

	SMOS L2 OS	Doc: SO-TN-ARG-GS-0014
	Table Generation Requirements Document	Issue: 3 Rev: 18 Date: 16 March 2021 Page: 70

$\sigma T3_model3$	0.1	K			3.4.1
$\sigma T4_model3$	0.1	K			3.4.1
σTh_model4	0.5	K			3.4.1
σTv_model4	0.5	K			3.4.1
$\sigma T3_model4$	0.1	K			3.4.1
$\sigma T4_model4$	0.1	K			3.4.1
Tg_TEC_gradient	10	TECu			4.8
RFI_std	1.2	dl			3.4.2
RFI_nsig	3	dl			3.4.2
RFI_c1	6.0	dl			3.4.2
RFI_c2	1.0	dl			3.4.2

2.4.3. Dielectric Constant

2.4.3.1. Klein & Swift

This module uses the Klein and Swift model that is described in ATBD section 4.1.

The values of each parameters are summarised in these table below. If necessary, these values should be modifiable during the commissioning phase.

Name of parameter	Value	Units	Range	Comments	ATDB ref.
m(0)	87.134	dl		constant	eq. 4.1.7
m(1)	-0.1949	dl		constant	eq. 4.1.7
m(2)	-0.01276	dl		constant	eq. 4.1.7
m(3)	0.0002491	dl		constant	eq. 4.1.7
m(4)	1.0	dl		constant	eq. 4.1.7
m(5)	$1.613 \cdot 10^{-5}$	dl		constant	eq. 4.1.7
m(6)	-0.003656	dl		constant	eq. 4.1.7
m(7)	$3.21 \cdot 10^{-5}$	dl		constant	eq. 4.1.7
m(8)	$-4.232 \cdot 10^{-7}$	dl		constant	eq. 4.1.7
t(0)	$1.768 \cdot 10^{-11}$	dl		constant	eq. 4.1.8
t(1)	$-6.086 \cdot 10^{-13}$	dl		constant	eq. 4.1.8
t(2)	$1.104 \cdot 10^{-14}$	dl		constant	eq. 4.1.8
t(3)	$-8.111 \cdot 10^{-17}$	dl		constant	eq. 4.1.8
t(4)	1.0	dl		constant	eq. 4.1.8
t(5)	$2.282 \cdot 10^{-5}$	dl		constant	eq. 4.1.8
t(6)	$-7.638 \cdot 10^{-4}$	dl		constant	eq. 4.1.8
t(7)	$-7.760 \cdot 10^{-6}$	dl		constant	eq. 4.1.8

ARGANS Ltd.

Commercial in Confidence

Page 70

Use, duplication, or disclosure of this document or any information contained herein is subject to the restriction on the title page of this document.

t(8)	1.105 10 ⁻⁸	dl		constant	eq. 4.1.8
s(0)	0.182521	dl		constant	eq. 4.1.9
s(1)	-0.00146192	dl		constant	eq. 4.1.9
s(2)	2.09324 10 ⁻⁵	dl		constant	eq. 4.1.9
s(3)	-1.28205 10 ⁻⁷	dl		constant	eq. 4.1.9
s(4)	0.02033	dl		constant	eq. 4.1.9
s(5)	0.0001266	dl		constant	eq. 4.1.9
s(6)	2.464 10 ⁻⁶	dl		constant	eq. 4.1.9
s(7)	1.849 10 ⁻⁵	dl		constant	eq. 4.1.9
s(8)	-2.551 10 ⁻⁷	dl		constant	eq. 4.1.9
s(9)	2.551 10 ⁻⁸	dl		constant	eq. 4.1.9

References

Klein, L. and Swift, C. (1977). An Improved Model for the Dielectric Constant of Sea Water at Microwave Frequencies. IEEE Transactions on Antennas and Propagation, AP-25(1):104–111.

2.4.3.2. Somaraju and Trumpf

This module uses the Sumaraju and Trumpf model that is described in ATBD section 4.1.4.

The values of each parameter are summarised in the table below.

Name of parameter	Value	Units	Range	Comments	ATDB ref.
f(0)	45.00	dl		constant	4.1.24
f(1)	5.0478e+00	dl		constant	4.1.24
f(2)	-7.0315e-02	dl		constant	4.1.24
f(3)	6.0059e-04	dl		constant	4.1.24
Ms(0)	3.70886e4	dl		constant	4.1.23
Ms(1)	- 8.2168e1	dl		constant	4.1.23
Ms(2)	4.21854e2	dl		constant	4.1.23
Ms(3)	0.00000000174 9069	dl		constant	4.1.23
Ms(4)	0.00000108853 5951	dl		constant	4.1.23
Ms(5)	- 0.00003897269 3320	dl		constant	4.1.23
Ms(6)	0.00322807742 5434	dl		constant	4.1.23
s(0)	2.903602	dl		constant	4.1.16

ARGANS Ltd.

s(1)	8.60700e-2	dl		constant	4.1.16
s(2)	4.738817e-4	dl		constant	4.1.16
s(3)	- 2.9910e-6	dl		constant	4.1.16
s(4)	4.3047e-9	dl		constant	4.1.16
s(5)	37.5109	dl		constant	4.1.16
s(6)	5.45216	dl		constant	4.1.17
s(7)	1.4409e-2	dl		constant	4.1.17
s(8)	1004.75	dl		constant	4.1.17
s(9)	182.283	dl		constant	4.1.17
s(10)	6.9431	dl		constant	4.1.17
s(11)	3.2841	dl		constant	4.1.18
s(12)	-9.9486e-2	dl		constant	4.1.18
s(13)	84.850	dl		constant	4.1.18
s(14)	69.024	dl		constant	4.1.18
s(15)	49.843	dl		constant	4.1.18
s(16)	- 0.2276	dl		constant	4.1.19
s(17)	0.198e-2	dl		constant	4.1.19
s(18)	2.903602	dl		constant	4.1.19
x(0)	5.7230e+00	dl		constant	4.1.25
x(1)	2.2379e-02	dl		constant	4.1.25
x(2)	-7.1237e-04	dl		constant	4.1.25

2.4.4. Foam

As discussed in the ATBD, at wind speeds greater than 12 m/s a non-negligible fraction of the sea surface may be covered by foam, and this foam can have a significant impact on brightness temperatures at L-band. As formulated in the ATBD, the foam impact can be provided in terms of L-band brightness temperature at H and V polarizations over the foam-covered area only.

With this formulation, the total brightness temperature for a given polarization, including non-foam and foam areas, is

$$T_{\text{surface}} = (1-F)(T_{\text{flat}} + T_{\text{rough}}) + T_{\text{foam}},$$

where F is the fraction of the surface covered by a foam layer (either crest of static foam). Thus, the processor requires not only foam brightness temperature but also total foam fractional coverage F. Thus, we provide 3 lookup tables for the foam correction that provide:

- Total foam fractional coverage (including static and crest foam).
- Total foam contribution to brightness temperature at H polarization.
- Total foam contribution to brightness temperature at V polarization.

The foam fractional coverage is a function only of the 10 m wind speed and the difference between the sea surface temperature and the air temperature at 2 m. The foam contribution to brightness temperature is a function of five parameters: SST, SSS, radiometer incidence angle, 10 m wind speed, and the difference between the sea surface temperature and the air temperature at 2 m. The following table summarizes the five dimensions used for the lookup tables.

Dimension	Number of Values	Units	Coordinate Values
SST	20	K	273, 276, 279, 282, 285, 288, 291, 294, 297, 299, 299.5, 300, 300.5, 301, 301.5, 302, 302.5, 303, 304, 306
SSS	22	PSU	0.0, 24.0, 28.0, 30.0, 32.0, 33.0, 33.5, 33.75, 34.0, 34.25, 34.5, 34.75, 35.0, 35.25, 35.5, 35.75, 36.0, 36.25, 36.5, 37.0, 38.0, 40.0
Radiometer incidence angle	28	deg	0, 3, 6, 9, 12, 15, 18, 21, 24, 27, 30, 33, 36, 39, 42, 45, 48, 51, 54, 57, 60, 63, 66, 69, 72, 75, 78, 81
Wind speed at 10 m height	31	m s ⁻¹	0, 1, 2, 3, 4, 5, 6, 7, 8, 9, 10, 11, 12, 13, 14, 15, 16, 17, 18, 19, 20, 21, 22, 23, 24, 25, 26, 27, 28, 29, 30
Air-sea temperature difference ($T_{\text{sea}} - T_{\text{air}}$)	29	K	-30, -20, -18, -16, -14, -12, -10, -8, -6, -5, -4, -3, -2, 1, 0, 1, 2, 3, 4, 5, 6, 8, 10, 12, 14, 16, 18, 20, 30

2.4.4.1. Generation method


As discussed above, there are two main components to the foam model. The first is a foam coverage model and the second is a foam emissivity model.

2.4.4.2. Foam coverage model

As formulated in the ATBD, the incremental foam fractional coverage for both static and crest foam is a function of

- generating breaking front speed c ,
- the 10 m wind speed, and
- the air-sea temperature difference.

Both static and crest foam incremental coverage functions are formulated in terms of a distribution function that yields total length of break crests per unit area per unit breaker speed. This distribution function is a modified form of that derived from measurements of Melville and Matusov (2002),

	<p style="text-align: center;">SMOS L2 OS Table Generation Requirements Document</p>	<p>Doc: SO-TN-ARG-GS-0014 Issue: 3 Rev: 18 Date: 16 March 2021 Page: 74</p>
---	--	---

$$\Lambda(WS, c) = A \left(\frac{WS}{10} \right)^3 \times 3.3 \times 10^{-4} \cdot e^{-.64B \left(\frac{c}{WS} \right)}$$

where A and B and constants to be specified. This distribution function differs from the empirical form of Melville and Matusov (2002) in that the exponent is a function of wave age rather than breaker phase speed.

Using the preceding formulation of the crest length distribution function, we can write the crest and static foam incremental coverages in terms of wind speed and breaker phase speed as

$$dF_c(WS, c) = \left[\frac{2\pi a_1}{g} c^2 \Lambda(WS, c) dc \right] \times e^{(\alpha_s \Delta T - \beta_s)}$$

and

$$dF_s(WS, c) = \left[\frac{2\pi a_2}{g} c^2 \Lambda(WS, c) dc \right] \times e^{(\alpha_s \Delta T - \beta_s)},$$

respectively. The final exponentials in the two previous equations are stability correction factors, which have a significant impact on the foam coverage. The free parameters in these correction factors are given values specified in the following table. The constants a_1 and a_2 in the above equations are constants that reflect the persistence time of the foam layers, which is typically much larger for static than for crest foam.

To compute the total contribution of foam to the measured brightness temperature, we must determine the distribution of foam as a function of characteristic foam thickness, from which time dependence has been removed by assuming that foam layers associated with fronts moving at a given speed have equal probability of being at any stage of development. Using this assumption together with a simple model for the time dependence of foam layer depth, we obtain for crest foam the depth

$$\bar{\delta}_{\tau^*}(c) = \frac{0.4c^2}{g},$$

and for static foam we obtain

$$\bar{\delta}_{\tau}(c) = \frac{0.4c}{2\pi a} \left[\frac{5c}{2g} + \tau' \left(1 - e^{-\frac{c}{g\tau'}(2\pi a - 5)} \right) \right].$$

In the above equations, g is the acceleration of gravity, c is the breaker phase speed, and τ' is the exponential decay time of the foam depth after the mean duration time of the breaking events (nominally taken to be 3.8 s for salt water). These expressions can be used to transform


ARGANS Ltd.

the differential foam coverage expressions into expressions for the incremental coverage per unit thickness. The following table shows the parameter values used in the foam coverage model.

Table: Foam Coverage Model Parameters

Parameter	Purpose	Value	Units
α_c	Factor multiplying sea-air temperature difference in exponential stability correction factor for crest foam	0.198	nd
α_s	Factor multiplying sea-air temperature difference in exponential stability correction factor for static foam	0.0861	nd
β_c	Offset in exponential stability correction factor for crest foam	0.91	nd
β_s	Offset in exponential stability correction factor for static foam	0.38	nd
A	Coefficient multiplying crest length distribution function	0.1	nd
B	Coefficient multiplying exponent in crest length distribution function	10.0	nd
τ'	Exponential decay time of foam after generating breaking event in seconds	3.8	s
a_1	Crest foam persistence time coefficient	0.8	nd
a_2	Static foam persistence time coefficient	5.0	nd

The foam correction will be applied to roughness models 1 and 2 when the wind speed value is above a specified threshold: $Tg_WS_foam_M1 = 100$ m/s and $Tg_WS_foam_M2 = 1$ m/s.

	SMOS L2 OS Table Generation Requirements Document	Doc: SO-TN-ARG-GS-0014 Issue: 3 Rev: 18 Date: 16 March 2021 Page: 76
---	--	---

2.4.5. Galactic Noise bistatic scattering

Bistatic scattering in the SMOS Level 2 Ocean Salinity processor, bistatic scattering coefficients are required for implementing corrections for galactic noise. These coefficients are functions of 6 variables:

- incoming radiation incidence angle
- incoming radiation azimuth angle
- outgoing azimuth angle
- outgoing incidence angle
- wind speed
- wind direction

From LUT size and generation perspectives, it is impractical produce a LUT directly as a function of these variables. In this note we review a revised implementation of the lookup table for bistatic scattering coefficients in which we have separated the dependency on wind direction from the dependencies on other variables, without introducing further approximations.

2.4.5.1 Formulation of scattering coefficients

For the lookup table, the bistatic scattering coefficients of the rough sea surface are estimated using the Small Slope Approximation theory [1]. The lower order-approximation (refer to as the SSA-1) is used here and is appropriate for both large- (the Kirchhoff regime) and small scale (the Bragg regime) roughness within a single theoretical scheme.

To facilitate discussion, we introduce a local cartesian coordinate system $(\hat{x}, \hat{y}, \hat{z})$ with basis vector \hat{x} pointing eastward, basis vector \hat{y} pointing northward, and basis vector \hat{z} pointing upwards normal to the horizontal surface.

Application of the SSA-1 approximation for scattering from the slightly rough ocean surface yields the following expression for a dimensionless bistatic scattering cross section $\sigma_{\alpha\alpha_o}^o$ for scattering of the incoming wave of polarization α_o into the outgoing wave of polarization α :

$$\sigma_{\alpha\alpha_o}(\vec{k}_s, \vec{k}_o) = \frac{1}{\pi} \left| \frac{2q_s q_o}{q_s + q_o} B_{\alpha\alpha_o}(\vec{k}_s, \vec{k}_o) \right|^2 e^{-(q_s + q_o)^2 \rho(0)} \cdot I_K \quad (1)$$

where I_K is often referred to as the Kirchhoff Integral and is given in cartesian coordinates by

$$I_K = \int_{-\infty}^{\infty} \int_{-\infty}^{\infty} \left\{ e^{(q_s + q_o)z} \rho(\vec{x}) - 1 \right\} e^{-i(\vec{k}_s - \vec{k}_o) \cdot \vec{x}} dx dy, \quad (2)$$

where we use the notation \vec{x} to denote the horizontal displacement vector and the integral is

ARGANS Ltd.

evaluated over all possible displacements in the horizontal plane. In Eqs. (1) and (2), (\vec{k}_s, \vec{k}_o) are the scattered and incident wavenumber vectors, $(q_s, q_o) = (\hat{z} \cdot \vec{k}_s, -\hat{z} \cdot \vec{k}_o)$ represents the vertical projection of the wavevectors and the kernel functions $B_{\alpha\alpha_o}(\vec{k}_s, \vec{k}_o)$ are


$$\begin{aligned}
 B_{vv}(\vec{k}_s, \vec{k}_o) &= \frac{\varepsilon - 1}{(\varepsilon q_s^{(1)} + q_s^{(2)})(\varepsilon q_o^{(1)} + q_o^{(2)})} \left[q_s^{(2)} q_o^{(2)} \frac{\vec{k}_s \cdot \vec{k}_o}{|\vec{k}_s| |\vec{k}_o|} - \varepsilon |\vec{k}_s| |\vec{k}_o| \right], \\
 B_{vh}(\vec{k}_s, \vec{k}_o) &= \frac{\varepsilon - 1}{(\varepsilon q_s^{(1)} + q_s^{(2)})(q_o^{(1)} + q_o^{(2)})} \frac{\omega}{c} q_s^{(2)} \frac{\hat{z} \cdot (\vec{k}_s \times \vec{k}_o)}{|\vec{k}_s| |\vec{k}_o|}, \\
 B_{hv}(\vec{k}_s, \vec{k}_o) &= \frac{\varepsilon - 1}{(q_s^{(1)} + q_s^{(2)})(\varepsilon q_o^{(1)} + q_o^{(2)})} \frac{\omega}{c} q_o^{(2)} \frac{\hat{z} \cdot (\vec{k}_s \times \vec{k}_o)}{|\vec{k}_s| |\vec{k}_o|}, \\
 B_{hh}(\vec{k}_s, \vec{k}_o) &= \frac{\varepsilon - 1}{(q_s^{(1)} + q_s^{(2)})(q_o^{(1)} + q_o^{(2)})} \frac{\omega}{c^2} \frac{\vec{k}_s \cdot \vec{k}_o}{|\vec{k}_s| |\vec{k}_o|},
 \end{aligned} \tag{3}$$

where ω is electromagnetic radian frequency (rad/s), c is the speed of light and $q_s^{(1,2)}$, and $-q_o^{(1,2)}$ are the vertical components of the scattered and incoming wavevectors in the first (air) and in the second (sea) medium. $\varepsilon = \varepsilon(\text{SSS}, \text{SST}, f)$ is the sea water dielectric constant at L-band which is a function of sea surface salinity (SSS), sea surface temperature (SST), and the electromagnetic frequency (f). We evaluate this function using the Klein and Swift dielectric constant model at a fixed SSS of 35 PSU and a fixed SST of 15°C. Also,

$$\begin{aligned}
 q_s^{(1)} &= \sqrt{\frac{\omega^2}{c^2} - |\vec{k}_s|^2}, q_s^{(2)} = \sqrt{\varepsilon \frac{\omega^2}{c^2} - |\vec{k}_s|^2}, \text{Im} q_s^{(1,2)} \geq 0, \\
 q_o^{(1)} &= \sqrt{\frac{\omega^2}{c^2} - |\vec{k}_o|^2}, q_o^{(2)} = \sqrt{\varepsilon \frac{\omega^2}{c^2} - |\vec{k}_o|^2}, \text{Im} q_o^{(1,2)} \geq 0.
 \end{aligned} \tag{4}$$

The incoming and scattered wavevectors cartesian components can be written as follows:

$$\begin{aligned}
 k_{ox} &= -|\vec{k}_o| \sin \theta_o \cos \phi_o = -K_o \sin \theta_o \cos \phi_o, \\
 k_{sx} &= |\vec{k}_s| \sin \theta_s \cos \phi_s = K_o \sin \theta_s \cos \phi_s, \\
 k_{oy} &= -|\vec{k}_o| \sin \theta_o \sin \phi_o = -K_o \sin \theta_o \sin \phi_o, \\
 k_{sy} &= |\vec{k}_s| \sin \theta_s \sin \phi_s = K_o \sin \theta_s \sin \phi_s, \\
 k_{oz} &= -|\vec{k}_o| \cos \theta_o = -K_o \cos \theta_o, \\
 k_{sz} &= |\vec{k}_s| \cos \theta_s = K_o \cos \theta_s, \\
 q_o &= |\vec{k}_o| \cos \theta_o = K_o \cos \theta_o, \\
 q_s &= |\vec{k}_s| \cos \theta_s = K_o \cos \theta_s,
 \end{aligned} \tag{5}$$

	<p style="text-align: center;">SMOS L2 OS Table Generation Requirements Document</p>	<p>Doc: SO-TN-ARG-GS-0014 Issue: 3 Rev: 18 Date: 16 March 2021 Page: 78</p>
---	--	---

where $K_0 = \frac{2\pi}{\lambda_0} = \frac{2\pi f}{c}$ is the free space electromagnetic wavenumber, $f = 1.413 \times 10^9$ Hz is the electromagnetic frequency at L-band, λ_0 (m) is the free space electromagnetic wavelength, $c = 3 \times 10^8$ m s⁻¹ is the free space speed of light, θ_o and θ_s are the incoming and scattered radiation incidence angles, and φ_o and φ_s are the incoming and scattered radiation azimuth angles. The minus sign is introduced in the definition of the incoming wavevector because in our convention the azimuth and incidence angles are determined from the perspective of an observer looking outward from the origin towards both the incoming and outgoing radiation, and the incoming wavevector is directed towards the origin while the scattered wavevector is directed away from the origin. Note, however, that q_p , which enters into the Kirchhoff diffraction integral, is defined to be minus the vertical component of the incoming wavevector, so that it is always nonnegative.

The surface correlation function $\rho(\vec{x})$ is defined by the relation:

$$\langle \exp[iQ(h(\vec{x}_1) - h(\vec{x}_2))] \rangle = \exp[-Q^2(\rho(0,0) - \rho(\vec{x}_1 - \vec{x}_2))], \quad (6)$$

where $\langle \cdot \rangle$ is the ensemble averaging operator that averages over the (assumed) spatially homogeneous statistical ensemble of sea surface roughness, described by the surface elevation function $h(\vec{x})$, and $Q = q_s + q_o$. If the sea surface elevation function is assumed to be a Gaussian random process, then ρ represents the correlation function of the surface elevation and can be expressed strictly in terms of the inverse Fourier transform of the roughness spectrum:

$$\rho(x, y) = \int_{-\infty}^{\infty} \int_{-\infty}^{\infty} W(\xi_x, \xi_y) e^{i\vec{\xi} \cdot \vec{x}} d\xi_x d\xi_y, \quad (7)$$

where $W(\xi_x, \xi_y)$ is the directional wavenumber spectrum of the rough sea surface as a function of surface wavenumber vector in cartesian number wavespace $\vec{\xi} = (\xi_x, \xi_y)$. In the present work, the sea surface elevation function is assumed to be a Gaussian random process and ρ is obtained from the inverse Fourier transform of the sea surface spectrum as computed using the model of Kudryavtsev al. [1999]. This wave model produces a spectrum that depends on 10 m wind speed u_{10} and the inverse wave age Ω , so that


$$W = W(\xi_x, \xi_y; u_{10}, \Omega). \quad (8)$$

The correlation function can be written more explicitly as

$$\rho(x, y; u_{10}, \Omega) = \int_{-\infty}^{\infty} \int_{-\infty}^{\infty} W(\xi_x, \xi_y; u_{10}, \Omega) e^{i\vec{\xi} \cdot \vec{x}} d\xi_x d\xi_y, \quad (9)$$

For the lookup table generation, we fix the inverse wave age to $\Omega = 0.83$ and vary the wind speed, so that the spectrum is a function only of the surface wavevector and 10 m wind speed:

ARGANS Ltd.

	SMOS L2 OS Table Generation Requirements Document	Doc: SO-TN-ARG-GS-0014 Issue: 3 Rev: 18 Date: 16 March 2021 Page: 79
---	--	---

$$W = W(\xi_x, \xi_y; u_{10}), \quad (10)$$

and

$$\rho(x, y; u_{10}) = \int_{-\infty}^{\infty} \int_{-\infty}^{\infty} W(\xi_x, \xi_y; u_{10}) e^{i\xi_x x + i\xi_y y} d\xi_x d\xi_y, \quad (11)$$

For simplicity, wind speed dependence is assumed, and we refer to the spectrum using the notation $W(\xi_x, \xi_y)$, and we refer to the corresponding correlation function by $\rho(x, y)$. Also, since the directional wavenumber spectrum exhibits simpler structure in polar coordinates than in cartesian coordinates, and since the electromagnetic scattering problem is naturally expressed in spherical coordinates, it is expedient to introduce polar coordinates for both physical space and surface wavenumber space. In physical space we have

$$x = r \cos \Phi; y = r \sin \Phi, \quad (12)$$

while in surface wavenumber space we have

$$\xi_x = \xi \cos \Phi_w; \xi_y = \xi \sin \Phi_w. \quad (13)$$

The Jacobian of the above transformation in wavenumber space is

$$J(\xi, \Phi_w) = \frac{\partial(\xi_x, \xi_y)}{\partial(\xi, \Phi_w)} = \begin{vmatrix} \left(\frac{\partial \xi_x}{\partial \xi}\right) & \left(\frac{\partial \xi_x}{\partial \Phi_w}\right) \\ \left(\frac{\partial \xi_y}{\partial \xi}\right) & \left(\frac{\partial \xi_y}{\partial \Phi_w}\right) \end{vmatrix} = \xi, \quad (14)$$

and so the integral expression for the correlation function becomes, after transforming coordinates,

$$\rho(r, \Phi) = \int_0^{\infty} \int_0^{2\pi} W_p(\xi, \Phi_w) e^{ir\xi[\cos(\Phi) \cos(\Phi_w) + \sin(\Phi) \sin(\Phi_w)]} \xi d\Phi_w d\xi, \quad (15)$$

or, after applying a trigonometric identity,

$$\rho(r, \Phi) = \int_0^{\infty} \int_0^{2\pi} W_p(\xi, \Phi_w) e^{ir\xi \cos(\Phi - \Phi_w)} \xi d\Phi_w d\xi, \quad (16)$$

where W_p is the wave spectrum in polar coordinates and ρ now represents the correlation function in polar coordinates. Using the Bessel function identity

$$e^{ib \cos \theta} = \sum_{n=-\infty}^{\infty} i_n J_n(b) e^{in\theta} = J_0(b) + 2 \sum_{n=1}^{\infty} i_n J_n(b) \cos(n\theta), \quad (17)$$

we can rewrite the previous expression for the correlation function as

ARGANS Ltd.

$$\rho(r, \Phi) = \int_0^\infty \int_0^{2\pi} W_p(\xi, \Phi_w) \sum_{n=-\infty}^{\infty} i_n J_n(r\xi) e^{in(\Phi - \Phi_w)} \xi d\Phi_w d\xi, \quad (18)$$

or

$$\rho(r, \Phi) = \sum_{n=-\infty}^{\infty} i_n \int_0^\infty \left[\int_0^{2\pi} W_p(\xi, \Phi_w) e^{in(\Phi - \Phi_w)} \xi d\Phi_w \right] J_n(r\xi) d\xi, \quad (19)$$

or

$$\rho(r, \Phi) = \int_0^\infty \left[\int_0^{2\pi} W_p(\xi, \Phi_w) \xi d\Phi_w \right] J_0(r\xi) d\xi + 2 \sum_{n=1}^{\infty} i_n \int_0^\infty \left[\int_0^{2\pi} \xi W_p(\xi, \Phi_w) \cos n(\Phi - \Phi_w) d\Phi_w \right] J_n(r\xi) d\xi, \quad (20)$$

For gaussian statistics, the wave spectrum has only even azimuthal harmonics, and in the remaining development we suppose that azimuthal structure of the wave spectrum can be represented entirely by wavenumbers 0 and 2. Moreover, we assume that the spectrum is symmetric about the wind direction ϕ_w , so that the surface spectrum can be written as

$$W_p(\xi, \Phi_w) = \frac{1}{2\pi\xi} W(\xi) [1 + \Delta(\xi) \cos 2(\Phi_w - \phi_w)], \quad (21)$$

where $W(\xi)$ is called the omnidirectional spectrum and $\Delta(\xi)$ is called the upwind-crosswind ratio for the spectrum. With this form for the spectrum, it is seen that

$$\int_0^\infty \left[\int_0^{2\pi} W_p(\xi, \Phi_w) \xi d\Phi_w \right] J_0(r\xi) d\xi = \frac{1}{2\pi} \int_0^\infty W(\xi) \int_0^{2\pi} J_0(r\xi) d\Phi_w = \int_0^\infty W(\xi) J_0(r\xi) d\xi. \quad (22)$$


Also, with the assumed form for the spectrum, only the term corresponding to $n = 2$ contributes in the sum in (20), and so

$$\begin{aligned} & 2 \sum_{n=1}^{\infty} i_n \int_0^\infty \left[\int_0^{2\pi} \xi W_p(\xi, \Phi_w) \cos n(\Phi - \Phi_w) d\Phi_w \right] J_n(r\xi) d\xi \\ &= -\frac{1}{\pi} \int_0^\infty W(\xi) \Delta(\xi) \int_0^{2\pi} \cos 2(\Phi_w - \phi_w) \cos 2(\Phi - \Phi_w) J_2(r\xi) d\Phi_w d\xi \\ &= -\frac{1}{\pi} \int_0^\infty W(\xi) \Delta(\xi) \int_0^{2\pi} \cos 2(\Phi_w - \phi_w) \cos 2(\Phi_w - \Phi) J_2(r\xi) d\Phi_w d\xi \end{aligned} \quad (23)$$

Now by a trigonometric identity we have, for arbitrary angles u and v ,

$$\begin{aligned} \cos 2(u - v) &= \cos 2u \cos 2v + \sin 2u \sin 2v, \\ \cos 2(u + v) &= \cos 2u \cos 2v - \sin 2u \sin 2v. \end{aligned} \quad (24)$$

Adding the two preceding equations, we have

	SMOS L2 OS Table Generation Requirements Document	Doc: SO-TN-ARG-GS-0014 Issue: 3 Rev: 18 Date: 16 March 2021 Page: 81
---	--	---

$$\cos 2 u \cos 2 v = \frac{1}{2} (\cos 2 (u - v) + \cos 2 (u + v)). \quad (25)$$

Letting $u = \Phi_w - \phi_w$ and $v = \Phi_w - \Phi$ we obtain

$$\cos 2 (\Phi_w - \phi_w) \cos 2 (\Phi_w - \Phi) = \frac{1}{2} (\cos 2 (\Phi - \phi_w) + \cos 2 (2\Phi_w - \Phi - \phi_w)). \quad (26)$$

so then Eq. (23) becomes

$$\begin{aligned} & 2 \sum_{n=1}^{\infty} i^n \int_0^{\infty} \left[\int_0^{2\pi} \xi W_p(\xi, \Phi_w) \cos n(\Phi - \Phi_w) d\Phi_w \right] J_n(r\xi) d\xi \\ &= -\frac{1}{2\pi} \int_0^{\infty} W(\xi) \Delta(\xi) \int_0^{2\pi} [\cos 2(\Phi - \phi_w) + \cos 2(2\Phi_w - \Phi - \phi_w)] J_2(r\xi) d\Phi_w d\xi \\ &= -\frac{1}{2\pi} \int_0^{\infty} W(\xi) \Delta(\xi) \int_0^{2\pi} \cos 2(\Phi - \phi_w) J_2(r\xi) d\Phi_w d\xi = -\int_0^{\infty} W(\xi) \Delta(\xi) \cos 2(\Phi - \phi_w) J_2(r\xi) d\xi \\ &= -\cos 2(\Phi - \phi_w) \int_0^{\infty} W(\xi) \Delta(\xi) J_2(r\xi) d\xi. \end{aligned}$$

Thus, the final expression for the correlation function in polar coordinates reduces to

$$\rho(r, \Phi) = \int_0^{\infty} W(\xi) J_0(r\xi) d\xi - \cos 2(\Phi - \phi_w) \int_0^{\infty} W(\xi) \Delta(\xi) J_2(r\xi) d\xi. \quad (27)$$

We now define

$$\begin{cases} \rho_0(r) = \int_0^{\infty} W(\xi) J_0(r\xi) d\xi \\ \rho_2(r) = \int_0^{\infty} W(\xi) \Delta(\xi) J_2(r\xi) d\xi \end{cases} \quad (28)$$

Using these definitions, the correlation function can be written as

$$\rho(r, \Phi) = \rho_0(r) - \rho_2(r) \cos 2 (\Phi - \phi_w), \quad (29)$$

where ϕ_w is the wind direction (towards which the wind is blowing), and where the isotropic part is given by $\rho_0(r)$ and the anisotropic azimuthal wavenumber 2 part is given by $\rho_2(r)$.

Returning now to the Kirchoff Integral, recall that in cartesian coordinates, we have

$$I_K = \int_{-\infty}^{\infty} \int_{-\infty}^{\infty} \left\{ e^{[(q_s + q_o)z] - 1} \right\} e^{-i(\vec{k}_s - \vec{k}_o) \cdot \vec{x}} dx dy. \quad (30)$$

We now transform the preceding equation into polar coordinates, just as we did for the correlation function. Introducing the following notation

ARGANS Ltd.

$$\begin{aligned} \vec{q} &= \vec{k}_s - \vec{k}_o = q_{Hx}\hat{x} + q_{Hy}\hat{y} + q_z\hat{z} \\ \Phi_{si} &= \tan^{-1}(q_{Hy}/q_{Hx}), \\ q_H &= |q_{Hx}\hat{x} + q_{Hy}\hat{y}|, \end{aligned} \quad (31)$$

we can write

$$(\vec{k}_s - \vec{k}_o) \cdot \vec{x} = q_H r \cos(\Phi - \Phi_{si}), \quad (32)$$

and so the Kirchhoff Integral in polar coordinates becomes

$$I_K = \int_0^\infty \int_0^{2\pi} \left\{ e^{[q_z^2 \rho_0(r) - q_z^2 \rho_2(r) \cos 2(\Phi - \phi_w)] - 1} e^{-iq_H r \cos(\Phi - \Phi_{si})} r d\Phi dr, \quad (33)$$

where we have used the harmonic representation of the correlation function in polar coordinates. If we now define

$$\begin{cases} I_{\Phi_1}(r) = \frac{1}{2\pi} \int_0^{2\pi} e^{-a(r)\cos 2(\Phi - \phi_w) - ib(r)\cos(\Phi - \Phi_{si})} d\Phi, \\ I_{\Phi_2}(r) = \frac{1}{2\pi} \int_0^{2\pi} e^{-ib(r)\cos(\Phi - \Phi_{si})} d\Phi, \end{cases} \quad (34)$$

where $a(r) = q_z^2 \rho_2(r)$ and $b(r) = q_H r$, then we can write

$$I_K = 2\pi \int_0^\infty [I_{\Phi_1}(r) e q_z^2 \rho_0(r) + I_{\Phi_2}(r)] r dr. \quad (35)$$

We now introduce the following identities


$$e^{-a \cos 2(\Phi - \phi_w)} = \sum_{m=-\infty}^{\infty} i_m J_m(ia) e^{2im(\Phi - \phi_w)} = J_0(ia) + 2 \sum_{m=1}^{\infty} i_m J_m(ia) \cos 2m(\Phi - \phi_w), \quad (36)$$

and

$$e^{-ib \cos(\Phi - \Phi_{si})} = \sum_{n=-\infty}^{\infty} i_n J_n(b) e^{in(\Phi - \Phi_{si})} = J_0(b) + 2 \sum_{n=1}^{\infty} i_n J_n(b) \cos n(\Phi - \Phi_{si}), \quad (37)$$

where J_m is the Bessel function of the first kind and order m . Substituting ((36)) and ((37)) into ((34)) and performing the integration over Φ , we obtain

$$I_{\Phi_1}(r) = J_0(ia) J_0(b) + 2 \sum_{m=1}^{\infty} \sum_{n=1}^{\infty} \delta(2m-n) J_m(ia) J_n(b) i_{m+n} \cos n(\Phi_{si} - \phi_w) \quad (38)$$

	SMOS L2 OS Table Generation Requirements Document	Doc: SO-TN-ARG-GS-0014 Issue: 3 Rev: 18 Date: 16 March 2021 Page: 83
---	--	---

where δ is the Dirac function. Using the relation $J_m(ia) = i^m I_m(a)$ where I_m denotes the modified Bessel function of the first kind and order m , we obtain:

$$I_{\Phi_1}(r) = I_0(a)J_0(b) + 2 \sum_{m=1}^{\infty} I_m(a)J_{2m}(b) \cos 2m(\Phi_{si} - \varphi_w). \quad (39)$$

For $I_{\Phi_2}(r)$, we have

$$I_{\Phi_2}(r) = \frac{1}{2\pi} \int_0^{2\pi} e^{-ib \cos(\Phi - \Phi_{si})} d\Phi = \frac{1}{2\pi} \int_0^{2\pi} \left[J_0(b) + 2 \sum_{n=1}^{\infty} J_n(b) \cos n(\Phi - \Phi_{si}) \right] d\Phi = J_0(b). \quad (40)$$

The formulation (35) for the Kirchhoff Integral allows calculation of bistatic scattering coefficients using a single numerical integration over the radial distance instead of four as with a cartesian coordinate formulation.

2.4.5.2 Lookup table implementation

Recalling the expressions for $I_{\Phi_1}(r)$ and $I_{\Phi_2}(r)$, we can write the Kirchhoff Integral as

$$I_K = 2\pi \int_0^{\infty} J_0(q_H r)(r) r dr + 2\pi \int_0^{\infty} \left[I_0(a)J_0(b) + 2 \sum_{m=1}^{\infty} I_m(a)J_{2m}(b) \cos 2m(\Phi_{si} - \varphi_w) \right] e^{iq_z^2 \rho_0(r)} r dr \quad (41)$$

or

$$I_K = 2\pi \int_0^{\infty} \left[J_0(q_H r)(r) + I_0(a)J_0(b) e^{iq_z^2 \rho_0(r)} \right] r dr + \sum_{m=1}^{\infty} I_K^m \cos 2m(\Phi_{si} - \varphi_w), \quad (42)$$

where, for m from 1 to ∞ ,

$$I_K^m = 4\pi \int_0^{\infty} I_m(a)J_{2m}(b) e^{iq_z^2 \rho_0(r)} r dr, \quad (43)$$

is the coefficient of harmonic $2m$ in a cosine series decomposition of the Kirchhoff Integral. If we further let

$$I_K^0 = 2\pi \int_0^{\infty} \left[J_0(q_H r)(r) + I_0(a)J_0(b) e^{iq_z^2 \rho_0(r)} \right] r dr \quad (44)$$

then we see that

$$I_K = I_K(\Phi_{si} - \varphi_w) = \sum_{m=0}^{\infty} I_K^m \cos 2m(\Phi_{si} - \varphi_w). \quad (45)$$

Recalling the expression for the bistatic scattering coefficients,

ARGANS Ltd.

$$\sigma_{\alpha\alpha_0}(\vec{k}_s, \vec{k}_o) = \frac{1}{\pi} \left| \frac{2q_s q_o}{q_s + q_o} B_{\alpha\alpha_0}(\vec{k}_s, \vec{k}_o) \right|^2 e^{-(q_s + q_o)^2 \rho(0)} \cdot I_K \quad (46)$$

we see that we can incorporate the polarization-dependent coefficients multiplying the Kirchhoff Integral into the sum over the Kirchhoff Integral harmonics. Doing so, we obtain harmonic decompositions of the bistatic scattering coefficients, so that we can write

$$\sigma_{\alpha\alpha_0}(\vec{k}_s, \vec{k}_o, u_0, \phi_w) = \sum_{m=0}^{\infty} \sigma_{\alpha\alpha_0}^m(\vec{k}_s, \vec{k}_o) \cos 2m(\Phi_{si} - \phi_w), \quad (47)$$

where we have explicitly included the dependence of the final scattering coefficients on the wind speed u_0 and wind direction ϕ_w (towards which the wind is blowing), and where


$$\sigma_{\alpha\alpha_0}^m(\vec{k}_s, \vec{k}_o) = \frac{1}{\pi} \left| \frac{2q_s q_o}{q_s + q_o} B_{\alpha\alpha_0}(\vec{k}_s, \vec{k}_o) \right|^2 e^{-(q_s + q_o)^2 \rho(0)} \cdot I_K^m \quad (48)$$

Note that the scattering coefficient harmonics are independent of wind direction. Moreover, these harmonics only depend on the incoming and scattered radiation incidence angles, the wind speed, and difference between the incoming and scattered radiation azimuth angles. Thus, switching from vector notation to angles, we can write the scattering coefficients as

$$\sigma_{\alpha\alpha_0}(\theta_o, \phi_o, \phi_s, \theta_s, u_0, \phi_w) = \sum_{m=0}^{\infty} \sigma_{\alpha\alpha_0}^m(\theta_o, \phi_o - \phi_s, \theta_s, u_0) \cos 2m(\Phi_{si} - \phi_w), \quad (49)$$

where θ_o is the incoming radiation incidence angle, ϕ_o is the incoming radiation azimuth angle, θ_s is the scattered radiation incidence angle. As defined previously, ϕ_w is the wind direction (towards which the wind is blowing) and $\Phi_{si} = \tan^{-1}(q_{Hy}/q_{Hx})$ is a function of the incidence and azimuth angles of the incoming and scattered radiation. Note that Φ_{si} depends upon the absolute radiation azimuth angles and so it is not invariant under a rotation about the vertical axis. This is not a problem for the implementation, however, since a change in the absolute radiation azimuth angles with no change in the difference between them requires only a re-evaluation of Φ_{si} and the harmonic sum and not a re-interpolation from the harmonic coefficient lookup table. This point can be important for optimization methods that attempt to reduce the number of interpolations.

As an example, if one is considering the impact of galactic noise on radiometer measurements, and one wishes to examine the change in impact as the radiometer is rotated in look azimuth while all other angles remain the same, then there is no need to re-interpolate bistatic

	SMOS L2 OS Table Generation Requirements Document	Doc: SO-TN-ARG-GS-0014 Issue: 3 Rev: 18 Date: 16 March 2021 Page: 85
---	--	---

harmonics. Instead, one can just rotate both incoming and scattered radiation azimuth angles and recompute the sum over the harmonics. The result is a significant increase in processing efficiency.

In the lookup table we provide the harmonic coefficients $\sigma_{\alpha\alpha_0}^m(\theta_o, \varphi_s - \varphi_o, \theta_s, u_{10})$ for even azimuthal wavenumbers 0 through 10 on a discrete grid. A breadboard C++ MEX code `bistaticHarmonics_SSA1_KA.cc` interpolates from that grid using cubic Hermite interpolation in all four dimensions, and from this routine one obtains the coefficients

$$\sigma_{\alpha\alpha_0}^m(\theta_o, \varphi_s - \varphi_o, \theta_s, u_{10}). \quad (50)$$

As a final step, the C++ MEX code `bistaticCoefficients_SSA1_KA.cc` implements the sum over the harmonics, given specific values for the incoming and scattered azimuths and wind direction. As it has been found that only the first few harmonics contribute significantly to the scattering coefficients, the sum is over only the first six even harmonics (including wavenumber 0), so the code computes

$$\sigma_{\alpha\alpha_0}(\theta_o, \phi_s, \phi_o, \theta_s, u_{10}, \varphi_w) = \sum_{m=0}^5 \sigma_{\alpha\alpha_0}^m(\theta_o, \phi_s - \phi_o, \theta_s, u_{10}) \cos 2m(\Phi_{si} - \varphi_w). \quad (51)$$

Here, as discussed before, the angle Φ_{si} is the angle of the difference between the scattered and incident wavevectors, and can be written as

$$\Phi_{si}(\theta_o, \phi_s, \phi_o, \theta_s) = \tan^{-1} \left(\frac{q_{Hy}}{q_{Hx}} \right) = \tan^{-1} \left(\frac{\sin \theta_s \sin \phi_s + \sin \theta_o \sin \phi_o}{\sin \theta_s \cos \phi_s + \sin \theta_o \cos \phi_o} \right) \quad (52)$$

where we have used the definition of the difference vector \vec{q}_H to write

$$q_{Hx} = \hat{x} \cdot (\vec{k}_s - \vec{k}_i) = |\vec{k}_s - \vec{k}_i| (\sin \theta_s \cos \varphi_s + \sin \theta_o \cos \varphi_o), \quad (53)$$


and

$$q_{Hy} = \hat{y} \cdot (\vec{k}_s - \vec{k}_i) = |\vec{k}_s - \vec{k}_i| (\sin \theta_s \sin \varphi_s + \sin \theta_o \sin \varphi_o), \quad (54)$$

In the above, the difference corresponds to a sum in terms of angles because we have chosen to use the convention that the azimuth angles for both incoming and scattered wavevectors are determined relative to an observer located at the origin, and the incoming wavevector is directed towards the origin so that the sign must be switched for the incoming wavevector.

It is found that linear interpolation introduces artifacts in all dimensions, but especially in incidence angle dimensions. In the C++ code we have implemented cubic Hermite interpolation in such a way that it is substantially faster than the default MATLAB

ARGANS Ltd.

	<p style="text-align: center;">SMOS L2 OS Table Generation Requirements Document</p>	<p>Doc: SO-TN-ARG-GS-0014 Issue: 3 Rev: 18 Date: 16 March 2021 Page: 86</p>
---	--	---

implementation of the same method. The basic idea behind the method is to ensure continuity of the first derivative of the interpolating function. To accomplish this, a four point stencil along each dimension surrounding the interpolation point is required, so in four dimensions we obtain a 256 point stencil, but the nature of the method is such that one can compute the coefficients once for all harmonics and reuse the weights, saving a large amount of processing time.

To implement the method, we apply the interpolation scheme separately along each of the four LUT dimensions and then combine all the weights into a set of 256 weights. In a given dimension, we consider the four nearest points (i.e., the stencil) surrounding the point at which we desire a value, say x . We assume that these points can be written as x_{k-1} , x_k , x_{k+1} , and x_{k+2} , where x is between x_k and x_{k+1} . Next, we assume that our interpolating function is a cubic of the form

$$p(\mu) = a + b\mu + c\mu^2 + d\mu^3, \quad (55)$$

where

$$\mu = \frac{x - x_k}{x_{k+1} - x_k} \quad (56)$$

and the coefficients depend upon the discrete function values at lookup table grid points. In the actual implementation, for a given interpolation location, a weight for each the four stencil points is computed based on the value of μ , which ranges from 0 to 1. If we define

$$\begin{aligned} a_0 &= 2\mu^3 - 3\mu^2 + 1 \\ a_1 &= \mu^3 - 2\mu^2 + \mu \\ a_2 &= \mu^3 - \mu^2 \\ a_3 &= -2\mu^3 + 3\mu^2 \end{aligned}, \quad (57)$$

then the weights for the four surrounding points are

$$\begin{aligned} w_{k-1} &= -\frac{1}{2}a_1 \\ w_k &= a_0 - \frac{1}{2}a_2 \\ w_{k+1} &= a_3 + \frac{1}{2}a_1 \\ w_{k+2} &= \frac{1}{2}a_2 \end{aligned} \quad (58)$$


and the final expression for the interpolated value at point x is

ARGANS Ltd.

Commercial in Confidence

Page 86

Use, duplication, or disclosure of this document or any information contained herein is subject to the restriction on the title page of this document.

	<p style="text-align: center;">SMOS L2 OS Table Generation Requirements Document</p>	<p>Doc: SO-TN-ARG-GS-0014 Issue: 3 Rev: 18 Date: 16 March 2021 Page: 87</p>
---	--	---

$$p(x) = \sum_{j=k-1}^{k+2} w_j y_j, \quad (59)$$

where y_j are values from the lookup table along the given dimension.

Near boundaries, where the stencil exceeds the boundary of the lookup table, zero normal gradient extrapolation is applied along each of the four LUT dimensions, so that it is assumed that lookup table values extend beyond the table boundaries with the values at the boundaries.

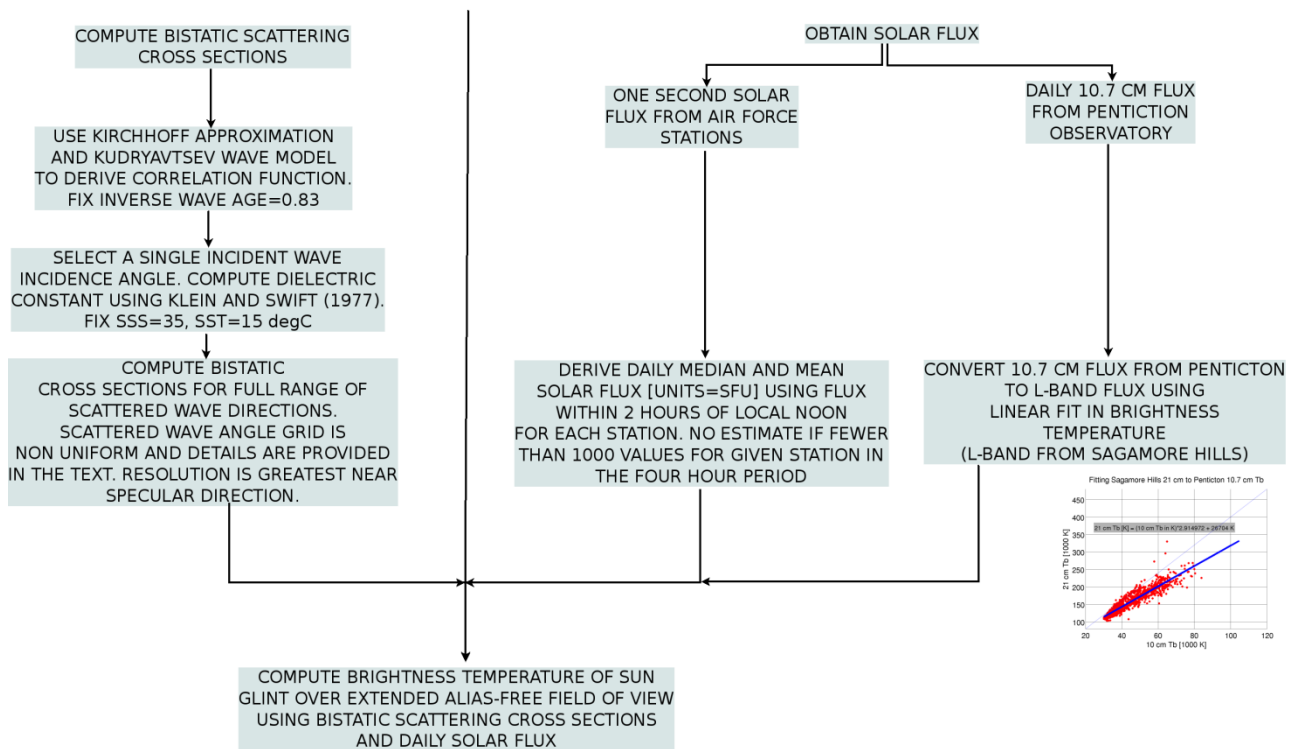
Reference

- [1] A. G. Voronovich, Small-slope approximation in wave scattering by rough surfaces, *Sov. Phys.-JETP*, vol. 62, pp. 65-70, 1985.
- [2] A. G. Voronovich, Small-slope approximation for electromagnetic wave scattering at a rough interface of two dielectric half-spaces, *Waves in Random Media*, vol. 4, pp. 337-367, 1994.

2.4.6. Sun glint

The following sections detail the computation of the sun glint LUTs that are required for the correction.

The diagram below provides an overview of the elements involved in computing the sun glint brightness temperature. The two essential elements required to compute the sun glint are bistatic scattering cross sections for the full range of scattering geometry and the sun brightness temperature at L-band.




The essential elements required are the bistatic scattering cross sections and the solar flux.

2.4.6.1. Bistatic scattering cross-sections

As explained in the ATBD, the scattering cross sections are compute by evaluating the Kirchhoff integral for a surface correlation function derived from the Kudryavtsev wave spectrum. The dielectric constant is obtained from the Klein and Swift 29177 model evaluated at a sea surface temperature of 18 degC and sea surface salinity of 35 psu.

The MATLAB script `pc_kud_cf.m` generates a lookup table of cross sections for one choice of 10-m wind speed and one value for the incoming wave incidence angle θ_o . The script computes the wave spectrum using the Kudryavtsev wave model and from this derives the

	SMOS L2 OS Table Generation Requirements Document	Doc: SO-TN-ARG-GS-0014 Issue: 3 Rev: 18 Date: 16 March 2021 Page: 89
---	--	---

surface correlation function. It then calls the function `coeffbistatic_cf.m` to compute the cross sections.

The structure of the cross-section lookup table is as follows:

```
>> cslut=load('lut.bistatic.kud.cf.ws_all.reduced.grazing_zero.mat')

cslut =    freq: 1.4135e+09 : L-band frequency (Hz)
          sss: 35
          sst: 15
          freq_units: 'Hz'
          sss_units: 'PSU'
          sst_units: 'degC'
          ws_units: 'm/s'
          theta_o_units: 'deg'
          theta_s_units: 'deg'
          phi_s_units: 'deg'
dielectricModel: 'KleinSwift' : dielectric model used to compute cross sections
  theta_o: [1x107 double] : incident wave incidence angle (deg)
  phi_s: [1x261 double] : scattered wave outgoing azimuth relative to incoming azimuth (deg)
  theta_s: [1x107 double] : scattered wave incidence angle (deg)
  ws: [4 5 6 7 10 15 25]
waveModel: 'Kudryavtsev_1999'
sigma_VV_0_ssa1: [4-D single]
sigma_VH_0_ssa1: [4-D single]
sigma_HV_0_ssa1: [4-D single]
sigma_HH_0_ssa1: [4-D single]
```

The following Kirchhoff cross sections are to be used to compute sun glint. Each variable is dimensioned by (wind speed, `theta_o`, `phi_s`, `theta_s`) with angles in degrees:

```
sigma_VV_0_ka: [4-D single]
sigma_VH_0_ka: [4-D single]
sigma_HV_0_ka: [4-D single]
sigma_HH_0_ka: [4-D single]
```

The discretization in incidence angle is not uniform, with an interval of 1 deg from 0 to 86 deg and 0.2 deg from 86 to 90 deg. Grid spacing in azimuth is also not uniform, being 2 deg beyond 30 deg from the specular direction, 1 deg between 10 and 30 deg from specular, and 0.5 deg between 2 and 10 deg from specular, and 0.1 deg within 2 deg of specular. This provides higher resolution near the specular direction where the HH and VV cross sections vary most rapidly.

Given the sun brightness temperature, `tbsun`, 10-m wind speed `tws`, and the scattering geometry, the scattered sun brightness temperatures in H and V polarization in the surface basis, (`Th`,`Tv`) are computed as follows (in MATLAB):

```
css.Mvv_ka = interpn(cslut.gws, cslut.gto, cslut.gps, cslut.gts, squeeze(cslut.sigma_VV_0_ka(:,:,:)), tws, go.theta_o(gind), phi_s, theta_s);
css.Mvh_ka = interpn(cslut.gws, cslut.gto, cslut.gps, cslut.gts, squeeze(cslut.sigma_VH_0_ka(:,:,:)), tws, go.theta_o(gind), phi_s, theta_s);
css.Mhv_ka = interpn(cslut.gws, cslut.gto, cslut.gps, cslut.gts, squeeze(cslut.sigma_HV_0_ka(:,:,:)), tws, go.theta_o(gind), phi_s, theta_s);
```

ARGANS Ltd.

Commercial in Confidence

```
css.Mhh_ka = interpn(cslut.gws, cslut.gto, cslut.gps, cslut.gts, squeeze(cslut.sigma_HH_0_ka(:,:,:)), tws, go.theta_o(gind), phi_s, theta_s);
```

```
css.sh_ka = css.Mhh_ka+css.Mhv_ka;  
css.sv_ka = css.Mvv_ka+css.Mvh_ka;
```

The final brightness temperatures of the sun glint are:

```
tsun_h_ka = double(css.sh_ka(:)./(4*pi*cosd(theta_s(:))*tbsun*sun_solid_angle);  
tsun_v_ka = double(css.sv_ka(:)./(4*pi*cosd(theta_s(:))*tbsun*sun_solid_angle);
```

Note that the interpolation above (MATLAB `interp()`) is linear in all four dimensions.

2.4.6.2. Solar flux LUT

In Appendix A, a list of solar fluxes were compared, listed in Table 5. Although the Penticton data set has the advantage of real-time availability, the rescaling from C-band to L-band is subject to error associated with a slow drift of the scaling factor over time. The 2-minute time series derived using the SMOS brightness temperatures and the forward ocean model generally yields a good correction, but this time time series is not yet complete.

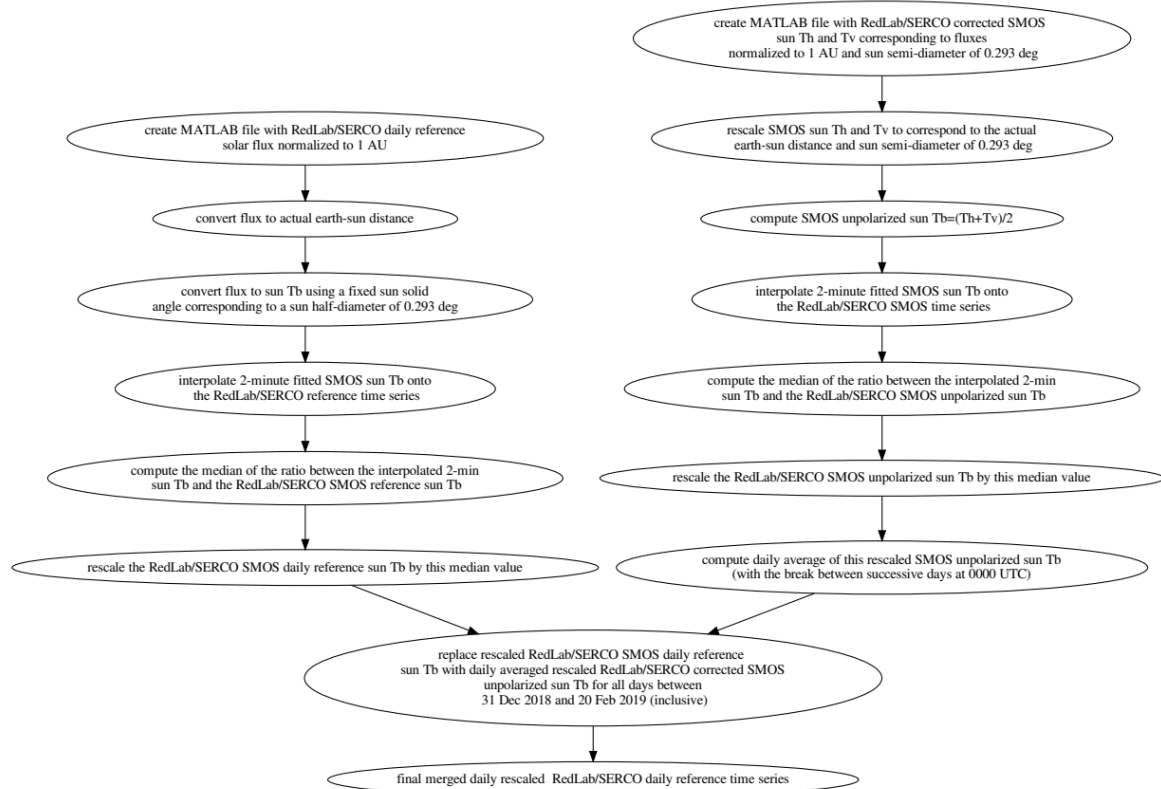


Figure 12: Flowchart showing the steps involved in producing the final daily (unpolarized) sun brightness temperature time series to be used in the Level 2 Ocean Salinity Processor.

Therefore, the time series used in the L2OS Processor is currently derived from a combination of the RedLab/SERCO daily reference (unpolarized) and the RedLab/SERCO corrected SMOS time series (unpolarized). The steps involved in producing the final time series are summarized in Figure 12. In order to obtain results close to what can be achieved using the 2-minute fitted solar flux, both RedLab/SERCO reference and SMOS time series are rescaled by the median ratio between the fitted sun T_b and the RedLab/SERCO sun T_b (unpolarized). The final time series is the RedLab/SERCO reference time series over most of the SMOS mission. The exception to this is the period between 31 December 2018 and 20 February 2019 (inclusive), during which the reference time series is biased due to a reduction in the available reference data.

Therefore, the final time series during this period is set to the daily average of the RedLab/SERCO corrected and rescaled SMOS unpolarized brightness temperature.

2.4.6.2.1.1. Format of the lookup table provided for the Level 2 OS Processor


Table 4 summarizes the format of the lookup table as provided to ARGANS for further reformatting into a file appropriate for use by the L2OS Processor.

Table 4: Solar Flux Lookup Table for the L2OS Processor

field name	definition	units
date	validity day for T_s	MATLAB datenum() format
sun_tb_lband_serco_reference_rescaled	sun T_s	kelvin
rescaling_factor	scale factor	dimensionless
sun_solid_angle_sr	nominal sun solid angle	sr

2.4.7. Switches & Filters

Name of parameter	Value	Units	Comments
Switch_iterative_scheme	true	bool	Switch for skipping iterative scheme (eg when running L2OS just to extract AUX_DTBXY_): true = execute, false = skip
Switch_OTT_AscDes	true	bool	If true use OTT with different LUTs for ascending and descending orbits

	SMOS L2 OS Table Generation Requirements Document	Doc: SO-TN-ARG-GS-0014 Issue: 3 Rev: 18 Date: 16 March 2021 Page: 92
---	--	---


Switch_GN2_AscDes	true	bool	If true use GAL2OS with different LUTs for ascending and descending orbits
Generate_DAP	true	bool	If false, no OSDAP2 is generated; if true, OSDAP2 is written
TEC_OTT_Strategy	2	dl	Strategy for extracting TEC from Stokes3 for OTT/DTBXY generation: 0 = use L1c TEC, 1 = extract for descending orbits only, 2 = extract for both ascending & descending orbits
TEC_Retrieval_Strategy	1	dl	Strategy for extracting TEC from Stokes3 for salinity retrievals: 0 = use L1c TEC, 1 = extract for descending orbits only, 2 = extract for both ascending & descending orbits
Switch_write_OTT	true	bool	If 'true' AUX_DTBXY_ will be generated, if 'false' no AUX_DTBXY_
OTT_Strategy	1	dl	Strategy used by OSCOTT to compute OTTs: 1 = mean, 2= gaussian mean (nominally 1)
OTT_Merge_FP	3	dl	OTT full polarisation merging: 0=no merging, 1=merge long & short XX/YY OTTs, 2=merge cross-pol Stokes 3 & 4 OTTs, 3 = both 1 & 2 (long/short & Stokes3/4)
OTT_Validity_Start	2	dl	Strategy for computing OTT & DTBCUR validity start time: 1 = first snapshot, 2 = mean (last-first snapshot), 3 = last snapshot, 4 = validity start of first snapshot orbit
OTT_Interpolation	1	dl	OTT interpolation option (0=nearest neighbour, 1=bilinear interpolation)
Detect_snapshot_out_of_range	Fg_ctrl_ignore, Fg_sc_land, Fg_sc_coast, Fg_sc_in_clim_ice, Fm_border, Fm_sun_point	filter	Filter applied to grid point and measurements before performing snapshot level out-of-range tests

ARGANS Ltd.

Commercial in Confidence

Page 92

Use, duplication, or disclosure of this document or any information contained herein is subject to the restriction on the title page of this document.

	SMOS L2 OS Table Generation Requirements Document	Doc: SO-TN-ARG-GS-0014 Issue: 3 Rev: 18 Date: 16 March 2021 Page: 93
---	--	---

Detect_snapshot_outliers	Fg_ctrl_ignore, Fg_sc_land, Fg_sc_coast, Fg_sc_in_clim_ice, Fm_EAFFOV, Fm_border, Fm_sun_point, Fm_out_of_range	filter	Filter applied grid point and measurements before performing snapshot level outlier tests based on std/ra
Detect_outliers	Fg_ctrl_ignore, Fg_sc_land, Fg_sc_coast, Fg_sc_in_clim_ice	filter	Filter applied to grid points before performing measurement level outlier tests
Detect_RFI_outliers	Fg_ctrl_ignore, Fg_sc_land, Fg_sc_coast, Fg_sc_near_land	filter	Filter applied to grid points before performing measurement level RFI outlier tests
Detect_measurement_outliers	Fg_ctrl_ignore, Fm_border, Fm_L1c_sun, Fm_L2_RFI_snapshot_out_of_range, Fm_L2_RFI_high_snapshot_std, Fm_L2_RFI_high_snapshot_std_Stokes3, Fm_L2_RFI_high_snapshot_std_Stokes4	filter	Filter applied to measurements before performing measurement level outlier tests
Set_RFI_flag_from_outlier_tests	Fm_L2_RFI_outlier	filter	Set Fm_L2_RFI from RFI outlier tests
Set_RFI_flag_from_snapshot_tests	Fm_out_of_range	filter	Set Fm_L2_RFI from RFI snapshot tests
Set_sun_flag_from_L1c	Fm_sun_glint_fov, Fm_sun_point	filter	Set Fm_L1c_sun measurement flag from L1c flag(s)
Set_RFI_flag_from_L1c	Fm_RFI_tails, Fm_RFI_XX, Fm_RFI_YY, Fm_RFI_point	filter	Set Fm_L1c_RFI measurement flag from L1c flag(s)
Measurement_decision_tree	Fm_resol, Fm_border, Fm_L1c_instrument_error, Fm_L1c_calibration_error	filter	Clear Fm_valid for suspicious measurements
Grid_point_decision_tree	Fg_ctrl_ignore, Fg_sc_land, Fg_sc_coast, Fg_ctrl_num_meas_min, Fg_sc_ice, Fg_ctrl_missing_ECMWF	filter	Clear Fg_ctrl_valid for ignored grid points
Poor_quality	Fg_ctrl_retrieval_failed, Fg_ctrl_range, Fg_ctrl_sigma, Fg_ctrl_chi2, Fg_ctrl_chi2_P, Fg_ctrl_marq, Fg_ctrl_reach_maxiter	filter	Set Fg_ctrl_poor_retrieval if retrieval results flagged as suspicious
Poor_quality_Acard	Fg_ctrl_retrieval_failed, Fg_ctrl_range_Acard, Fg_ctrl_sigma_Acard, Fg_ctrl_chi2, Fg_ctrl_chi2_P, Fg_ctrl_marq, Fg_ctrl_reach_maxiter	filter	Set Fg_ctrl_poor_retrieval for Acard if retrieval results flagged as suspicious



SMOS L2 OS
Table Generation Requirements Document

Doc: SO-TN-ARG-GS-0014
Issue: 3 Rev: 18
Date: 16 March 2021
Page: 94

Poor_geophysical	Fg_ctrl_many_outliers, Fg_ctrl_sunlint, Fg_ctrl_moonglint, Fg_ctrl_num_meas_low, Fg_sc_TEC_gradient, Fg_sc_suspect_ice, Fg_sc_rain, Fg_oor_rough1_ws, Fg_oor_GN1_ra, Fg_oor_GN1_dec, Fg_oor_sunlint_theta_sun, Fg_oor_sunlint_phi, Fg_oor_sunlint_theta, Fg_oor_sunlint_ws, Fg_oor_GN2_dec, Fg_oor_GN2_ra, Fg_oor_GN2_ws, Fg_oor_GN2_theta, Fg_oor_GN2_psi	filter	Set Fg_ctrl_poor_geophysical if geophysical conditions may have contaminated retrievals
Poor_geophysical_Acard	Fg_ctrl_sunlint, Fg_ctrl_moonglint, Fg_ctrl_num_meas_low, Fg_sc_TEC_gradient, Fg_sc_rain, Fg_oor_rough1_ws, Fg_oor_GN1_ra, Fg_oor_GN1_dec, Fg_oor_sunlint_theta_sun, Fg_oor_sunlint_phi, Fg_oor_sunlint_theta, Fg_oor_sunlint_ws, Fg_oor_GN2_dec, Fg_oor_GN2_ra, Fg_oor_GN2_ws, Fg_oor_GN2_theta, Fg_oor_GN2_psi	filter	Set Fg_ctrl_poor_geophysical for Acard if geophysical conditions may have contaminated retrievals
Dg_user	Fm_LO_calibration	filter	Criteria for Dg_user DAP counter
Acard_measurement_decision_tree	Fm_resol, Fm_border, Fm_L1c_instrument_error, Fm_L1c_calibration_error	filter	Clear Fm_valid for suspicious measurements
Acard_grid_point_decision_tree	Fg_ctrl_ignore, Fg_sc_land, Fg_sc_coast, Fg_ctrl_num_meas_min, Fg_ctrl_missing_ECMWF	filter	Clear Fg_ctrl_valid for ignored grid points
OTT_region_filter	Fg_ctrl_ignore, Fg_sc_land, Fg_sc_coast, Fg_sc_near_land, Fg_sc_suspect_ice, Fg_ctrl_missing_ECMWF, Fg_sc_rain, Fg_sc_low_wind, Fg_sc_high_wind, Fm_sun_point, Fm_L1c_RFI	filter	Select grid points and measurements for OTT computation (generating AUX_DTBXY_)
OTT_snapshot_filter	Fm_L2_RFI_snapshot_out_of_range, Fm_L2_RFI_high_snapshot_std, Fm_L2_RFI_high_snapshot_std_Stokes3, Fm_L2_RFI_high_snapshot_std_Stokes4, Fm_L1c_software_error, Fm_L1c_instrument_error, Fm_L1c_calibration_error	filter	Select snapshots for OTT computation (generating AUX_DTBXY_)
OTT_stats_filter	Fm_EAFFOV, Fm_border, Fm_sun_point, Fm_sun_tails	filter	Select measurements for computing filtered statistics
Compute_angle_ignore_filter	Fg_sc_land, Fg_sc_coast, Fg_ctrl_num_meas_min, Fg_ctrl_missing_ECMWF	filter	Set Fg_ctrl_ignore to skip grid points when computing angles

ARGANS Ltd.

Commercial in Confidence

Page 94

Use, duplication, or disclosure of this document or any information contained herein is subject to the restriction on the title page of this document.

2.4.8. Atmosphere

Name	Value	Range	Units	Comments	ATBD ref
Atmosphere nadir optical thickness τ_{atm}					§ 4.9.1.2.2
k0_tau_O2	+8.03325e+003	na.	[neper]	Oxygen optical thickness parameters fit.	Eq (8)
kT0_tau_O2	-1.03999e+002	na.	[neper/K]		
kP0_tau_O2	+2.82992e+001	na.	[neper/hPa]		
kT02_tau_O2	+2.62584e-001	na.	[neper/K^2]		
kP02_tau_O2	+6.43081e-003	na.	[neper/hPa^2]		
kT0P0_tau_O2	-9.42431e-002	na.	[neper/K/hPa]		
k0_tau_H2O	-1.47866e+002	na.	[neper]	H2O optical thickness parameters fit.	Eq (10)
k1_tau_H2O	+1.50999e-001	na.	[neper/hPa]		
k2_tau_H2O	+3.75477e+000	na.	[neper m ² /kg]		
Atmospheric layer equivalent temperature T_{atm}					§ 4.9.1.2.2
k0_DT_O2	-7.78882e-001	na.	[K]	Oxygen temperature contribution parameters fit.	Eq (9)
kT0_DT_O2	+1.37576e-001	na.	[]		
kP0_DT_O2	-1.14919e-003	na.	[K/hPa]		
kT02_DT_O2	-1.15781e-004	na.	[1/K]		
kP02_DT_O2	+1.28474e-006	na.	[K/hPa^2]		
kT0P0_DT_O2	-1.11330e-005	na.	[1/hPa]		
k0_DT_H2O	+8.18092e+000	na.	[K]	H2O temperature contribution parameters fit.	Eq (11)
k1_DT_H2O	+2.79377e-004	na.	[K/hPa]		
k2_DT_H2O	+3.72190e-002	na.	[K m ² /kg]		

2.4.9. Cardioid model

The cardioid model used to retrieve a pseudo-dielectric constant uses the following parameters

Name of parameter	Value	Units	Range	Comments	ATDB ref.
Acard_prior	1	dl		Prior estimator for retrieval	4.10
sigma_Acard	50	dl		Prior std for retrieval	4.10
Bcard	0.8	dl		Fixed parameter	4.10
Ucard_prior	45	°		Prior estimator for retrieval	4.10

ARGANS Ltd.

Commercial in Confidence

Page 95

Use, duplication, or disclosure of this document or any information contained herein is subject to the restriction on the title page of this document.

Tg_SST_ice_Acard	271	K		Maximum effective temperature to detect sea ice	4.10
Tg_Acard_ice	40	dl		Maximum A_card value to detect sea ice	4.10
Tg_lat_ice_Acard	50	°		Minimum latitude to detect sea ice	4.10

References

Boutin, J., J.L. Vergely, and P. Waldteufel (2007) On the use of an effective L-band pseudo-dielectric constant for qualifying SMOS measurements over the ocean. *IEEE Trans. Geosci. Remote* (submitted)

2.4.10. 2.4.10 RFI

RFI contaminated values will be identified using the methods explained in section 3.4 of ATBD. Two parameters are needed for this computation and their values are provided in the Measurement discrimination User Parameters Table section (2.4.2) of this TGRD.

The RFI flag coming from L1c will be kept in SSS L2 output product.

2.4.11. 2.4.11 Convergence

The convergence algorithm is described in section 4.14 of the ATBD. The table below summarises the values of the parameters used in the algorithm. These values might be modifiable according to tests performed during calibration/validation activities after SMOS launch.


Name of parameter	Value	Units	Range	Comments	ATDB ref.
λ_{ini}	0.001	dl	0-1	Initial Marquardt's diagonal amplifier	4.14
δ_{χ}	10^{-3}	dl		Chi variance ratio for convergence test 1	4.14

ARGANS Ltd.

Commercial in Confidence

Page 96

Use, duplication, or disclosure of this document or any information contained herein is subject to the restriction on the title page of this document.

	<p style="text-align: center;">SMOS L2 OS Table Generation Requirements Document</p>	<p>Doc: SO-TN-ARG-GS-0014 Issue: 3 Rev: 18 Date: 16 March 2021 Page: 97</p>
---	--	---

δsig	10^{-2}	dl		Parameter variation ratio for convergence test 2	4.14
Tg_it_max	20	dl		Maximum number of iterations allowed	4.14
Tg_Q χ	1.35	dl		Threshold to set the quality flag of the retrieval process	4.14
Tg_chi2_P_max	0.95	dl		Maximum admissible value for Dg_chi2_P	4.14
Tg_chi2_P_min	0.05	dl		Maximum admissible value for Dg_chi2_P	4.14
k _d	0.1	dl		Factor for multiplying Marquardt's diagonal amplifier	4.14
Tg_lambda_diaMax	100	dl		Maximum acceptable Marquardt increment	
SSS_prior	35	psu		SSS prior for retrieval	4.14
Tg_SSS_max	40	psu		Maximum salinity acceptable	4.14
Tg_SSS_min	30	psu		Maximum salinity acceptable	4.14
Tg_sigma_max	5	dl		Maximum SSS retrieved	4.14

ARGANS Ltd.

Commercial in Confidence

Page 97

Use, duplication, or disclosure of this document or any information contained herein is subject to the restriction on the title page of this document.

				sigma acceptable	
Acard_prior	1	dl		Acard prior for retrieval	4.14
Tg_Acard_max	70	dl		Maximum A_card acceptable	4.14
Tg_Acard_min	0	dl		Minimum A_card acceptable	4.14
Tg_sigma_max_Acard	5	dl		Maximum A_card retrieved sigma acceptable	4.14
δ SST	0.01	K	[150,300]	SST increment to compute the derivatives	4.14
δ SSS	0.01	psu		SSS increment to compute the derivatives	4.14
δ Acard	0.01	dl		Acard increment to compute the derivatives	4.14
δ U*	0.01	m/s		U* increment to compute the derivatives	4.14
δ WSx	0.01	m/s		Neutral wind speed component x increment to compute the derivatives	4.14
δ WSy	0.01	m/s		Neutral wind speed component y increment to	4.14

ARGANS Ltd.

Commercial in Confidence

Page 98

Use, duplication, or disclosure of this document or any information contained herein is subject to the restriction on the title page of this document.

				compute the derivatives	
δWS	0.01	m/s		Neutral WS increment to compute the derivatives	4.14
$\delta \Omega$	0.01	dl		Ω increment to compute the derivatives	4.14
$\delta \phi$	0.01	ρ		ϕ increment to compute the derivatives	4.14
δTEC	0.01			TEC increment to compute the derivatives	4.14
δHs	0.01	m		Hs increment to compute the derivatives	4.14
$\delta MSQS$	0.01	dl		MSQS increment to compute the derivatives	4.14
dT_dS_0	-0.224	K/psu		Coefficients for the Tb/SSS dependence	4.14.2.2
dT_dS_1	-0.0157	1/psu		Coefficients for the Tb/SSS dependence	4.14.2.2
Overall_Quality_Threshold_Low	10%	dl		Threshold for a low SSS quality index	4.14.2.2
Overall_Quality_Threshold_High	30%	dl		Threshold for a high SSS quality index	4.14.2.2

2.4.12. 2.4.12 TEC and Faraday rotation

The Faraday angle ω_{Fa} for each view is provided by L1c data (field #09 or #10 in tables 26 or 27, depending on polarization mode), or computed from TEC computed from L1c Stokes 3 data

In the case where L1c TEC data is used, and TEC_n is retrieved, the Faraday angle is introduced in the direct model:

$$\omega_{Fa} \approx cst_far * TEC_n * (B \cdot U_{LS}) / \cos(\vartheta_g) \text{ (}^\circ\text{)}$$

where:

$$cst_far = 6950$$

TEC_n is the total vertical electron content obtained from L1c field #15 for each view. The range of TEC_n is about 5 to 50.

$(B \cdot U_{LS})$ is the scalar product of the magnetic field vector B by the unitary vector U_{LS} giving the direction of the line of sight. The magnitude $|B|$ of B is obtained from L1c field #16 (expressed in nanotesla). The range of $|B|$ is about 2 to 5 10^{-5} Tesla.

$B = [(\cos(inc_B) \sin(dec_B), \cos(inc_B) \cos(dec_B), -\sin(inc_B))]$. L1c provides (fields #17 and #18) the declination dec_B and inclination inc_B of B in a local geographical frame $Oxyz$ (Ox towards East, Oy toward North, Oz upwards).

$U_{LS} = [\sin(\vartheta_g) \cos(\vartheta_n), \sin(\vartheta_g) \sin(\vartheta_n), \cos(\vartheta_g)]$ in polar geographical coordinates ϑ_g (elevation away from the Oz axis) and ϑ_n (azimuth from origin Ox , counter clockwise). It is expected that the EE CFI may provide directly ϑ_n and ϑ_g . Alternatively, ϑ_g could be inferred from the incidence angle (provided by the L1c) through adding the Earth centre angle; ϑ_n could be computed from the DGG node coordinates, assuming the coordinates of the subsatellite point are provided by the EE CFI.

In the case where TEC is computed from L1c Stokes 3:

Name of parameter	Value	Units	Comments	ATDB ref.
Rearth	6371.009	km	Radius of the earth	4.18
H_{sat}	796.0	km	Altitude of SMOS	4.18
H_{tec}	400.0	km	Assumed altitude of TEC	4.18
ξ_{min}	-0.05	dl	Lower xi limit for selecting measurements in the A3 FOV	

ARGANS Ltd.

Commercial in Confidence

Page 100

Use, duplication, or disclosure of this document or any information contained herein is subject to the restriction on the title page of this document.

ξ_{\max}	0.05	dl	Upper xi limit for selecting measurements in the A3 FOV	
η_{\min}	0.20	dl	Lower eta limit for selecting measurements in the A3 FOV	
η_{\max}	0.25	dl	Upper eta limit for selecting measurements in the A3 FOV	
maxdA3	10	tecu	Upper limit for A3TEC measurement selection	
ξ_{TEC}	3.0	dl	Correlation length for TEC estimation (by latitude)	
latWinSize	10.0	degrees	Size of the latitude window for computing A3TEC error	
σ_{OTT}	10.0	dl	Sigma prior for A3TEC OTT estimation	4.18
σ_{TEC_0}	2.0	dl	Sigma prior for A3TEC TEC estimation	4.18
σ_{TEC_1}	30.0	dl	A3 retrieved TEC smoothing factor	4.18
SnapshotWindowMin	5	dl	Minimum number of snapshots for computing A3TEC std(TB) in the latitudinal window, below which Default_A3Sig is used	
defaultA3sig	5.0	dl	Default A3 sigma used if too few snapshots	

2.4.13. Global SSS quality index

This table contains the values of the scaling coefficients SC_i used for the computation of the global quality indices $Dg_quality_SSS1$, $Dg_quality_SSS2$ and $Dg_quality_SSS3$.

SC_i values will be updated during the mission.

SC_i	SC_i value	SC_i unit
SC11	0.2	$K\ km^{-1}$
SC21	10	K
SC22	10	K
SC23	0	K
SC24	0.3	dl

ARGANS Ltd.

Commercial in Confidence

Page 101

Use, duplication, or disclosure of this document or any information contained herein is subject to the restriction on the title page of this document.



SC25	0.3	dl
SC26	100	K
SC27	40	K
SC28	0	K
SC31	0	K
SC32	40	K
SC33	100	K
SC34	100	K
SC35	40	K
SC36	40	K
SC41	40	K
SC42	40	K
SC43	40	K
SC44	24	K
SC45	24	K
SC46	24	K
SC47	24	K
SC48	0	K
SC49	0	K
SC50	0	K
SC51	0	K
SC52	0	K
SC53	0	K
SC54	0	K
SC55	0	K
SC56	0	K
SC57	0	K

Appendix A: Solar Flux datasets for sun glint correction

The second element required to compute sun glint is the solar flux. Three options are currently available: high-resolution one-second data from Air Force stations and daily noon solar flux from Penticton. The daily noon fluxes are available with a one-day delay while the one-second data are available with a delay of several months.

A.1. One second solar flux data

One-second solar flux data at L-band are available from the following stations:

Location	Lat	Lon	Local Noon (reporting time)
Learmonth (LEAR)	22.13S	114.60E	0500 UTC
Palehua (PALE)	21.24N	158.06W	2300 UTC
Sagamore Hill (SGMR)	42.38N	70.49W	1700 UTC
San Vito (SVTO)	40.40N	17.43E	1200 UTC

Example Linux commands to obtain December 2014 solar flux data files from the four stations are listed below:

```
wget -m -np 'http://www.ngdc.noaa.gov/stp/space-weather/solar-data/solar-features/solar-radio/rstn-1-second/palehua/2014/12/'
wget -m -np 'http://www.ngdc.noaa.gov/stp/space-weather/solar-data/solar-features/solar-radio/rstn-1-second/learmonth/2014/12/'
wget -m -np 'http://www.ngdc.noaa.gov/stp/space-weather/solar-data/solar-features/solar-radio/rstn-1-second/sagamore-hill/2014/12/'
wget -m -np 'http://www.ngdc.noaa.gov/stp/space-weather/solar-data/solar-features/solar-radio/rstn-1-second/san-vito/2014/12/'
```

The one-second data are downloaded, uncompressed, and then merged into ASCII files, one per station:

```
learmonth.all.txt
palehua.all.txt
san-vito.all.txt
sagamore-hill.all.txt
```

The first few lines of the file 'sagamore-hill.all.txt' are the following:

```
K7OL20100101120338 2 0 1 22 47 50 61 172
K7OL20100101120339 2 0 1 22 47 50 63 172
K7OL20100101120340 2 0 1 23 47 50 61 172
K7OL20100101120341 2 0 1 22 47 50 61 172
K7OL20100101120342 2 0 1 22 47 50 61 172
K7OL20100101120343 2 0 1 23 47 48 61 172
```

Each line corresponds to a single measurement and begins with a station identifier and the data of measurement. This is followed by the solar flux for each of the following frequencies in megahertz: 245, 410, 610, 1415, 2695, 4995, 8800, 15400.

The complete text files are then broken up into years for ease of processing, and then each yearly file is converted into a MATLAB file. The final set of MATLAB files is:

```
learmonth.2010.mat
```

ARGANS Ltd.

Commercial in Confidence



learmonth.2011.mat
learmonth.2012.mat
learmonth.2013.mat
learmonth.2014.mat
learmonth.2015.mat
palehua.2010.mat
palehua.2011.mat
palehua.2012.mat
palehua.2013.mat
palehua.2014.mat
palehua.2015.mat
sagamore-hill.2010.mat
sagamore-hill.2011.mat
sagamore-hill.2012.mat
sagamore-hill.2013.mat
sagamore-hill.2014.mat
sagamore-hill.2015.mat
san-vito.2010.mat
san-vito.2011.mat
san-vito.2012.mat
san-vito.2013.mat
san-vito.2014.mat
san-vito.2015.mat

Each of these files contains the following fields:

```
>> a=load('sagamore-hill.2013.mat')
```

a = date: [16064422x1 double] : measurement date in MATLAB datenum() format

solar flux (sfu) at 8 frequencies:

```
sfu_00245: [16064422x1 double]  
sfu_00410: [16064422x1 double]  
sfu_00610: [16064422x1 double]  
sfu_01415: [16064422x1 double]  
sfu_02695: [16064422x1 double]  
sfu_04995: [16064422x1 double]  
sfu_08800: [16064422x1 double]  
sfu_15400: [16064422x1 double]
```

The next step involves computing the daily mean, median, standard deviation, minimum, and maximum solar fluxes within a 4-hour window centred around local noon at each station. If fewer than 1000 fluxes are available within the window, the daily flux is set to the missing value (MATLAB NaN). The result is one daily flux file for each station and year.

The next step involves merging the daily solar fluxes into one file for all years and stations. The resulting file, 'daily_solar_flux.mat' has the following fields:

```
>> a=load('daily_solar_flux.mat')
```


a = One structure per station:
svto: [1x1 struct]
sgmr: [1x1 struct]
lear: [1x1 struct]

ARGANS Ltd.

Commercial in Confidence

Page 104

Use, duplication, or disclosure of this document or any information contained herein is subject to the restriction on the title page of this document.

	<p style="text-align: center;">SMOS L2 OS Table Generation Requirements Document</p>	<p>Doc: SO-TN-ARG-GS-0014 Issue: 3 Rev: 18 Date: 16 March 2021 Page: 105</p>
---	--	--

pale: [1x1 struct]

Example substructure for Sagamore Hill station:

>> a.sgmr

```
ans =
    date: [1x2191 double] : date in datenum() format
    sfu_01415_median: [1x2191 double] : median solar flux in 4-h window
    sfu_01415_mean: [1x2191 double] : maximum solar flux in 4-h window
    sfu_01415_min: [1x2191 double] : minimum solar flux in 4-h window
    sfu_01415_std: [1x2191 double] : standard deviation of solar flux 4-h window
    sfu_01415_count_good: [1x2191 double] : number of measurements in 4 hour window
```

In the next step the solar flux statistics are converted to brightness temperatures using the factor 'sfu_to_tb_21cm' defined below:

```
kboltzmann = 1.38e-23;
omega_sun = 8.2e-5; % sun solid angle in steradians
sfu_to_tb_21cm = 1e-22*.21^2/(2*kboltzmann)/omega_sun;
```

The resulting daily brightness temperature statistics are then averaged with a running window with a six-day window width. This is done for each station separately and the results are stored in the file 'daily_solar_flux_filtered.mat' with the following structure:

>> a=load('daily_solar_flux_filtered.mat')

```
a =
    svto: [1x1 struct]
    sgmr: [1x1 struct]
    lear: [1x1 struct]
    pale: [1x1 struct]
    running_mean: [1x1 struct]
```

Running means are stored in the following structure :

>> a.running_mean

```
ans = sgmr: [1x1 struct]
    date: [1x2191 double]
    svto: [1x1 struct]
    lear: [1x1 struct]
    pale: [1x1 struct]
    median: [1x2191 double] : median of running mean Tbs from SGMR, PALE, and SVTO stations
    min: [1x2191 double]
    max: [1x2191 double]
```

This leaves several possible time series that may be used as the solar flux for sun glint calculations. One possibility is to use the (time,flux) pair MATLAB FILE 'daily_solar_flux_filtered.mat': (a.running_mean.date, a.running_mean.median).

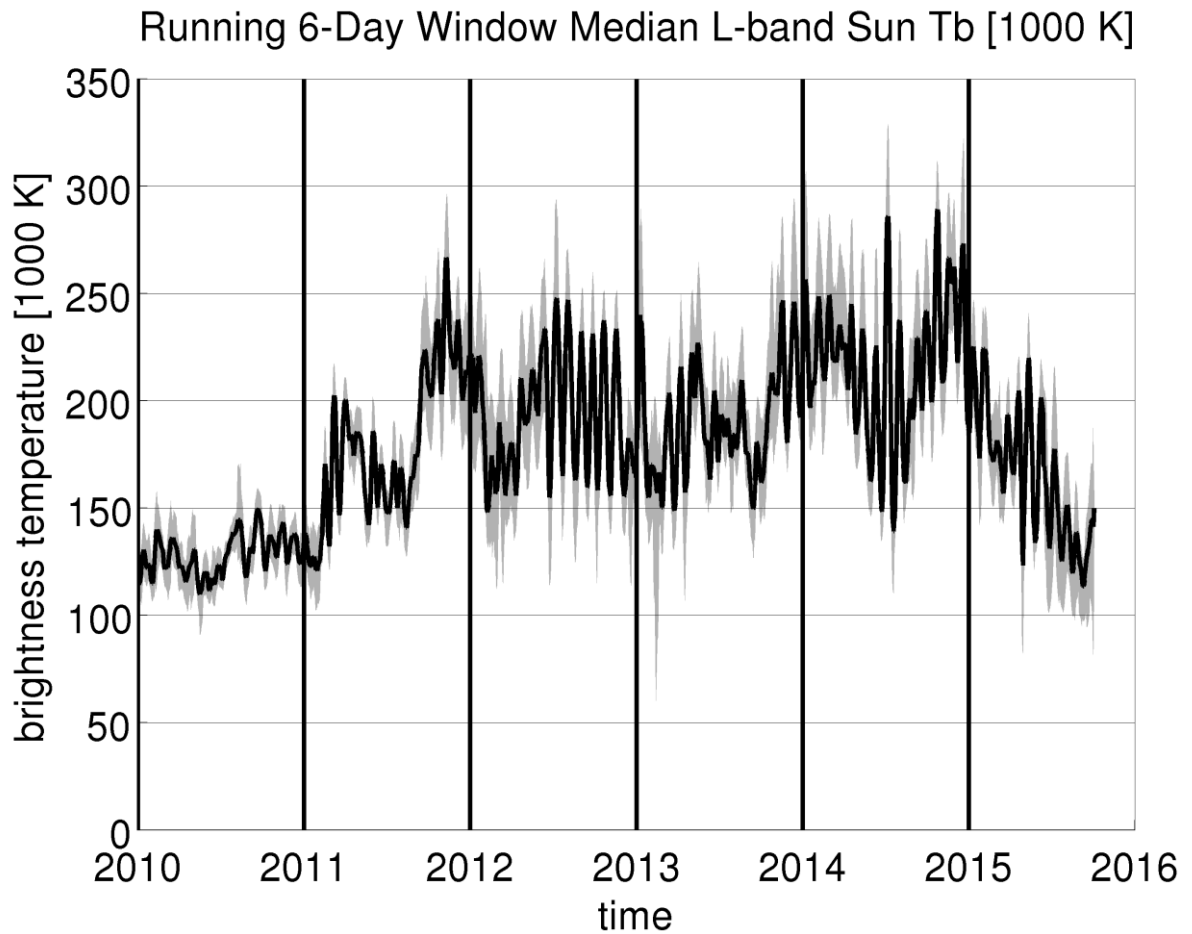


Figure 13: Time series of the six-day running mean of daily median of the 1-s sun brightness temperatures reported by stations in Sagamore Hill, Palehua, and San Vito. This running mean is used to compute the sun glint model solutions. Gray shading shows the range of sun brightness temperatures obtained by computing the daily maximum and minimum of the smoothed solar fluxes +/- two standard deviations.

A.2. Daily noon solar flux data

Unfortunately, the one-second data from the above stations are not available within any particular specified time and the delay may reach several months. Hence these data are not suitable for a real-time application. However, daily average solar flux at 10.7 cm is available in near real-time from the following station in western Canada:

Location	Lat	Lon	Local Noon (reporting time)
Penticton	49.30N	119.35W	2000 UTC

The Penticton data are available within one day of the measurement from the following site:

<http://www.spaceweather.com/rsga.txt>

The preceding file is referred to as the 'Report of Solar and Geophysical Activity' (RSGA) and it is jointly produced by NOAA and the US Air Force. These RSGA data files are also available from the SMOS DPGS here:

ftp://dpgs_ads:dis2DgafLO@131.176.251.162//application_cache/data/ftp/reference/auxdata/YYYYMMDDRSGA.txt

where YYYYMMDD should be replaced by the year, month, and day of the report.

Within each RSGA file are lines of the form :

```
IV. Penticton 10.7 cm Flux
Observed      06 May 090
Predicted    07 May-09 May 085/085/085
90 Day Mean   06 May 095
```

The daily flux is obtained from the line beginning with the word 'Observed'. However, for real-time applications the forecasted fluxes may also be used.

For SMOS the 10.7 cm fluxes must be transformed into L-band brightness temperatures. This is done by making a linear fit of the 10.7 cm brightness temperatures to 21 cm brightness temperatures from Sagamore Hill Observatory.

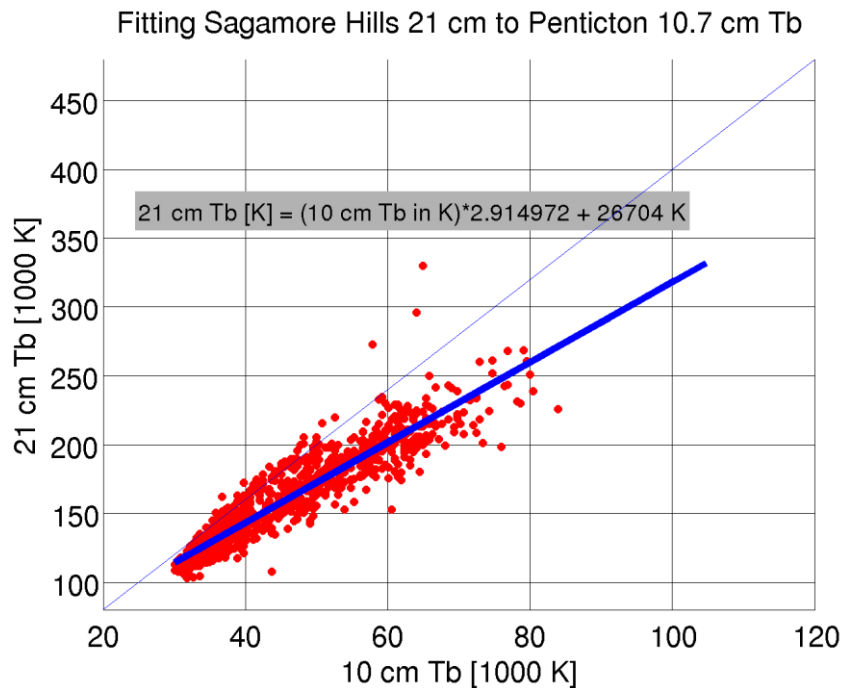


Figure 14: Linear fit between 10.7 cm and 21 cm sun brightness temperatures.

The following transformation factors are used to convert solar flux (in solar flux units or sfu) to brightness temperature (K) at 21 cm and 10 cm wavelengths:

```
kboltzmann = 1.38e-23;
omega_sun = 8.2e-5;
sfu_to_tb_21cm = 1e-22*.21^2/(2*kboltzmann)/omega_sun;
sfu_to_tb_10cm = 1e-22*.10^2/(2*kboltzmann)/omega_sun;
```

Contents of the MATLAB file solar_sfu.mat :

```
sfu_10cm: [1x2364 double]
date: [1x2364 double]: Date in MATLAB datenum() format
tb_10cm: [1x2364 double]: daily brightness temp. (K) at 10.7 cm from Penticton
sfu_21cm_sgmr: [1x2364 double]: daily L-band solar flux from one-second SGMR data (sfu)
tb_21cm_sgmr: [1x2364 double]: daily brightness temp. (K) from SGMR
tb_21cm_from_10cm: [1x2364 double]: daily L-band sun brightness temp. From linear fit to 10.7 cm
sfu_21cm_from_10cm: [1x2364 double]: daily solar flux at 21 cm from 10.7 cm Penticton flux
```

Thus, as an alternative to the one second flux, the following (time,flux) series may be used for sun glint calculations: MATLAB file 'solar_sfu.mat': (a.date, a.tb_21cm_from_10cm).

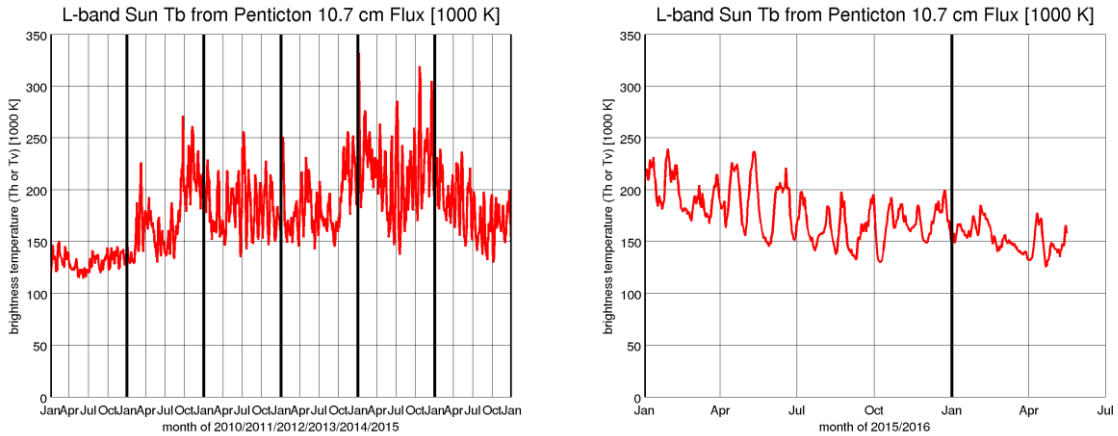


Figure 15: Left: Time series of daily L-band sun brightness temperature obtained from linear fit to 10.7 cm brightness temperature as described above. Right: zoom on 2015/2016 brightness temperatures, showing the slow overall decrease in solar flux during this period.

A.3. Use of solar flux derived from SMOS data

During the research phase associated to the L2 OS v700 baseline, a novel methodology has been identified to measure solar flux valid for SMOS application. The method makes use of telemetric information to extract the influx of L-band radiation coming from the sun, which enables a more accurate estimation of L-band measurements at the exact same frequency than SMOS and better fitted for glint correction.


The details of the generation of the “raw” solar flux are explained in the associated TGRD for such product, RedLab-SER-SM-REP-001. In the following sections, details are provided in how such product has been adapted to produce the LUT required for the sun glint correction and found within AUX_SUN_BT auxiliary file.

A.3.1. Review of sun glint formulation

The principle use of the solar flux time series in the L2OS processor is the calculation of the contribution of sun glint to the scene brightness as measured by MIRAS. At the surface, the brightness temperature of the scattered solar radiation in polarization p may be expressed as

$$T_{ssp} = \frac{T_s(t)\Omega_s}{4\pi \cos(\theta_s)} [\sigma_{pp}(\phi_o, \theta_o, \phi_s, \theta_s; u_{10}) + \sigma_{pq}(\phi_o, \theta_o, \phi_s, \theta_s; u_{10})], \quad (1)$$

where $T_s(t)$ is the brightness temperature of the sun averaged over the solar disc at 1.4 GHz at time t, p and q represent the polarizations H or V, and $(\sigma_{pp}, \sigma_{pq})$ are the bi-static scattering cross-sections of the sea surface, expressed as functions of the scattering geometry. The incidence and azimuth angles from the scattering surface toward the sun are ϕ_o and θ_o , respectively, and the corresponding angles towards the satellite are ϕ_s and θ_s . Ω_s is the (time-

	<p style="text-align: center;">SMOS L2 OS Table Generation Requirements Document</p>	<p>Doc: SO-TN-ARG-GS-0014 Issue: 3 Rev: 18 Date: 16 March 2021 Page: 110</p>
---	--	--

varying) solid angle of the sun at L-band, which is related to its (fixed) cross-sectional area A_s by

$$\Omega_s(t) = \frac{A_s}{d_s^2(t)}, \quad (2)$$

where $d_s(t)$ is the (varying) earth-sun distance given in [CCC20] as

$$d_s(t) = \text{AU} \left(1 - \frac{0.03344}{2} \cos(0.0172N_{\text{day}} - 0.0688) \right), \quad (3)$$

where N_{day} is the day of year. The sun glint scales as the product of the sun brightness temperature and the sun solid angle, which is proportional to the solar flux. The solar flux F_s , with units of solar flux units ($\text{sfu} = 10^{-22} \text{ W m}^{-2} \text{ Hz}^{-1}$), is related to sun brightness temperature by the equation

$$F_s = \frac{2k_b T_s}{\lambda^2} \Omega_s, \quad (4)$$

where λ is the radiation wavelength and k_b are Boltzmann's constant ($1.3810^{-23} \text{ J K}^{-1}$). The sun solid angle at L-band is usually taken to be around $8.2 \times 10^{-5} \text{ sr}$ but this varies as a function of the earth-sun distance since the cross-sectional area of the sun is constant. Although the sun brightness temperature does not vary with earth-sun distance d_s , the solar flux varies inversely with the earth-sun distance, so it can be useful to introduce a solar flux normalized to an earth-sun distance of 1 AU,

$$F_{ns} = \frac{2k_b T_s}{\lambda^2} \Omega_{ns}, \quad (5)$$

where now both F_{ns} and Ω_{ns} correspond to an earth-sun distance d_{ns} of 1 AU. Noting that by definition

$$\Omega_{ns}(t) = \frac{A_s}{d_{ns}^2(t)} = \Omega_s(t) \left(\frac{d_s^2(t)}{d_{ns}^2(t)} \right), \quad (6)$$

the normalized flux may be expressed in terms of the actual flux by

$$F_{ns} = \frac{2k_b T_s}{\lambda^2} \Omega_s(t) \frac{d_s^2(t)}{d_{ns}^2(t)} = F_s \frac{d_s^2(t)}{d_{ns}^2(t)}. \quad (7)$$

A.3.1. Sources of solar flux data considered


Table 5 below summarizes the data sets that are compared in this document. The daily Penticton C-band data are transformed into an estimate of the daily L-band solar flux using a linear fit between the Penticton C-band data and daily averaged L-band solar flux data from the Radio Solar Telescope Network (RSTN). The RedLab/Serco solar flux and SMOS linear fit data sets are discussed in the following subsections.

Table 5: Solar Flux sources alternatives

field name	description	time resolution
daily Penticton C-band (RSGA)	daily time series derived from Penticton C-band measurements rescaled to L-band	1 value per day
RedLab/SERCO daily reference	daily time series derived from carefully calibrated multi-frequency radioastronomy measurements	1 value per day
RedLab/SERCO uncorrected SMOS	solar flux derived from MIRAS brightness temperatures	1 value for T_x and T_y per orbit
RedLab/SERCO corrected SMOS	solar flux derived from MIRAS brightness temperatures and adjusted using the RedLab/SERCO daily reference	1 value for T_x and T_y per orbit
SMOS linear fit over ocean	solar flux derived by fitting ocean scene brightness model to MIRAS first Stokes parameter	1 value approximately every 2 minutes

A.3.2. The RedLab/Serco Solar Flux Data Sets

RedLab/Serco have developed solar flux datasets based on an analysis of both radiotelescope measurements and brightness temperatures obtained from MIRAS. The so-called 'reference' dataset based on radiotelescope measurements provides daily L-band solar flux normalized to a 1 AU earth-sun distance, while the dataset based upon SMOS brightness temperatures typically provides several solar fluxes values each day. Details of the derivation of these datasets are provided in [CCC20]. The time series data provided by Serco are normalized to a 1 AU earth-sun distance, and these are rescaled to the actual sun distance using (7) for comparison with fluxes obtained from the linear fit described below.

	<p style="text-align: center;">SMOS L2 OS Table Generation Requirements Document</p>	<p>Doc: SO-TN-ARG-GS-0014 Issue: 3 Rev: 18 Date: 16 March 2021 Page: 112</p>
---	--	--

A.3.3. Solar flux obtained from the MIRAS measurements

During the months of November, December, January and February the sun glint has a strong impact on the scene brightness on the western side of the field of view in descending passes south of about 40° S latitude, where the sun glint can exceed 10 K at the swath edges. Noting that the sun glint is proportional to the solar flux for any given surface roughness conditions (cross sections), it is possible to estimate the flux directly from the residual obtained after subtracting the ocean forward scene brightness model solutions without sun glint from the total OTT-corrected SMOS brightness temperatures. As discussed in subsection 7, the sun glint estimated from SMOS data can be expressed as

$$\Delta T_p^{(sg)} = \left[T_p^{(miras)}(\xi, \eta, t) - \Delta T_p^{OTT}(\xi, \eta) \right] - T_{tp}^{(nsg)}, \quad (8)$$

where T_{tp}^{nsg} is the forward ocean scene brightness model solution without sun glint. The model sun glint can be expressed as the product of the model glint for some nominal solar flux and the ratio of the actual to nominal solar flux. This nominal flux (corresponding to $T_s = T_s^n = 100000 \text{ K}$), is

$$T_{ssp}^n = \frac{T_s^n \Omega_s}{4\pi \cos(\theta_s)} [\sigma_{pp}(\phi_o, \theta_o, \phi_s, \theta_s; u_{10}) + \sigma_{pq}(\phi_o, \theta_o, \phi_s, \theta_s; u_{10})], \quad (9)$$

In terms of this nominal sun glint, the model sun glint corresponding to a sun brightness temperature $T_s(t)$ is


$$T_{ssp} = T_{ssp}^n \frac{T_s(t)}{T_s^n} = \left[T_{ssp}^n (\sigma_{pp}(\phi_o, \theta_o, \phi_s, \theta_s; u_{10}), \sigma_{pq}(\phi_o, \theta_o, \phi_s, \theta_s; u_{10})) \right] \frac{T_s(t)}{T_s^n}. \quad (10)$$

where the dependence of the nominal sun glint solution upon the scattering cross sections (and hence surface roughness or wind speed u_{10}) is made explicit.

The preceding equation shows that the ratio of the actual to nominal sun brightness temperature is equal to the ratio of the model solutions evaluated at the actual and nominal sun glint model solutions,

$$T_s(t) = T_s^n \frac{T_{ssp}}{T_{ssp}^n}. \quad (11)$$

If the model solution at the actual sun brightness temperature T_{ssp} is replaced by the residual sun glint obtained from the SMOS data ΔT_p^{sg} , the result is an estimate of the sun brightness temperature from the data,

	<p style="text-align: center;">SMOS L2 OS Table Generation Requirements Document</p>	<p>Doc: SO-TN-ARG-GS-0014 Issue: 3 Rev: 18 Date: 16 March 2021 Page: 113</p>
---	--	--

$$T_s(t) = T_s^n \frac{\Delta T_p^{(sg)}}{T_{ssp}^n}. \quad (12)$$

Since the sun brightness temperature does not depend upon viewing geometry, the preceding equation also holds for dwell-line average sun glint solutions,

$$T_s(t) = T_s^n \frac{\langle \Delta T_p^{(sg)} \rangle}{\langle T_{ssp}^n \rangle}, \quad (13)$$

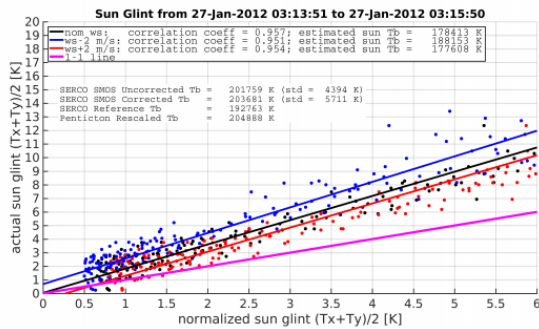
where it is assumed that the sun brightness temperature is constant within each dwell line average. To estimate the solar flux, a linear fit is made to the set of all $(\langle T_{ssp}^n \rangle, \langle \Delta T_p^{sg} \rangle)$ collected within 2-minute time intervals in the portion of orbits strongly affected by sun glint. The product of the nominal sun brightness temperature ($T_s^n = 100000 \text{ K}$) and the slope of this linear fit yields the sun brightness temperature from the (SMOS-model) residuals. This approach is advantageous because it is not strongly affected by forward model errors at any given point.

Examples of this linear fit are shown in Figure 16. In these examples the correlation coefficients exceed 0.95 and the estimated sun brightness temperatures are consistently lower than those obtained from rescaled Penticton 10.7 cm measurements and the RedLab/Serco data. Varying the wind speed by +/- 2 m/s in the calculation of the nominal sun glint results in a small variation of the estimated solar flux but this variation does not account for differences between the different data sources.

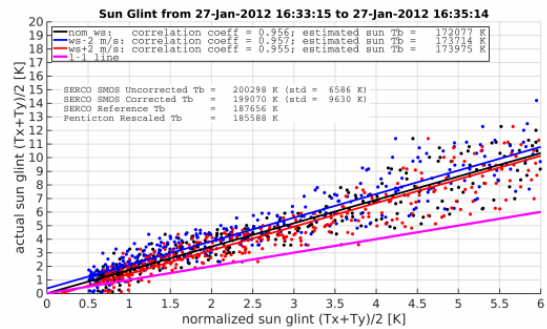
A.3.4. Comparing the solar flux time series

The linear fits described in the previous section have been performed over the months of December and January from 2010-2019 and the results have been compiled into a high-resolution time series for just these months. An example comparison between this time series and the other available series for two days is provided in Figure 17. A few observations may be made:

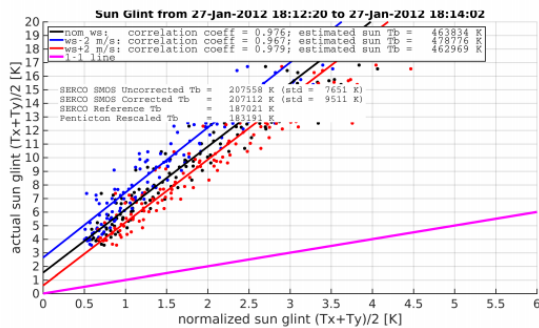
- Even in terms of the 20-min averages, the variability of the linear fit solar flux within each day is larger than that of any other source.
- The variability of the 2-min fit solar flux within each 20-min window (max-min) is of the same magnitude as the intra-day variability.
- The uncertainty associated with +/- 2 m/s variation in the wind speed and source of wind speed (CCMP OR ECMWF) is much smaller than the intra-day variations.
- The 20-min average linear fit solar fluxes are generally lower than all other sources.



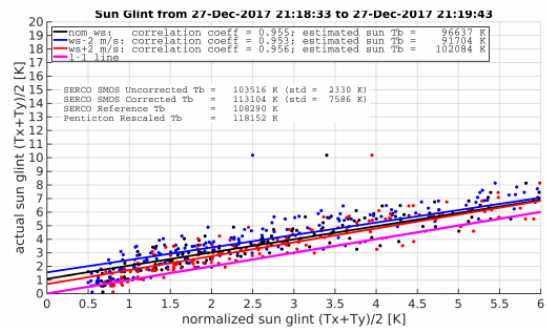
(a)



(b)



(c)



(d)

Figure 16: Scatterplots of actual versus nominal sun glint (first Stokes divided by two, as discussed in the text) for four distinct 2-min time intervals during which sun glint strongly affects the measured brightness. (a)-(c) are three-time intervals on 27 Jan 2012, and (c) corresponds to a solar flare during which there is a large increase in the solar flux lasting just a few minutes. (d) is a two-min interval on 27 Dec 2017 which corresponds to a quiet sun period (and low sun brightness temperature). The black lines correspond the linear fits at the wind speed provided by the CCMP product, while the red and blue lines are linear fits for CCMP wind speed +/- 2 m/s, respectively.

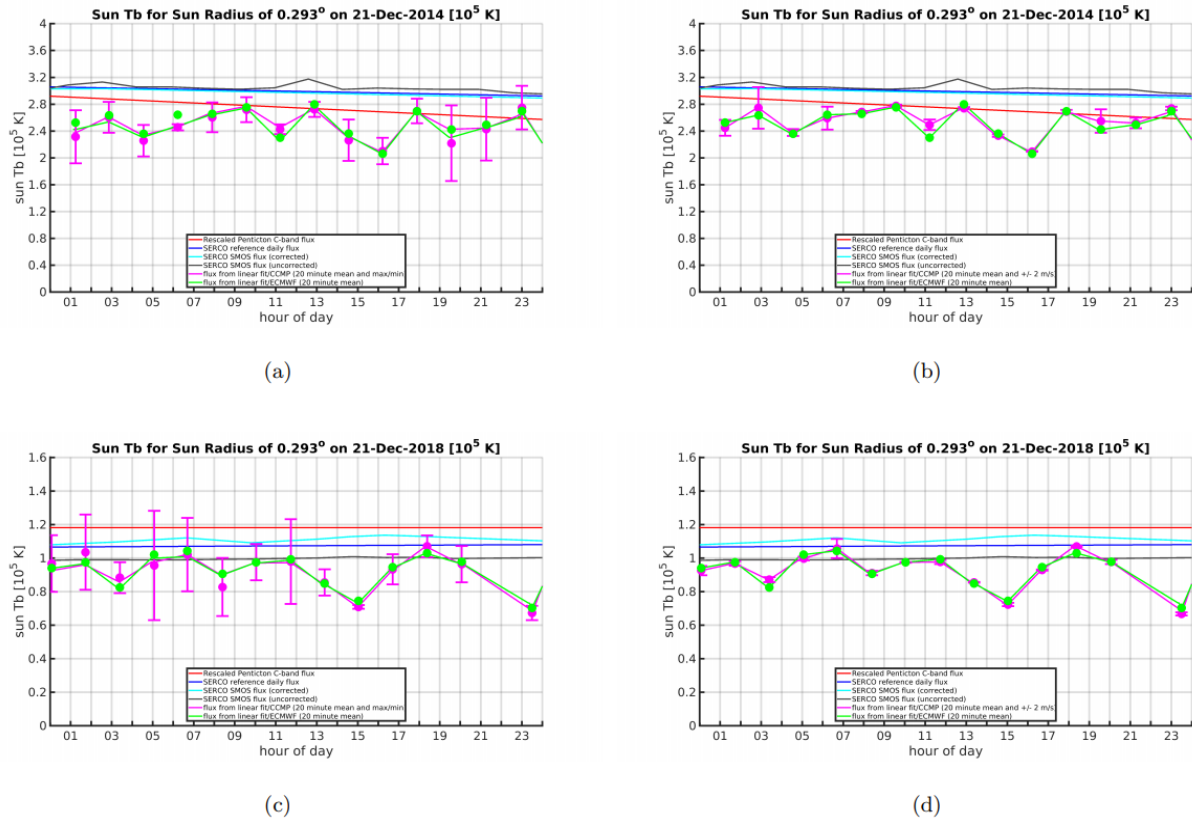


Figure 17: Daily time series of sun Tb from various sources, include the rescaled Penticton 10.7 cm measurements, the RedLab/Serco reference and SMOS time series, and 20-min averages of the linear fit using both CCMP and ECMWF wind speed to compute the nominal sun glint solutions. Upper panels are for 21 dec 2014 (active sun), while the lower panels are for 21 Dec 2018 (quiet sun). Vertical bars in the left panels show the range of linear fit sun Tb within each 20-min averaging wind, while the bars in the right panels show the range associated with varying the CCMP wind speed by +/- 2 m/s in the nominal sun glint solution.

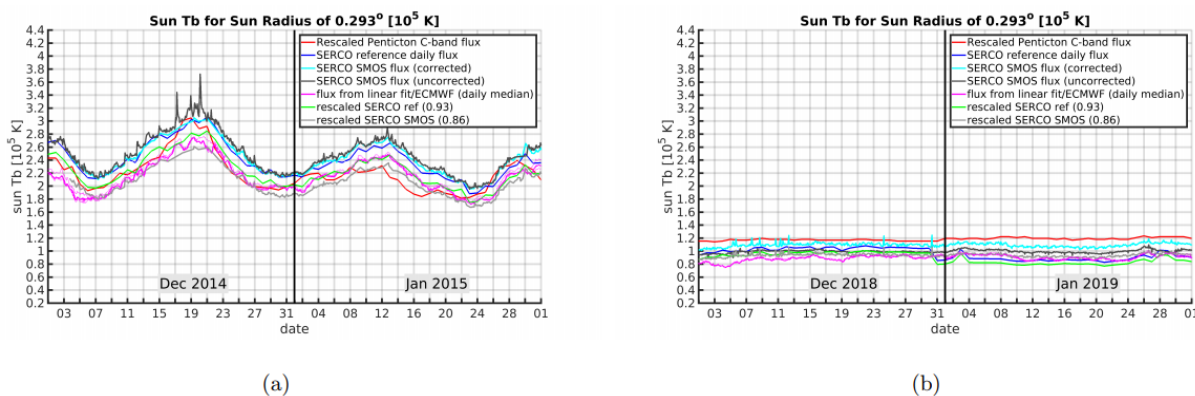


Figure 18: Time series of various sources of sun Tb over the months of December and January for (a) 2014-2015 and (b) 2018-2019. Shown are both the nominal (i.e. as provided) and rescaled RedLab/Serco fluxes, where the rescaling is obtained as the median of the ratio between the linear fit and RedLab sun Tb time series over the entire mission. A median filter with a running 1-day window has been applied to the 2-min linear fit sun Tb time series to make it comparable to the daily time series.

A rescaled version of the RedLab/Serco reference time series (daily fluxes) is used for the sun glint calculation in the Level 2 Salinity Processor. A single rescaling factor has been determined for the entire time series, and this factor is computed as the median of the ratio of the linear fit sun Tb (based upon ECMWF 10-m wind speed) to the RedLab/Serco reference sun Tb (adjusted to the actual earth-sun distance). Figure 18 compares the available solar flux time series for December and January of 2014-2015 and 2018-2019. This figure illustrates the same tendency of the linear fit solar fluxes to be generally lower than the other (non-rescaled) fluxes. Rescaling the RedLab/Serco fluxes by a factor near 0.9 brings them into better agreement with the linear fit fluxes.

The right panel in Figure 18 shows a distinct drop in the RedLab/Serco reference time series (green curve) on 31 Dec 2018, and this corresponds to the start of a period extending through 20 Feb 2019 during which both the 1.0 and 2.0 GHz reference source data are unavailable (see [CCC20] for details). As a final adjustment the rescaled reference time series during this period is replaced by the daily averaged rescaled corrected SMOS time series.

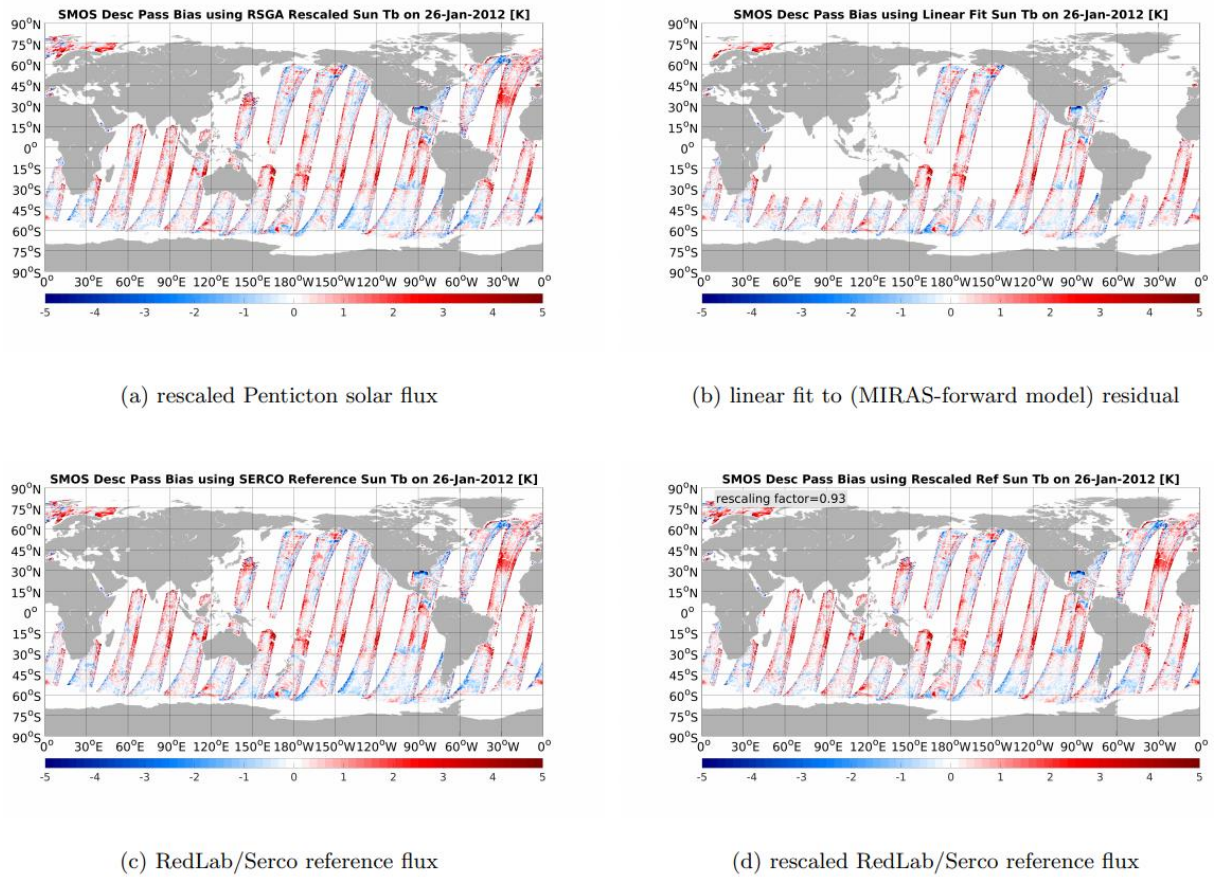



Figure 19: Dwell-line average bias between SMOS and the total forward ocean scene brightness (first Stokes parameter divided by two) model including sun glint computed using four sources of solar flux (SMOS-model).

	<p style="text-align: center;">SMOS L2 OS Table Generation Requirements Document</p>	<p>Doc: SO-TN-ARG-GS-0014 Issue: 3 Rev: 18 Date: 16 March 2021 Page: 117</p>
---	--	--

A.3.5. Example global bias map

Figure 19 shows examples of global maps of the dwell-line averaged bias between SMOS and the total forward model with sun glint solutions from four different sources of solar flux: (a) rescaled Penticton 10.7 cm; (b) linear fit; (c) RedLab/Serco reference daily time series; and (d) rescaled RedLab/Serco reference daily time series.

Use of the Penticton 10.7 cm time series results in overcorrection in most of the swaths in this example, while the linear fit (by construction) results in very little over or under correction except in one swath (south of Australia) where some overcorrection is evident.

In this case both the RedLab/Serco maps show evidence of sub-optimal correction, but with the residual bias reduced somewhat with the rescaled time series.

A.3.7. The total model solution

This section reviews the complete ocean scene brightness model used to derive the sun brightness temperatures from the SMOS brightness temperatures and to evaluate the various solar flux time series.

Considering all of the components of the scene brightness at L-band, the complete model solution for the upwelling brightness temperatures above the atmosphere but below the ionosphere (before Faraday rotation) in the surface polarization basis is, in horizontal polarization,

$$T_{th}^{(full)} = (\tau_d \tau_v) [T_{esh} + T_{sch} + T_{ssh} + R_h T_{ea}] + T_{ea} + (\tau_d \tau_v) [(1 - F_f) T_{erh} - F_f T_{esh} - e_{rh} T_{ea}] \quad (14)$$

and in vertical polarization

$$T_{tv}^{(full)} = (\tau_d \tau_v) [T_{esv} + T_{scv} + T_{ssv} + R_v T_{ea}] + T_{ea} + (\tau_d \tau_v) [(1 - F_f) T_{erv} - F_f T_{esv} - e_{rv} T_{ea}] \quad (15)$$

where the terms in red represent the sun glint and the other variables are listed in Table 6, at the end of this section. The total model solutions without the sun glint contributions are thus

$$T_{th}^{(nsg)} = (\tau_d \tau_v) [T_{esh} + T_{sch} + R_h T_{ea}] + T_{ea} + (\tau_d \tau_v) [(1 - F_f) T_{erh} - F_f T_{esh} - e_{rh} T_{ea}] \quad (16)$$

$$T_{tv}^{(nsg)} = (\tau_d \tau_v) [T_{esv} + T_{scv} + R_v T_{ea}] + T_{ea} + (\tau_d \tau_v) [(1 - F_f) T_{erv} - F_f T_{esv} - e_{rv} T_{ea}]. \quad (17)$$

After passage of the radiation upward through the ionosphere and after transformation into the Ludwig-3 [Lud73] instrument polarization basis, the Stokes vector elements of the total and no-sunglint model solution are

$$\begin{pmatrix} T_{tx}^{(\text{full,nsg})} \\ T_{ty}^{(\text{full,nsg})} \\ T_{t3}^{(\text{full,nsg})} \\ T_{t4}^{(\text{full,nsg})} \end{pmatrix} = \begin{pmatrix} \cos^2 \beta & \sin^2 \beta & -\cos \beta \sin \beta & 0 \\ \sin^2 \beta & \cos^2 \beta & \cos \beta \sin \beta & 0 \\ \sin(2\beta) & -\sin(2\beta) & \cos(2\beta) & 0 \\ 0 & 0 & 0 & 1 \end{pmatrix} \begin{pmatrix} T_{th}^{(\text{full,nsg})} \\ T_{tv}^{(\text{full,nsg})} \\ T_{tU}^{(\text{full,nsg})} \\ T_{tV}^{(\text{full,nsg})} \end{pmatrix}, \quad (18)$$

where the angle β account for both rotation of the polarization plane during passage through the ionosphere and rotation of the polarization basis from the surface basis to the Ludwig-3 basis. In the following subsections the various components of the preceding total model are described.

The difference between the brightness temperatures from SMOS and the forward model in (instrument basis) polarization p is

$$\Delta T_p(\xi, \eta, t) = T_p^{(\text{miras})}(\xi, \eta, t) - T_{tp}^{(\text{full})}. \quad (19)$$

then the corresponding OTT is

$$\Delta T_p^{\text{OTT}}(\xi, \eta) = \langle \Delta T_p \rangle_t(\xi, \eta, t). \quad (20)$$

where the average is taken over some long time interval (more than one day).

Using the preceding notation, the sun glint (in the instrument basis) can be estimated from the OTT-corrected measurements and the forward model as

$$\Delta T_p^{(\text{sg})} = \left[T_p^{(\text{miras})}(\xi, \eta, t) - \Delta T_p^{\text{OTT}}(\xi, \eta) \right] - T_{tp}^{(\text{nsg})}. \quad (21)$$

For the developments described in this note only the first Stokes parameter is used to derive the glint and evaluate the various sources of solar flux data, and the polarization subscript is dropped when referring to the first Stokes parameter (divided by two).

A.3.8. References

[CCC20] Daniele Casella, Lorenzo Di Ciolo, and Raffaele Crapolicchio. L-band solar flux table generation requirements document. Technical report, RedLab and Serco Italia, June 2020.

[Lud73] Arthur C. Ludwig. The definition of cross polarization. IEEE Trans. Antennas Propag., AP-21(1):116– 119, January 1973.


	<p style="text-align: center;">SMOS L2 OS Table Generation Requirements Document</p>	<p>Doc: SO-TN-ARG-GS-0014 Issue: 3 Rev: 18 Date: 16 March 2021 Page: 119</p>
---	--	--

Table 6: Quantities in the total Scene Brightness Model

Variable	Physical Quantity
$T_{th}^{(full)}$	H-pol total brightness temp. in the surface pol. basis [K]
$T_{tv}^{(full)}$	V-pol total brightness temp. in the surface pol. basis [K]
$T_{tU}^{(full)}$	third Stokes parameter total brightness temp. in the surface pol. basis [K]
$T_{tV}^{(full)}$	fourth Stokes parameter total brightness temp. [K]
$T_{tx}^{(full)}$	H-pol total brightness temp. in the instrument pol. basis [K]
$T_{ty}^{(full)}$	V-pol total brightness temp. in the instrument pol. basis [K]
$T_{t3}^{(full)}$	third Stokes parameter total brightness temp. in the instrument pol. basis [K]
$T_{t4}^{(full)}$	fourth Stokes parameter total brightness temp. [K]
τ_d	1-way atmospheric transmittance associated with molecular oxygen absorption [nd]
τ_v	1-way atmospheric transmittance associated with water vapor absorption [nd]
T_{esh}	H-pol brightness temp. of specular emission H-pol (surface pol. basis) [K]
T_{erh}	H-pol brightness temp. of rough surface emission H-pol (surface pol. basis) [K]
T_{sch}	H-pol brightness temp. of scattered celestial sky radiation (surface pol. basis) [K]
T_{esv}	V-pol brightness temp. of specular emission H-pol (surface pol. basis) [K]
T_{erv}	V-pol brightness temp. of rough surface emission H-pol (surface pol. basis) [K]
T_{scv}	V-pol brightness temp. of scattered celestial sky radiation (surface pol. basis) [K]
T_{ea}	brightness temp. of (unpolarized) atmospheric 1-way emission [K]
R_h	H-pol surface power reflection coefficient (surface pol. basis) [K]
R_v	V-pol surface power reflection coefficient (surface pol. basis) [K]
e_{rh}	H-pol rough surface emissivity [K]
e_{rv}	V-pol rough surface emissivity [K]
F_f	foam fraction from rough surface emission model [nd, range: 0-1]
T_{ssh}	H-pol brightness temp. of scattered solar radiation (sun glint) (surface pol. basis) [K]
T_{ssv}	V-pol brightness temp. of scattered solar radiation (sun glint) (surface pol. basis) [K]

ARGANS Ltd.

Commercial in Confidence

Page 119

Use, duplication, or disclosure of this document or any information contained herein is subject to the restriction on the title page of this document.

Appendix B: TGRD to IODD traceability matrix

Parameters set in the TGRD are also listed in the IODD and grouped in files. In general, a file contains one Look-up Table. For individual parameters such as physical constants, many parameters are gathered in a file. The table below summarizes the tables and parameters defined in TGRD and indicates the file in which they are stored along with reference section in IODD.

Table 7: TGRD to IODD traceability matrix

Parameter / Look-Up Table	TGRD section	File name	IODD section	Note
Land sea mask-Measurement discrimination	2.2.2.1	AUX_DISTAN	2.5	
Sea ice mask-Measurement discrimination	2.2.2.2	AUX_DISTAN	2.5	
Roughness_1	2.2.3	AUX_RGHNS1	2.4.4	
Roughness_2	2.2.4	AUX_RGHNS2	2.4.5	
Roughness_3	2.2.5	AUX_RGHNS3	2.4.6	
Galactic noise 1	2.2.6	AUX_GAL_OS	2.4.8	
Galactic noise 2	2.2.7	AUX_GAL2OS	2.4.9	
Land contamination	2.2.8	AUX_MSOTT	2.5.3	
SMOS-based climatology	2.2.9	AUX_SSSCLI	2.5.1	
AGDP tables	2.3.1	AUX_AGDPT_	2.5.4	
OTT tables	2.3.2	AUX_OTTxF/D_	2.5.2	
Physical Constants	2.4.1	AUX_CNFOSD/F	2.5.4	
Measurement discrimination	2.4.2	AUX_CNFOSD/F	2.5.4	
Dielectric constant	2.4.3	AUX_FLTSEA	2.4.3	
Foam	2.4.4	AUX_FOAM_	2.4.7	
Sunglint	2.4.6	AUX_SGLINT	2.4.10 & 2.4.11	
Solar flux TB	2.4.6.2	AUX_SUN_BT	2.4.11	
Switches & Filters	2.4.7	AUX_CNFOSD/F	2.5.4	
Atmosphere	2.4.8	AUX_ATMOS_	2.4.12	
Cardioid model	2.4.9	AUX_CNFOSD/F	2.5.4	
Bias correction				Not implemented yet
RFI	2.4.10			Empty
Convergence	2.4.11	AUX_CNFOSD/F	2.5.4	
TEC & Faraday rotation	2.4.12	AUX_CNFOSD/F	2.5.4	
Global quality index	2.4.13	AUX_CNFOSD/F	2.5.4	

ARGANS Ltd.

Commercial in Confidence

Page 120

Use, duplication, or disclosure of this document or any information contained herein is subject to the restriction on the title page of this document.